CONCENTRATION AND OPTICAL MEASUREMENT OF AQUEOUS ANALYTES IN AN ORGANIC SOLVENT SEGMENTED CAPILLARY UNDER A HIGH ELECTRIC FIELD

by

HONG ZHENG, B.S.

A THESIS

IN

CHEMISTRY

Submitted to the Graduate Faculty
of Texas Tech University in
Partial Fulfillment of
the Requirements for
the Degree of

MASTER OF SCIENCE

Approved

Accepted

May, 1994

ACKNOWLEDGEMENT

I would like to thank my research advior Dr. Purnendu K. Dasgupta, for his support, guidance, and patience in the course of my graduate research at Texas Tech University. His time spent on the correction of this final version of the thesis is appreciated.

My sincere thanks goes to Dr. Kiumars Ghowsi and Dr. Dennis Shelly, for their valuable review of this thesis and being part of my thesis committee.

I am grateful forever to all my friends and family members for their understanding, help, and encouragement throughout these years. I am deeply indebted to my parents in China.

Finally, a heartfelt thanks goes out to Young Zhu, for his constant encouragement, help, and his belief in my abilities. Thank you.

TABLE OF CONTENTS

LIST OF FIGURES

CHAPTER I

INTRODUCTION

On-line concentration and optical detection of aqueous analytes in an organic solvent segmented small diameter silica capillary under high electric field is a new concept in chemical analysis. Although the basic instrumental setup is similar to that for capillary zone electrophoresis (CZE), the underlying physico-chemical processes are different. There include polarization, ion exchange, and extraction, rather than separation based on differences in electrophoretic velocities as in CZE systems.

The system is complex. A consummate explanation to all of the phenomena observed for the experimental systems has been elusive. Therefore, the introductory part briefly describes several relevant fields. These include solvent extraction, especially "on-line" solvent extraction flow injection analysis; capillary-high electric field systems and electrochemical processes at the boundary of two immiscible phases.

1.1 Solvent Extraction in the Analysis of Metal Ions

1.1.1 General Review

Solvent extraction is one of the most powerful methods in separation science, because of its ease of operation, simple apparatus, fast analysis and wide applicabilities. It is efficient in the determination of trace and ultratrace levels of metals.[1] Since we are usually concerned with metal samples in aqueous solutions, solvent extraction discussed here implies the use of an aqueous-organic solvent pair.

Solvent extraction systems are generally classified into two categories on the basis of the nature of the extractable species.[2] The formation of uncharged species is a prerequisite for extraction into organic solvents which generally have low dielectric constants. The first category is termed chelate extraction systems; the extracted species

are neutral chelates. The second category is termed ion association extraction systems. In this case, neutral extractable species are formed by the association of ions; it is classified into three subtypes. The first type is characterized by the metal being incorporated into a very large ion that contains a bulky organic group, an example is $Fe(o\text{-}Phen)_3^{2+}$. The second type is termed oxonium extraction system. In this type of ion association extraction system, the formation of an extractable species depends on the action of oxygen-containing organic compounds, such as tributylphosphate which can replace the coordinated water molecules from metal ions. The third type is characterized by the formation of reverse micelles of appropriate high molecular weight surfactants into which metal ions are incorporated. The hydrophobic outer portion of the reverse micelle permits extraction by an organic solvent, while the metal ions at the polar core of the micelle are shielded from the organic solvent.

Solvent extraction phenomena have been known since ancient time. Solvent extraction as a separation technology was known by the 19th century. As early as 1824, it was found that uranyl nitrate could be extracted by diethyl ether; however, it was not of particular interest at that time. This extraction actually involves the formation and extraction of an ion association complex. The great expansion of solvent extraction came after World War II, along with the blooming of nuclear technology and analytical chemistry. During several decades of the development of solvent extraction, the scope has continuously grown. It now includes, for example, studies of complexation chemistry, separation and purification processes, the chemistry of solvents, extractants and diluents, the mechanism of distribution reactions, etc. There is considerable interest in the progress of solvent extraction from both industrial and academic sectors. The dominant interest is in the nuclear energy area.[3]

Solvent extraction has been recognized by analytical chemists as a powerful method of separation since the 1940s. Several comprehensive volumes on solvent extraction in

connection to colorimetric analysis have also been published.[2,4-6] Several standard methods of analysis used in industrial and clinical laboratories routinely utilize extraction followed by colorimetric analysis. Extant literature tabulates a set of comprehensive fundamental data for evaluating solvent extraction and the colorimetric determination of metals. For a specific metal ion to be analyzed, the listing may include colorimetric reagents, the reactions, the nature of the media (e.g., organic extractants), absorption spectra, the extinction coefficient, the range over which Beer's Law is obeyed, the details of the experimental procedure and the possible interferences.[2,4]

1.1.2 "On-Line" Solvent Extraction--Solvent Extraction Flow Injection Analysis (FIA)

In spite of its high selectivity and sensitivity, manual solvent extraction procedures suffer from some significant disadvantages. It is not only tedious and time-consuming but also hazardous. Conventional solvent extraction processes consume a large amount of solvents, most of these are toxic.

"On-line" solvent extraction technology brings opportunities to overcome some problems inherent in conventional solvent extraction procedures. Solvent extraction continuous flow analysis was the first "on-line" solvent extraction system. Although air segmented systems were first to utilize such organic solvent extraction, flow-injection based systems are presently more common. Solvent extraction FIA is usually performed in the microscale range, and it is easily automated. The consumption of chemicals and time is at least an order of magnitude lower, compared with a manual procedure. It also offers other advantages such as high sensitivity and reproducibility, ease of operation, and high sample throughput.[7]

Karlberg and Thelander[8] and Bergamin[9] independently devised the first solvent extraction FIA procedure. The aqueous sample, which can be extracted into the organic phase, is injected into an aqueous carrier stream to which the organic phase is

continuously added. After passing through the extraction coil, the organic phase can be separated from the aqueous phase and carried through the flow cell for continuous measurement.[10] In many cases, it is also possible to perform an optical measurement of the extractant segment without phase separation.[11-13]

The solvent extraction process in such an "on-line" system basically occurs in the extraction coil, e.g., a tubular Teflon® coil. During the extraction process, the extractable species are transported from the homogeneous aqueous phase into the immiscible organic segments through the interface. The interfacial area available for extraction is composed of the menisci between the two phases, and a film surrounding the segments.[14-16] Usually, the liquid with the higher affinity to the tubing material forms the film, e.g., the organic phase in Teflon tubing and the aqueous phase in glass tubing. This film provides additional surface contact between the two immiscible phases. An extractable species diffuses through the interface until extraction equilibrium is reached. The extraction efficiency in the extraction coil is usually high, and the extraction is often complete in several seconds. The degree of extraction is dependent on the residence time of extractable species in the extraction coil. So, the coil length and the flow rate are the two important factors.[17]

As in most flow injection analysis systems, a peristaltic pump is usually used to deliver aqueous and organic streams in such "on-line" solvent extraction systems. An aqueous stream is generated by a peristaltic pump directly; while an organic stream is usually generated by the use of liquid/liquid displacement techniques. In order to maintain segmentation reproducibility of the organic phase, the diameter of the organic phase inlet tubing usually varies between 0.10 to 0.35 mm I.D., depending on the character of the solvent and its flow rate.[10] Although "on-line" solvent extraction FIA procedures consume much less chemicals than a manual extraction, sample and reagent consumption can still be higher than desired, e.g., when very little sample is available and reagents are

very expensive. Miniaturization of the flow systems is, therefore, advantageous. It is not only beneficial for "on-line" solvent extraction systems, but also for other FIA systems. The advantages of miniaturization are obvious: e.g., less waste is generated, less space is occupied, and sample throughput is improved. Super miniaturized FIA systems have been discussed both theoretically and experimentally.[18-20]

1.2 Chemical Analysis in a Silica Capillary Using High Electric Field

1.2.1 Introduction

The popularity of small diameter silica capillaries for performing separations in a high electric field dates from the last decade. In 1981, Jorgenson and Lukacs published the first paper showing the use of a 75 μm i.d. open tubular silica capillary to perform zone electrophoresis.[21] It was apparent that the electrophoresis in small diameter silica capillary tubes offers several exciting advantages, e.g., high separation efficiency, fast analysis, small sample and reagent consumption. Possibilities to perform separations of macromolecules in trace quantities and to develop small-volume separation-based sensors are alluring prospects in the area of analytical biotechnology and beyond.[22]

The key advantage of CZE, as presently performed, is dependent on the use of a small diameter silica capillary tube. Heat dissipation is very efficient in this case. Therefore, a high electric field can be applied, which results in high separation efficiency and a short analysis time. The bulk flow inside the capillary is usually due to the electroosmotic flow. It has a flat profile and is usually strong enough to cause all solutes to elute at one end of capillary.

Capillary electrophoresis (CE) is regarded as the newest of the three major instrumental separation techniques introduced within last thirty years (gas chromatography 1960, and high performance liquid chromatography (HPLC) 1970).[23] Many researchers

are involved in the development of this new technique. Books, reviews and a large number of papers have been published in recent years.

Although most publications concerning chemical analysis using capillary-high electric field systems are directly or indirectly focused on separation, several extant papers describe some new concepts or new approaches of utilizing such systems. Regnier and co-workers introduced a type of reaction-based chemical analysis using capillary electrophoresis systems, termed electrophoretically mediated microanalysis. By using different electrophoretic mobilities of charged species, spatially distinct zones of chemical reagents can be electrophoretically merged under the electric field.[24,25] Liu and Dasgupta reported that the electroosmotic flow induced by high electric field in a 75 μm bore fused silica capillary can be used as the miniaturized pumping mechanism for flow injection analysis.[26,27]

1.2.2 Elements of a Capillary Based High Electric Field Analysis System

1.2.2.1 Sample Injection

Three categories of sample introduction technique are often used: pressure differential sample introduction; electromigrative sample introduction; other approaches to sample introduction, e.g., split flow injection, sample loop injection.

There are three main techniques of creating a pressure differential. The first one is gravity injection. The sample vial is raised to a certain height above the receiving vial at the other end of capillary. A hydrostatic pressure is created by the weight of liquid in the height difference Δh of the raised capillary. The sampling rate $S_{(\Delta h)}$ [cm/s] is defined as:

$$S_{(\Delta h)} = (\rho g r^2 \Delta h) / (8 \eta L_t), \qquad (1.1)$$

where ρ is the electrolyte density [g/ml], r is the capillary internal radius [cm], g is the acceleration due to gravity, η is the viscosity of water at 20°C [poise], and L_t the total length of capillary [cm].[28] The second method for creating a controlled hydrodynamic flow of sample into the capillary is pressurizing the sample vial. The sample vial to which Δp is directly applied is hermetically sealed. The sampling rate $S_{(\Delta p)}$ [cm/s] is defined as:

$$S_{(\Delta p)} = (\pi r^2 \Delta p) / (8\eta L_t), \qquad (1.2)$$

where Δp is the pressure differential [$g/(cm \cdot s^2)$]. The third method applies vacuum to the electrolyte vial at the opposite end of capillary to introduce the sample. The major drawback of pressure differential sample introduction is the dependence of the process on sample viscosity.[28]

As a method for sample introduction, electromigration is unique for CE systems. It applies a voltage across the sample vial and the destination vial, therefore sample analytes migrate into the capillary. Since different sample analytes have different electrophoretic mobilities, they move into the capillary with different velocities. So the injected sample is different from the original sample, this is called "bias of electrokinetic injection."[29]

Hydrodynamic and electromigrative procedures are the most frequently used routine sampling methods in CZE. There are some supplementary injection methods which satisfy different sampling requirements. Split-flow sample introduction is one such method.[30,31] An HPLC-type syringe is connected to a split-vent tubing and a perpendicularly positioned capillary tubing. The volume (V_c) introduced into the capillary is defined as:

$$V_c = (d_c/d_s)^4 (L_s/L_t) V_{inj}, \qquad (1.3)$$

where d_c and d_s are the capillary and venting tube diameters, respectively, L_s is the length of venting tubing, L_t is the total capillary length, V_{inj} is the volume injected from the HPLC syringe. The advantage of the split-flow design is that small sample injection is achievable and any movement of capillary is avoided during the injection. The disadvantage of split-flow sampling is: any possible obstruction of the flow in the venting tubing or in the capillary can distort the ratio of hydrodynamic resistance and lead to poor reproducibility of the actual sample volume introduced into the capillary.[32]

Another supplementary sample injection design is rotary valve injector. Rotary injectors are widely used in HPLC. If metallic parts of such a valve come in contact with the electrolyte in a CE system, bubbles are generated.[33] Loop injectors with wetted parts made from nonreactive polymers are now commercially available. The injection procedure is the following: first the sampling tubing is connected to a cylindrical cavity inside the injector which defines the volume of the sample (typ. $\leq$60 nl), then rotate the valve 90 degrees, the sample volume inside the rotor is now placed in line with the capillary.[33] The advantage of the valve injector design is that it overcomes drawbacks inherent in hydrodynamic and electromigrative injection procedures. However, the major limitation of such an injector is the lower limit of the sample volume that can be introduced.

In this laboratory, a special valve injector was designed.[66] The sample stream, brought in/out by capillaries C_3 and C_4 is perpendicular to the two main capillary segmants C_1 and C_2 at their joint (see Figure 1.1). Normally C_1 is butt-joined to C_2. When C_2 is moved away from C_1 by a pneumatic actuator, a space is created by C_1 and C_2 and the sample is automatically drawn into this space. Now if the liquids to C_3 and C_4 are shut off and the capillary C_2 is returned back to the original position, the sample introduced into the joint space previously created is forced to go into the C_1/C_2 conduit. A screw on the stationary block holding C_1 allows the adjustment of the displacement of the capillary in a microscale fashion. Thus it is feasible to vary the injection volume with

such a valve. The relative standard deviation (RSD) for repeated injections is lower than 2% ($n \geq 8$, see Figure 1.2). Several modifications of this basic design were explored and further details are given in Appendix A.

1.2.2.2 Capillary and Electrolyte Vials

The capillary used is polyimide coated fused silica capillary. The inner diameter is usually between 10 to 100 μm, the outer diameter is between 300 to 400 μm. The two most important U.S. suppliers of fused silica capillaries are Polymicro Technologies, Inc., Phoenix, Arizona, and Scientific Glass Engineering, Inc., Austin, Texas. The narrow diameter of the capillary and the good thermal conductivity of silica facilitate the dissipation of heat generated by the electric resistance of the electrolyte inside the capillary. The polyimide coating increases the physical strength and the flexibility of the otherwise fragile silica capillary. In order to overcome hysteresis effects, a new capillary is usually pretreated with concentrated NaOH followed by washing with water.

Both ends of the capillary are immersed in suitable electrolyte solutions during operation when the high voltage (HV) is applied. Each electrolyte vial contains an electrode, one is connected to HV and the other to ground of the HV supply. Typically the receiving vial has the ground electrode. In our experiments, the electrolyte carriers used are the same as those usually used in CE systems. A frequently occurring problem in CE analysis is caused by air bubbles trapped inside the capillary. The presence of air bubbles leads to fluctuation of the baseline in the electropherograms and even disconnection of the electric field. This problem can be solved by degassing the carrier electrolyte solutions with sonication and flushing the capillary with freshly degassed carrier. Another important requirement is to place the two electrolyte vials at exactly the same height, in order to prevent hydrostatic flow.

1.2.2.3 High Voltage Power Supply and Controller

The high voltage required in this system is provided by a regulated direct current power supply. The maximum value of high voltage is 30 kV, and the maximum value of current is usually below 500 μA. The main reason for limiting maximum current is due to safety considerrations. Also, while silica has a relatively good thermal conductivity, it can not dissipate all the heat generated at very high currents. Overheating leads to boiling of the electrolyte solution in the capillary.[22]

The high voltage power supply and controller usually have provisions for choosing positive or negative polarity of the high voltage. Different modes of operation, e.g., constant-voltage mode, constant-current mode, are also usually available.

1.2.2.4 Detector

There are several detection methods for capillary systems, such as UV/visible absorbance detectors, fluorescence detectors, mass spectrometric detectors, amperometric detectors, conductometric detectors, radiometric detectors, Raman-scattering based detectors, and refractometric detectors. Several performance criteria, e.g., sensitivity, selectivity, linear range, and signal-to-noise ratio, have to be considered for the choice of the appropriate detector for a given application. Since the UV/visible detection method is the simplest and the most common method, and most of the work described in this thesis is based on this kind of detection, the following discussion focuses solely on UV/visible detectors.

Most of the commercially available capillary electrophoresis systems are equipped with UV/visible detectors. Several companies also offer accessories to change a HPLC detector for use with capillary systems. "On-column" UV/visible detection minimizes extracolumn dispension problems. To enable light to pass through the capillary, the polyimide coating on the detection window must be removed first. It is usually burned off

by a butane lighter, either directly or by using hot concentrated H_2SO_4. The exposed segment of the fused silica is then inserted into the light path of a photometric detector and properly aligned and fixed in place. The incident light beam, typically focused by a sapphire ball lens, passes through the capillary perpendicularly and reaches a photodiode detector. The sensitivity of on-column detection is usually low due to the extremely short light paths, ≤ 100 μm. The first approach to improve detection sensitivity is by expanding the path lengths of the optical cell. Bubble cells[34], U cells and Z cells[35-37] have been introduced, accordingly. The optical paths can be expanded by using different cell geometries as described above.

In this laboratory, the optical path has been expanded, in a manner similar to bubble cells, by connecting a small piece of larger diameter capillary as the detection window directly to the separation capillary.[38] The observed sensitivity is often increased by a factor more than the ratio of the two diameters. This extra increase in sensitivity is credited to diminution of stray light in the large capillary system. Rectangular capillaries were introduced by Tsuda[69] et al., for increasing detection sensitivity. Such cells have been tested in our laboratory.[39] The longer dimension of the cross section is used as the optical path, the sensitivity is improved accordingly by the appropriate factor. However, our experience is that separation efficiency in these capillaries (50 μm × 500 μm or 50 μm × 1000 μm cross section) is much lower than that of the 75 μm inner diameter round silica capillaries whether due to difficulties in introducing as a sufficiently small amount of sample or due to inefficient heat dissipation. In addition, initial experiments were done with uncoated glass capillaries. Their extreme fragility makes it difficult to align and fix the capillary in the detector. A rectangular geometry also makes it difficult to perform simple tasks such as flushing with a syringe. This is nontrivial since homemade instrumental set-ups usually do not contain pneumatic flushing arrangments.

Another approach to increase optical path length is to make a light beam travel several times through a relatively narrow segment of a modified fused silica capillary. A multireflection cell is prepared as the follows: about 1 cm polyimide coating is burned off to create a transparent window; a silver layer is deposited on that window by the redox reaction of $Ag(NH_3)_2^+$ and glucose; the silver coating is protected by a layer of black paint; two 0.35 mm wide apertures are created 0.8 mm apart on the silvered window. A laser beam is focused at a certain incident angle through one aperture, and detected at the other aperture. Note that this type of multireflection cell can only work effectively with a coherent light source.[40]

In this laboratory, we have also studied multireflection detection in a capillary system using the cell as an etalon as originally outlined by Dasgupta.[41] Conventional light sources can be used, a laser source is not necessary. The detection cell is prepared as follows:[67] a small portion of polyimide coating is burned off to expose a transparent segment of capillary; make ~75% of the capillary surface a perfect mirror (~100% reflectivity), and ~25% of the surface a partial mirror (95% reflectivity, 5% transmissibility) by physical deposition of different thicknesses of aluminum in a vapor deposition apparatus; a small aperture (<150 μm) is made on perfect mirror side through which light is introduced; a photodiode is coupled to the partial mirror side (see Figure 1.3). The incident light beam is multireflected inside the capillary and the overall device behaves as a nonlinear absorbance amplifier. Although significant absorbance enhancements were observed in the initial planar test cell format, this gain could not be realized in the tubular capillary format, further details are given in Appendix B.

1.2.2.5 Data-Processing System

Several types of data-processing systems are available, e.g., chart recorders, integrators and appropriately equipped personal computers (PC). All of these satisfy an

user's general requirements for recording detector responses in a CZE system. However, PC-based data acquisition systems display significant advantages over the other systems, including convenient data management, data transformation, carrying out routine automatic analysis, etc.. Typically commercial CE instruments are supplied with PC-based data acquisition systems as options.

1.2.3 Electroosmotic Flow

Electroosmotic flow is the electrokinetic phenomenon involving interactions between a charged surface in contact with an ionic electrolyte solution.[42]

Figure 1.4 schematically shows how the polarity of the surface charge determines the direction of the electroosmotic flow. There are usually two types of species in the immediate vicinity of the negatively charged capillary wall: water molecules with oriented dipoles and hydronium cations. Since only a small portion of negative wall charges is compensated by the two above species, the wall is still left with a number of negative charges without any positive counterparts in this vicinity. Thus, a negative zeta potential is created. This overall negatively charged wall is counterbalanced from a larger distance by a corresponding number of cations. There are two regions of liquid next to the solid interface: first, the relatively rigid inner Helmholtz layer, next to the wall; second, the more diffuse and less organized outer Helmholtz layer, a little farther from the solid-liquid interface. If both Helmholtz layers are formed and oriented in an electric field, it is possible to induce a movement of less tightly attached hydronium and other cations in the outer Helmholtz layer toward the cathode. Since the cations are interlocked with water molecules, their movement creates the whole bulk flow, termed electroosmotic flow.[43,47] Because of the unusual nature of driving force, the profile of electroosmotic flow is different from that of hydrodynamic flow (Figure 1.5). The magnitude of electroosmotic flow can be calculated according to the Smoluchowski equation:[44]

$$v_{eof} = -(\varepsilon\zeta/\eta)E, \qquad (1.4)$$

where ε is the dielectric constant of the electrolyte, ζ the zeta potential [V], η the viscosity [Poise], and E the applied electric field [V/cm].

The generation of electroosmotic flow in a silica capillary is dependent on its surface silanol groups dissociated in aqueous solution. The pKa value of the dissociation equilibrium shown below is ~7.7:[70]

$$(OH)_3Si\text{-}OH = (OH)_3Si\text{-}O^- + H^+. \qquad (1.5)$$

Therefore, in pure water or neutral-to-alkaline solution, fused silica shows a negative value of zeta potential. The absolute value of the potential is dependent on the number of dissociated silanol groups, and increases with pH accordingly. By about ~pH 2, the dissociation of all surface silanol groups is completely suppressed, the value of the zeta potential is close to zero, the electroosmotic flow also approaches zero. Below pH 2 the silica surface exhibits a positive charge:

$$(OH)_3Si\text{-}OH + HX = (OH)_3Si\text{-}OH_2^+ + X^-, \qquad (1.6)$$

so, the zeta potential is positive. The zeta potential for silica capillary can be manipulated by other means as well.[45-51]

1.3 Electrochemical Processes at the Interface Between Two Immiscible Electrolytes

The investigation of electrochemical processes at the interface between two immiscible electrolyte solutions is essential to understand processes occurring in an ion exchange membrane as well as ion transport phenomena in biological systems.

Nernst carried out pioneering research in this area at the beginning of this century and suggested that the proportion of cations and anions carrying charges across the interface can be measured experimentally. Assume that at the water/organic solvent phase boundary (w/o), an equilibrium exists between a particular cationic species I in both phases. The equilibrium potentials at the interface can be described by:

$$\Delta_o^w\varphi = \Delta_o^w\varphi_i^\circ + RT / Z_iF \ln(a_i(o) / a_i(w)). \qquad (1.7)$$

This is the general form of Nernst equation, where $\Delta_o^w\varphi$ is the difference of inner electric potentials between the two phases, $\Delta_o^w\varphi_i^\circ$ is the difference of standard electric potential of species I in two phases, Z_i is the magnitude of charge on species I, and a_i is the activity in both phases. The Gibbs free energy for phase transfer (ΔG_{tr}°) can be calculated using the Nernst equation.

Next, consider a uni-uni valent salt A^+B^- in a distribution equilibrium between the water phase and organic phase. We have:

$$\Delta_o^w\varphi = [-\Delta G_{tr}^\circ{}_{B^-}{}^{o\to w} + RT / \ln(a_+(o) / a_+(w))] / F + [\Delta G_{tr}^\circ{}_{A^+}{}^{o\to w} - RT / \ln(a_-(o) / a_-(w))] / F. \qquad (1.8)$$

For a dilute solution, $a_+(o) \approx a_-(o)$ and $a_+(w) \approx a_-(w)$, the distribution potential is:

$$\Delta_o^w\varphi_{distr} = (\Delta G_{tr}^\circ{}_{A^+}{}^{o\to w} - \Delta G_{tr}^\circ{}_{B^-}{}^{o\to w})/F. \qquad (1.9)$$

If both the cation and the anion have the same hydrophobicity or hydrophilicity, then $\Delta_o{}^w\varphi_{distr} = 0$. If the cation is more hydrophobic than the anion, $\Delta G_{tr}{}^\circ{}_{A^+}{}^{o\rightarrow w} < \Delta G_{tr}{}^\circ{}_{B^-}{}^{o\rightarrow w}$, then $\Delta_o{}^w\varphi_{distr}$ is negative.[52]

Nernst theory is reflected directly in the charges in the electric double layer formed at such interfaces. For example, if the cation is more hydrophobic than the anion, it tends to cross the interface to move into the organic phase; while the anion tends to stay in the aqueous phase. Bulk transfer across the phase boundary does not occur. So, both ions remain at the interface of two immiscible solutions and form the charged envelopes of the electric double layer. In this context, it may also be useful to mension that the term facilitated transport, used in membrane science, denotes mass transfer across a membrane when such transfer is enhanced by a chemical reaction in the receptor phase.[53] Facilitated ion transfer is also observed in the cases of transfer between two electrolytes contained in two immiscible phases.[54]

Potential-sweep voltammetry is the main technique used for studying electrolysis phenomena at the interface between two immiscible electrolytes.[55,56] The basic component of the experimental arrangement is a four electrode potentiostat. It is capable of imposing a programmed potential difference at two Luggin capillaries with tips placed close to the interface. A number of other methods have also been applied to investigate the electrolysis at the interface between two immiscible electrolytes, e.g., chronopotentiometry,[57] polarography with dropping electrolyte electrode,[58] faradaic impedance measurement,[59] current scan voltammetry,[60] etc.. Alkali metal ions, tetraalkylammonium cations, choline, acetylcholine, picrate, perchlorate, iodide, thiocyanate, nitrate, dodecylsulphate, and cationic forms of various tetracycline derivatives have been studied with their transportation properties across the interface of two

immiscible electrolytes. Facilitated ion transfer has also been studied for alkali and alkaline earth metal ions. Ionophores facilitate the metal ions transfer in these cases.[61,62]

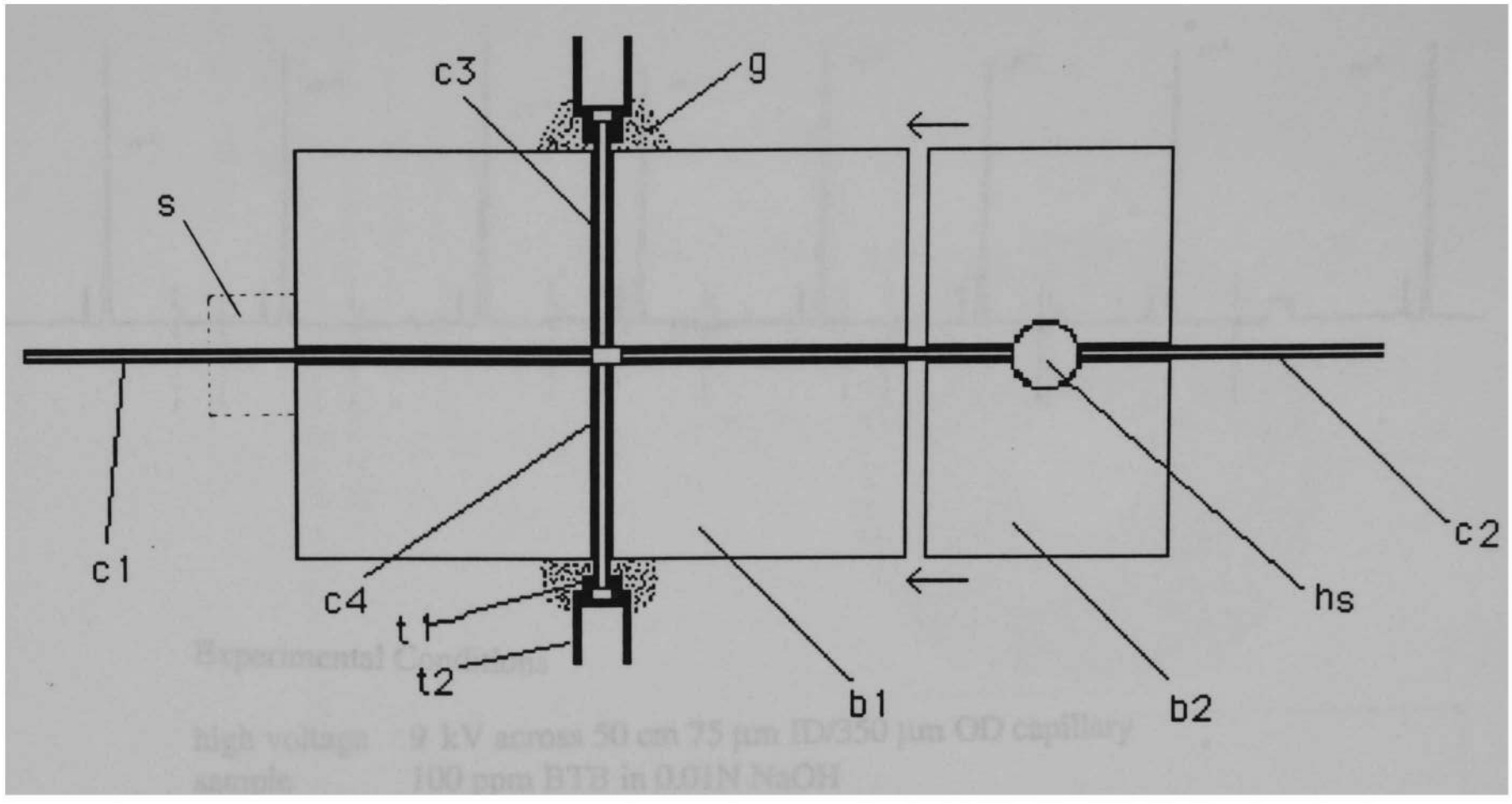

b1, b2	Plexiglas blocks	t1	Polyvinyl Chloride (PVC)
c1, c2	75 µm ID / 350 µm OD electrophoresis capillaries	t2	Teflon tubing
c3, c4	250 µm ID / 350 µm OD sampling capillaries	g	glue
hs	hole for screw to fix c2	s	screw for adjusting capillary displacement

Figure 1.1 First Version of the Valve Injector.

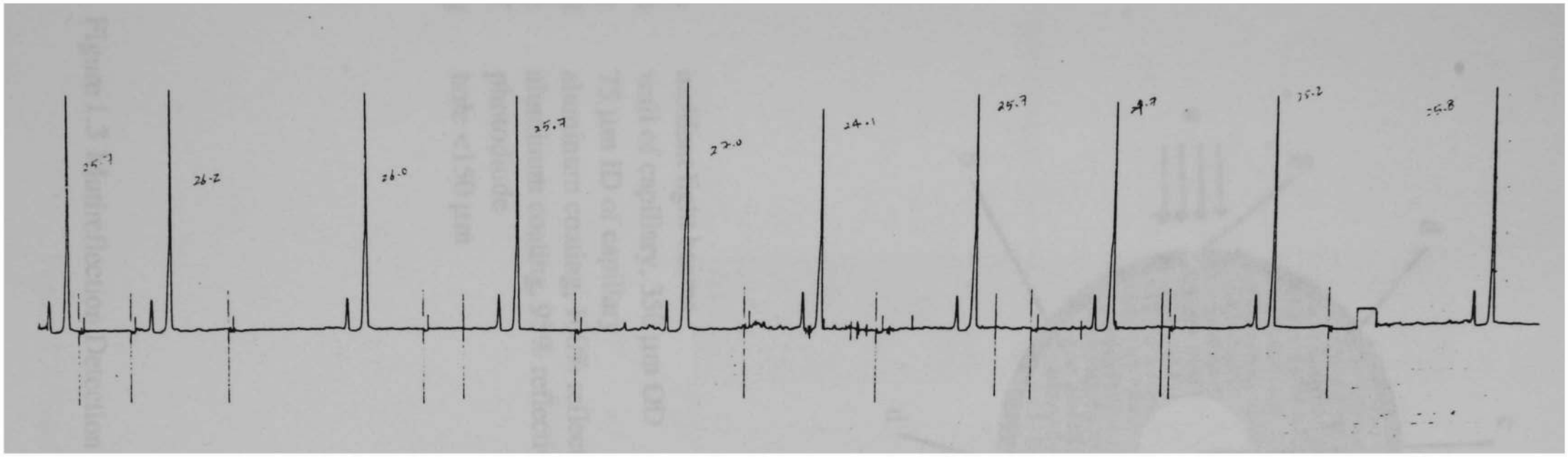

Experimental Conditions

high voltage	9 kV across 50 cm 75 µm ID/350 µm OD capillary
sample	100 ppm BTB in 0.01N NaOH
electrolyte	2 mM $Na_2B_4O_7$
detector	LED-605 nm, silicon photodiode, log ratio amplifier
full scale	0.1 AU
paper speed	60 mm / hr.

Figure 1.2 Results from the First Version Valve Injector .

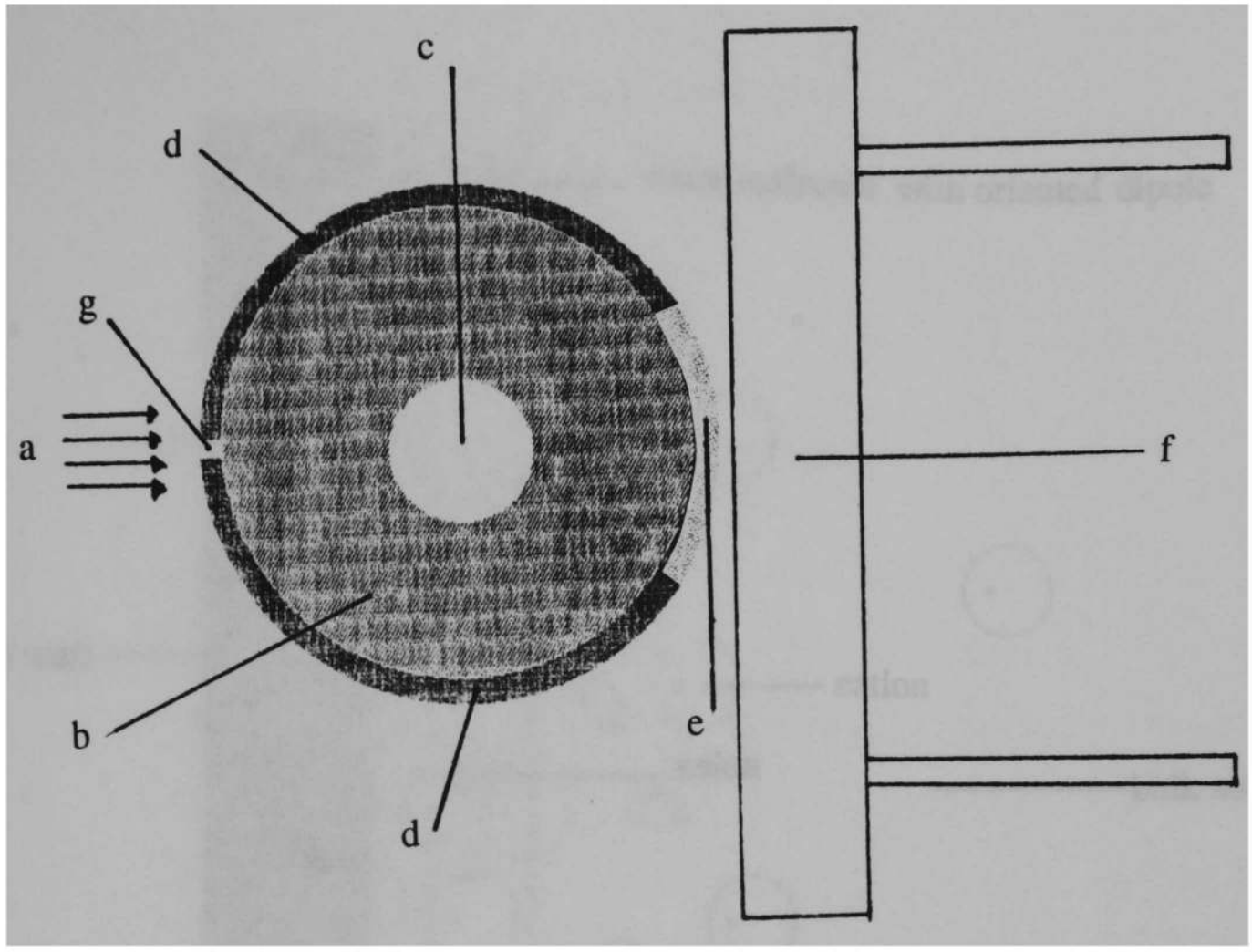

a incident light beams
b wall of capillary, 350 μm OD
c 75 μm ID of capillary
d aluminum coating, 100% reflectivity
e aluminum coating, 95% reflectivity 5% transmissibility
f photodiode
g hole <150 μm

Figure 1.3 Mutireflection Detection in Capillary System Using Conventional Light Beams.

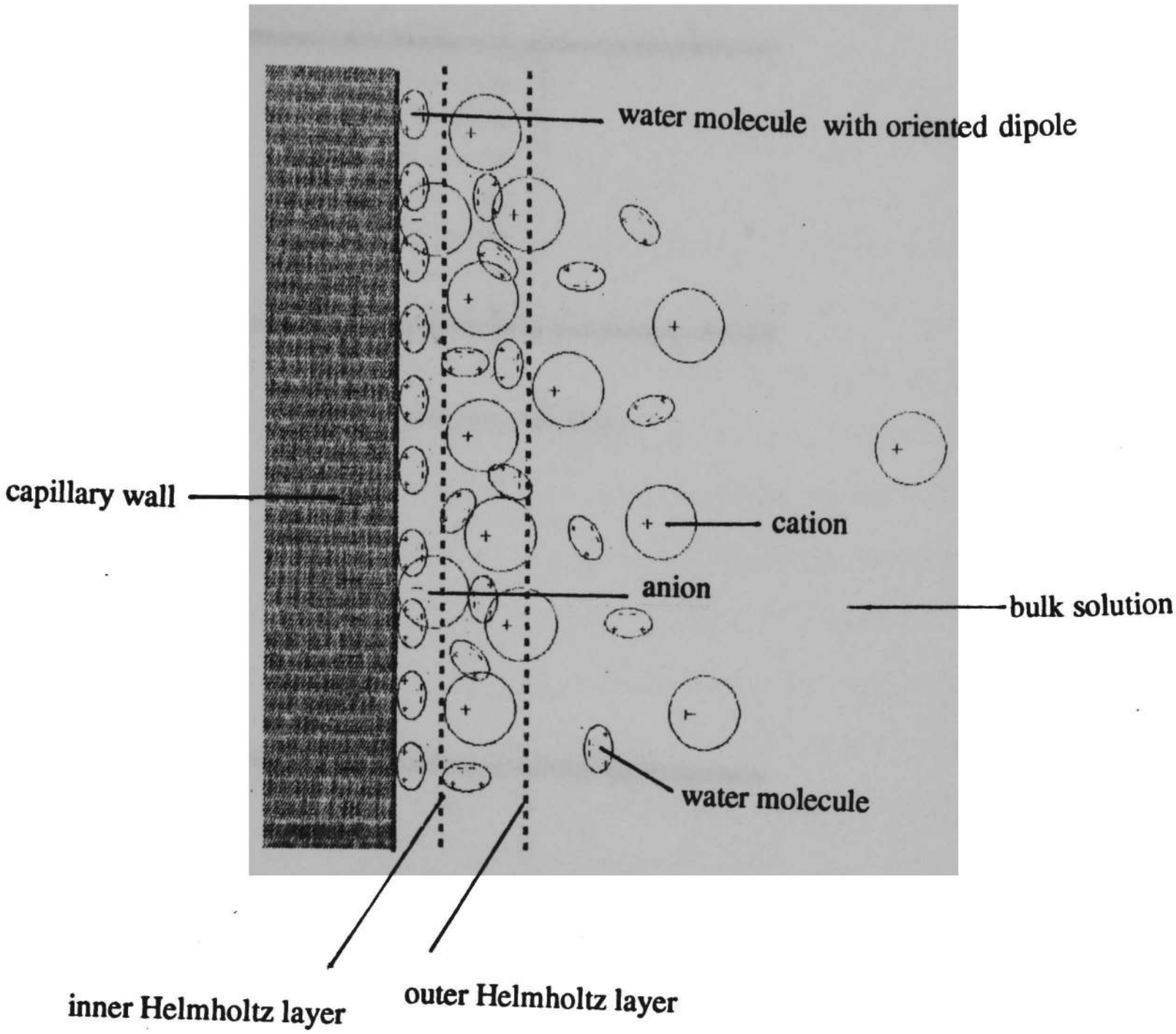

Figure 1.4 Electrical Double Layer.

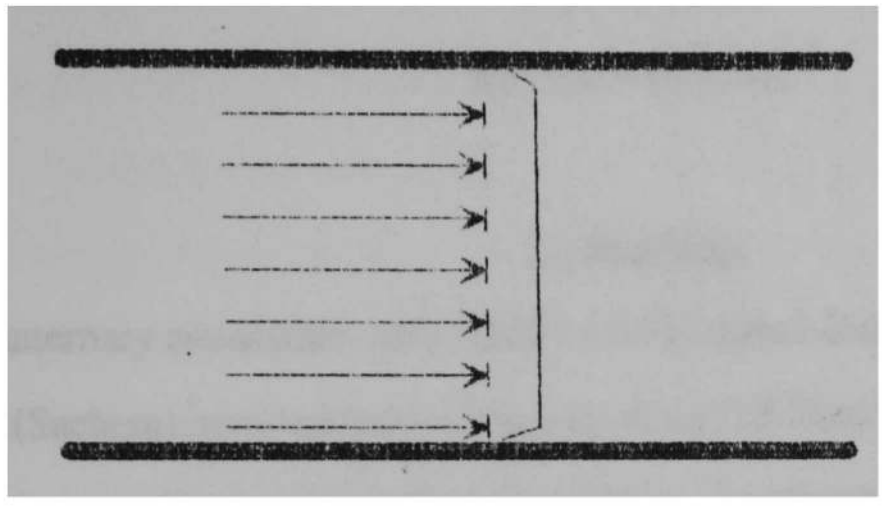

(a) Electroosmotic Flow.

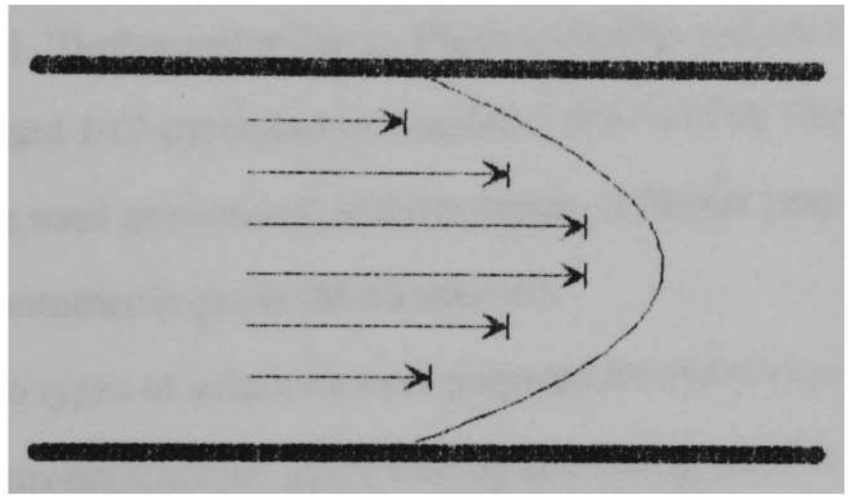

(b) Hydrodynamic Flow.

Figure 1.5 Flow Profiles.

CHAPTER II

EXPERIMENTAL

2.1 Reagents

Quaternary ammonium salts (QAS) used included tetrabutylammonium perchlorate (TBAP) (Sachem); tetrabutylammonium bisulfate (TBABs) (Aldrich), tetrabutylammonium bromide (TBAB) (Aldrich), tetrabutylammonium iodide (TBAI) (Aldrich), tetraethylammonium perchlorate (TEAP) (Aldrich), tetrapropylammonium perchlorate (TPrAP) (Alfa Products), tetrapentylammonium bromide (TPAB) (Aldrich), tetrahexylammonium bromide (THAB) (Aldrich) and tetraoctylammonium bromide (TOAB) (Aldrich). Extractable dyes used included Eosin Y (Baker) and Crystal Violet (Logical Stain Co.). Chelating reagents used included 4-(2-pyridylazo)-resorcinol (PAR) (G.F.S.), 1,10-phenanthroline (o-Phen) (Aldrich), sodium diethyldithiocarbamate (DEDC) (Fisher), and 1-(2-pyridylazo)-2-naphthol (PAN) (City Chemical Corp.). All reagents used were used as received, without drying or further purification. Chloroform used was spectrophotometric grade (Mallinckrodt).

Two types of solutions were prepared for every experiment. One was an aliquot of 1 ml spectrophotometric grade $CHCl_3$ containing variable amounts of quaternary ammonium salt. The second was a 2 mM $Na_2B_4O_7$ solution with and without ppb to ppm levels of extractable species, e.g., dyes, metal chelates. The pH of the borate solution was ~9.2.

2.2 Apparatus

Two 1.5 ml capacity micro centrifuge sample vials were located on a rotatable turret (see Figure 2.1). One vial contained the aqueous sample; the other vial held the QAS containing organic solvent. Polyimide coated silica capillary c (~50 cm in length, 75 μm

I.D./350 μm O.D.; Polymicro Technologies, Phoenix, AZ) could be moved by two pneumatic actuators for dipping/lifting into/from individual vials. The anode electrode, a 0.25 mm diameter Pt-wire, was affixed to the turret end of capillary. The polyimide coating was removed at a distance of ~40 cm from the turret end of capillary for a space of ~1 cm. The exposed window is aligned and fixed onto a photometric detector equipped with ball lenses for the use with capillaries (Linear Model UVIS 200 / Spectra-Physics). The capillary itself thus constitutes the radial path detector cell. The far end of the capillary went to the cathode vial containing the same running electrolyte as the anode vial, 2 mM $Na_2B_4O_7$. Except as specifically mentioned, it is typically placed at the same height as the source vial. The high voltage power supply and a control module for adjusting operating mode, voltage magnitude and polarity is built from CZE 1000 PN30 Modules (Spellman, Plainview, NY). All instrument functions, including sampling, could be automated through a programmable micro controller (LS-100, Minarik Electric, Los Angeles, CA). The digital outputs of the DAS-12 data acquisition board and supplied software (Analogic Corporation, Wakefield, MA) were used for initiating the collection of the data. A strip chart recorder (OmniScribe, Austin, TX) was also used.

2.3 Experimental Protocol

The following steps are typically practiced for analysis: (a) rinse the capillary with 50 μL electrolyte solution containing the extractable analyte; (b) dip the capillary into the organic sample vial and apply high voltage (+15 kV) for 10 seconds, the measured sample introduction rate is 12 ± 1.5 nl/s; (c) lift the capillary, rotate the turret and dip the capillary into the aqueous running electrolyte vial; (d) apply high voltage, e.g., +15 kV, until the organic segment passes through the detector; (e) repeat steps a - d as many times as desired.

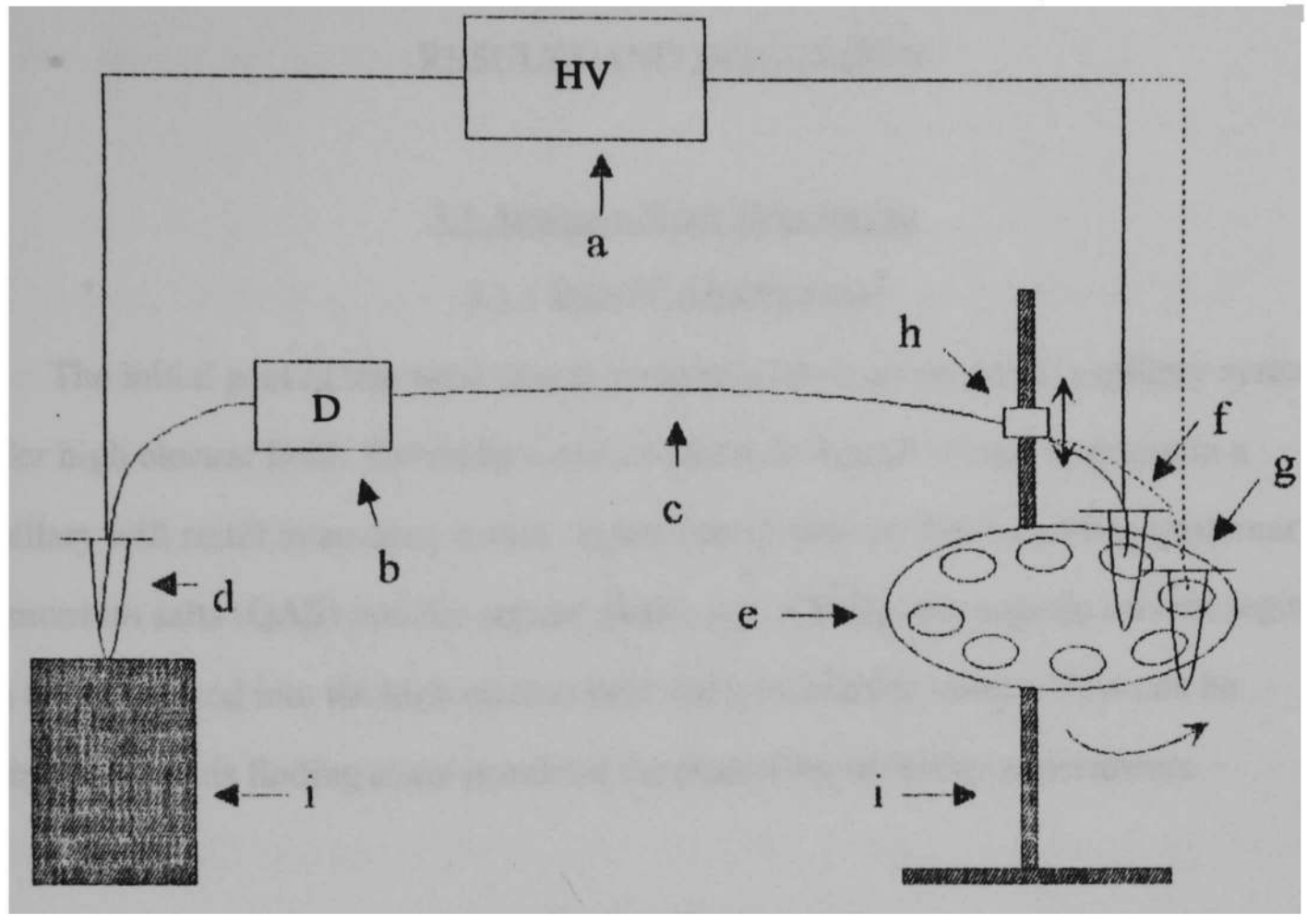

a high voltage supply
b LINEAR UVIS 200
c capillary 75 µm ID/350 µm OD
d cathode vial, 2 mM sodium borate rotable turret
f aqueous sample vial
g organic sample vial
h pneumatic valve for vertical movement of capillary
i support

Figure 2.1 Experimental Set-up.

CHAPTER III

RESULTS AND DISCUSSION

3.1 Aqueous Blank Experiment

3.1.1 Initial Considerations

The initial goal of this work was to perform solvent extraction in capillary systems under high electric field. Normally a non-conductive organic solvent segment in a capillary will result in an open circuit. It was found early on that by adding quaternary ammonium salts (QAS) into the organic phase, e.g., $CHCl_3$, the organic solvent segments can be introduced into the high electric field and a reasonable current flow can be maintained. This finding alone permitted the possibility of further experiments.

3.1.2 Output Characteristics

Several concentration and extraction systems of aqueous-organic solutions have been studied and are discussed in this thesis. It is best to start with characterizing the output of a blank, i.e., a sample containing no extractable analyte. So the response recording of the system when a blank sample is injected is merely due to the organic segment passing through the detector. The organic segment contains no extracted analyte and this then represents the system background.

This background output is shown in Figure 3.1. A negative rectangular pulse is produced as the organic segment passes through. Such output is early understood from a ray tracing diagram (Figure 3.2). The refractive index of $CHCl_3$ (n_D 1.444) is much closer to the refractive index of the silica conduit (n_D 1.46) than is that of the aqueous phase (22 C°, n_D 1.333). Consequently, reflection losses at the silica/solvent and the solvent/silica interfaces are much lower when the organic segment passes through. In addition, the total divergence of the exit beam is less when the intervening medium is $CHCl_3$. If the

absorbance of aqueous phase is set as the base line having zero absorbance, the organic segment predictably shows negative absorbance.

3.1.3 Output Reproducibility

Figure 3.3 shows a typical output resulting from repeated injection of QAS containing $CHCl_3$. The aqueous solution is 2 mM $Na_2B_4O_7$ pH 9.2; the organic sample vial contains 0.1 g/ml TBAP in $CHCl_3$. The relative standard deviation (RSD) of the retention time is 0.51%; while the RSD of the peak width is 1.72% (n = 13). The retention time and the amount of organic phase injected are obviously quite reproducible.

Quaternary ammonium salts available in this laboratory other than TBAP were also tested at the 0.29 M concentration (equi-molar concentration as 10 w/v % TBAP) with the exception of TEAP and TPrAP which do not dissolve sufficiently in $CHCl_3$. With these latter salts, stable operating conditions are not obtained. With TBABs, TBAB, TBAI, TPAB and THAB, the retention time of the organic segment was essentially the same as that with TBAP.

The effect of the concentration of the QAS was also studied with TBAP. The results show that the retention time of the organic segment does not vary significantly with the TBAP concentration for [TBAP] = 0.05, 0.1, 0.2, 0.3, 0.4 g/ml $CHCl_3$.

3.1.4 Mechanism of the Movement of the Organic Segment Under High Electric Field

3.1.4.1 Driving Force--Electroosmotic Flow

How does the organic segment migrate with such a reproducible retention time? The rate of movement of the organic segment is essentially the same as the bulk electroosmotic flow produced in the absence of any organic segment. There is little doubt therefore that the bulk electroosmotic flow generated by the capillary wall in contact with

the aqueous electrolyte is responsible for the movement of the organic segment under electric field.

As mentioned in Chapter I, there are two motive forces for migration in a silica capillary under high electric field. One is electroosmotic flow, the bulk flow of liquid due to the effect of the electric field on counterions adjacent to the charged capillary wall. The other is electrophoretic movement, this is the migration of charged species to the oppositely charged electrode under an external electric field. Under our experimental conditions, e.g., 2 mM borate buffer, pH 9.2, the electroosmotic velocity of the bulk solution is much greater than the electrophoretic velocity of any individual ion.

Since $CHCl_3$ is hydrophobic and the silica surface is hydrophilic, it is reasonable to expect that there exists an aqueous film between the organic segment and the wall of capillary. Such a film would be particularly likely in the presence of a QAS--it would distribute itself between the organic segment and the aqueous film with the orientation of the hydrophobic cation and the counterion at the interface helping to stabilize the aqueous film between the organic segment and the silica capillary. After the organic segment is introduced and high voltage is applied across the whole capillary, the existence of the film maintains the continuity of the electric double layer, provides a passage for charge transport and the continuity of the electroosmotic flow.

Support for this hypothesis is provided by a number of experimental observations. In one experiment, two capillary segments are connected by PVC tubing and with several millimeters of the PVC tubing is exposed internally at the joint. As long as a purely aqueous electrolyte solution is used and high voltage is applied, current readings and electroosmotic flow are both stable. When a QAS-containing organic segment is injected, the circuit becomes open as soon as the organic segment reaches the exposed PVC tube. As soon as the organic segment reaches the hydrophobic PVC conduit, there is no affinity for the wall to maintain an aqueous film and the aqueous film surrounding the segment

disappears. In the absence of an electric double layer at the wall, the effective resistance of the zone containing the organic segment is dramatically increased. Most of the voltage now appears on this zone and overheating results in bubble production in the segment leading eventually to circuit disconnection.

In a second experiment, the silica capillary was filled with QAS-doped $CHCl_3$; and a marker such as an aqueous electrolyte segment or a colored compound, e.g., diphenylthiocarbazone dissolved in $CHCl_3$, was injected by gravity; high voltage was then applied. The current readings were stable but no flow was observed. The above experiment was also conducted using transparent hydrophobic capillary tubing of fluorinated ethylene propylene (FEP) copolymer. Since the FEP material is transparent, it could be clearly seen that there is no migration of the marker inside the tubing. In both cases there is no conducting double layer at the wall and thus no net flow.

3.1.4.2 Function of the Quaternary Ammonium Salts

3.1.4.2.1 Ion Transport Through the Organic Segment under electric Field

The dissolved QAS in the organic segment may play another role beyond maintaining an aqueous film between the organic phase and the capillary wall. If there are no QAS compounds in an organic segment that is introduced by gravity, an open circuit occurs essentially within 10 seconds of applying the high voltage. The QAS concentration must have some minimum value for stable and continuous operation. For TBAP, a concentration of 0.05 g/ml $CHCl_3$ is minimally needed.

Ion transport can occur from the QAS loaded organic segment in two different ways. First, in addition to the leakage of the QAS as a whole at both ends of the segment into the aqueous phase, it is possible for the unpaired quaternary ammonium cation (Q^+) to migrate from the organic phase towards the cathode and an equivalent amount of the anionic constituent of the QAS (X^-) to similarly migrate towards the anode. Second,

cationic and anionic constituents of the aqueous electrolyte can in principle enter the organic phase causing the exodus of an equivalent amount of Q^+ and X^- respectively from the opposite ends of the segment. Because of the very low polarizabilities of either Na^+ or $B(OH)_4^-$ (the form in which borate exists in aqueous solution), is poor (these are "hard" acid/bases), the second pathway may not be very important.

It is not clear as to how much of the charge transport across the organic segment zone occurs by ion transport through/from the segment itself, relative to that through the aqueous film. An experiment was conducted in which a PVC capillary containing two metallic electrodes separated by ca. 40 μm was put in just prior to the grounded (cathode) end of the capillary. (This is essentially a bifilar wire conductance cell developed by others in this laboratory, supplied courtesy of Dr. S. Kar.) The voltage across the two metallic electrodes was measured to assess the field strength in a given zone as it passes through the probe. It was found that the field strength in the zone containing the 10% TBAP doped $CHCl_3$ is ~5 times greater than the aqueous 2 mM $Na_2B_4O_7$ electrolyte. For an electric field that is five times greater, a proportionately smaller cross section for transport is adequate to maintain a steady state of charge transport across the segment. For a capillary of 75 μm bore in which a t μm thick film surrounds the organic phase, geometric considerations readily indicate that the aqueous film cross section is 20% of that of the capillary cross section when t is 7.5 μm. In other words, for a 7.5 μm thick aqueous film around a 60 μm diameter organic segment, transport through the aqueous film alone is sufficient to maintain the steady state current. The exact aqueous film thickness is unknown.

Leakage of the QAS from the organic segment is readily apparent from the temporal current profile shown in Figures 3.4 and 3.5. A quantitative understanding can be gleaned as follows. The measured specific conductance ρ of a 2 mM $Na_2B_4O_7$ solution is

~300 μS/cm. Consequently, the electric resistance R of a 50 cm long 75 μm bore. (cross section 4.42×10^{-5} cm^2) capillary is readily calculated from:

$$R = L_t/(A\rho). \tag{3.1}$$

Thence the current following in the circuit when 15 kV is applied is given by:

$$i = (15{,}000A\rho) / L_t, \tag{3.2}$$

and substitution of the numerical values given above yields i = 4 μA, in reasonable agreement with the starting current values of 4.3 μA observed in Figures 3.4 and 3.5.

We hypothesize that as the organic segment is introduced, the aqueous film around it is first initially thicker and then decreases to a steady state value as the movement is fully established. At this point, the resistance represented by the organic zone is maximum and the overall current value is minimum. At an organic solvent introduction rate of 12 ± 1.5 nl/s a 10 s introduction results in a 120 ± 15 nl segment, in a 75 μm capillary this is 2.7 ± 0.3 cm long. In either Figures 3.4 and 3.5 one can observe that the minimum current is ~ 3.6 μA. If the initial resistance of the aqueous electrolyte filled capillary is R_{in} and that of the capillary containing an organic segment is R_{seg},

$$R_{seg}/R_{in} = 4.3/3.6 = 1.2. \tag{3.3}$$

If the resistance per cm of the aqueous electrolyte is R_{aq} and that for the organic zone is R_{org}, it follows that,

$$R_{in} = L_t R_{aq}, \quad \text{and,} \tag{3.4}$$

$$R_{seg} = (L_t - L_{org})\, R_{aq} + L_{org}\, R_{org}, \qquad (3.5)$$

where L_{org} is the length of the organic segment. Putting in numerical values and combining equations 3.3 - 3.5 results in:

$$[(47.3 \mp 0.3)\, R_{aq} + (2.7 \pm 0.3)\, R_{org}] / (50\, R_{aq}) = 1.2. \qquad (3.6)$$

Thence one obtains:

$$R_{org} / R_{aq} = 4.8 \pm 0.6. \qquad (3.7)$$

Indeed, this is the ratio of the field strength in the two zones experimentally observed with a bifilar probe, as previously mentioned. In fact, the ratio represented by equation (3.7) can only produce a lower limit of R_{org} because during the movement of the segment, QAS leakage from it has already started to occur, lowering the resistance of the aqueous electrolyte. In the absence of any such leakage, the minimum current observed in Figures 3.4 and 3.5 would have been lower still. The above calculations does not take that into account.

How much of the QAS from the organic segment leaks into the aqueous electrolyte? A lower limit estimate is possible in the following manner. Consider that in Figure 3.5, the peak current is ~8.3 μA, ~4 μA greater than the initial baseline value. From the known equivalent conductance of tetrabutylammonium (19.1) and perchlorate (67.9), it is readily computed that this excess current can be produced if 3.4 mM NBu_4ClO_4 (equivalent to 7.4 nmole, 2.5 μg) is *uniformly* distributed in the capillary. The amount of NBu_4ClO_4 present in the segment, 200 mg, is very much higher than this. However, the leaked QAS

can not possibly be uniformly distributed in the capillary, but likely decreases in an exponential fashion with increasing distance from the organic segment. The uniform distribution with increasing distance assumption produces, of course, the lower limit of the amount of QAS leaked from the segment.

It is noteworthy that the peak current is lower when the QAS loading is lower (Figure 3.4 vs. Figure 3.5). Also note that due to the persistent presence of the leaked out QAS in the medium, the current level does not return to the original level even after the organic segment has left the capillary.

It is also interesting to note that if a highly hydrophobic QAS, such as TOAB, is used in the organic segment, the current decreases after the introduction of the organic segment to ~3 μA and does not increase again. This suggests that in the case of a highly hydrophobic QAS, no significant leakage occurs.

3.1.4.2.2 Polarization of the Organic Segment under Electric Field

We hypothesize that the organic segment is significantly polarized in the electric field (Figure 3.6). We envision that the net positive charge density is greater in the front part of the segment closest to the cathode; while the net negative charge density is greater in the rear part of the segment closest to the anode. At the organic segment menisci, it is logical to expect that the orientation is as represented in Figure 3.6.

3.2 Experiments with an Extractable Hydrophobic Cation

Crystal violet (see Figure 3.7) is a hydrophobic cationic dye. It shows strong absorption at ~600 nm. The extraction and concentration of crystal violet in the capillary under high electric field was studied as a typical example of this type of extraction.

3.2.1 Properties of Crystal Violet

Crystal violet is a blue-violet powder. It is usually supplied in the chloride form. It is soluble in water, and the solubility is ~0.1 g/100 ml. The aqueous solution is violet, $\lambda_{max} = 591$ nm, $\varepsilon_{max} \approx 10^5$. The concentration decreases during storage likely due to absorption losses. The solubility of crystal violet is much greater in polar organic solvents, e.g., ethanol, chloroform.[64]

3.2.2 Output Characteristics

Figure 3.8 shows the typical output of crystal violet. The solid line is the extraction signal detected at 600 nm; the dashed line is the "background" signal detected at 720 nm, where there is no absorption from crystal violet. It was previously verified that in the absence of injected crystal violet, the background signals at 600 and 720 nm are identical. Figure 3.9 shows the net absorption due to crystal violet obtained by subtracting the background from its original signal.

Note that the detector used is not a dual wavelength detector and the "signal" and the "background" data comes from two separate runs. The accuracy of the "net" signal obtained this way therefore is limited both by run-to-run reproducibility (for example, in the width of the organic segment introduced) and in the judgment necessary in establishing coincidence of the abscissa values of two separate runs for the purposes of subtraction. The purpose of displaying the net signals in this work is for qualitative information only, every detail should not be emphasized.

It is apparent that crystal violet is extracted and concentrated in the front part of organic segment. The concentration distribution of crystal violet shows an exponential decay from a maximum value near the interface, in much the same way the positive charge distribution in the front (cathode) end of the segment was envisioned in section 3.1.4.2.2 regarding charge polarization in the segment.

3.2.3 Mechanism of Extraction and Concentration

3.2.3.1 Mechanism of Extraction

How does crystal violet move into the organic segment under high electric field? Is it the same mechanism as in "on-line" flow injection extraction?

Since there is an aqueous film surrounding the organic segment in a silica capillary, the interfacial area for extraction consists of the menisci as well as the area of the aqueous film between the organic segment and the wall.

One can envision two modes by which extraction can occur. First, the organic segment can be extracting from the surrounding solution as it moves along. If crystal violet is present in both the front and the rear of the moving organic segment, extraction should primarily be occurring through the rear because while the organic segment is moving by the electroosmotic flow, the crystal violet in the rear of the segment is moving both by electroosmotic and electrophoretic flow in the same direction and would thus enter the segment. Conversely, the direction of the electric field precludes significant extraction through the front meniscus and extraction through the aqueous wall film can only occur by hydrodynamic circulation of solution from the solution ahead of this segment into the film. Note that experimentally, the capillary is first washed/filled with the solution containing crystal violet, so some dye is always present ahead of the organic segment. Whether crystal violet is present in the rear of the segment or not depends on whether, after the organic segment is introduced, the capillary is put into an anode vial that does or does not contain crystal violet in addition to $Na_2B_4O_7$.

Experimental results show that within experimental uncertainty there is no difference in the net extraction signal whether crystal violet is present in the rear of the segment or not. The mechanism described in the foregoing and involving direct liquid-liquid extraction can not therefore be important.

The second and likely mechanism is that crystal violet, being a hydrophobic cationic dye, is adsorbed on the negatively charged wall of the silica tubing. When the organic segment passes through, the dye adsorbed on the wall is taken into the organic segment via the aqueous interface film.

For crystal violet, the amount extracted is dependent on the concentration of TBAP in the organic segment. For Figures 3.8 and Figure 3.10, the experimental conditions are basically the same except that twice the TBAP concentration is used in the second case. It is readily noticed that the extracted amount is less with an increased concentration of TBAP. There may be two reasons for this. A greater concentration of NBu_4^+ cation in the front of the organic segment may hinder the entrance of crystal violet through this part. Second, the aqueous film thickness may increase with increasing TBAP concentration, reducing extraction efficiency.

3.2.3.2 Calculation of the Extraction Amount

The amount of extraction of crystal violet can be calculated using Beer's Law:

$$A = \varepsilon bc. \tag{3.8}$$

For crystal violet, ε has been determined to be (see section 3.2.4 on calibration data for the extraction of crystal violet) 0.771 $AU \cdot cm^{-1} \cdot ppm^{-1}$ at 600 nm. The actual path length in a 75 μm bore capillary is averaged across the optical aperture. This value was determined to be 37 μm by comparing absorbance values for the same crystal violet containing borate solution being measured in a 1 cm cell versus the capillary, in each case using only the borate solution as the zero absorbance reference. To use equation 3.8, the peak area of a peak such as that shown in Figure 3.10 is computed in AU·s. The mass of the analyte in the peak is then available from:

$$\text{Analyte mass (mg)} = [\text{Peak Area (AU·s)} \times \text{Flow rate (L/s)}] / [\varepsilon\ (\text{AU·cm}^{-1}\text{·ppm}^{-1}) \times \text{b (cm)}]. \quad (3.9)$$

Here, Peak Area (AU·s) is integrated from Figures 3.9 and 3.11; the flow rate can be calculated from the retention time and the bore and the length of the capillary.

The data for Figure 3.9 indicate that 124 pg of crystal violet is extracted and that for Figure 3.11 indicate that 73 pg of crystal violet is extracted. The total amount of crystal violet present in the capillary from the segment to the detector (for this experiment, this length was 36.2 cm), as the segment is first introduced, was 366 pg. The efficiency of extraction can thus be taken to be 33.9 and 19.9% for the two cases represented in Figures 3.9 and 3.10, respectively.

3.2.3.3 Spatial Distribution of Crystal Violet within the Organic Segment

Figures 3.8 and 3.10 make it apparent that the dye is distributed in the organic segment such that most of the dye is at the front interface, decreasing with increasing distance from the interface. It may seem that even though arguments have been made in the previous section that extraction through the front meniscus is unlikely, such a process will give rise to the observed distribution. It can be proven that the observed distribution is a result of the electric field, not the extraction process.

Crystal violet was first dissolved into $CHCl_3$ along with TBAP. This sample was introduced into the capillary containing aqueous borate electrolyte and then eluted out under high voltage. The observed crystal violet distribution in the organic segment is the same as that observed in the extraction experiments. This shows that even if crystal violet is originally distributed in a homogeneous fashion in the organic segment, it is redistributed under the high electric field and concentrates in the front part of organic

segment towards the cathode. When a longer organic segment containing crystal violet is introduced, a higher peak signal results since a greater mass of crystal violet is injected and redistributed.

3.2.4 Calibration Data for the Extraction of Crystal Violet

Crystal violet solutions 0 - 1 ppm, were made in 2 mM $Na_2B_4O_7$. Figure 3.12 shows the output signals of different concentrations of crystal violet. Figure 3.13 shows the calibration curve. In this plot, the ordinate plotted is the positive peak height at the interface. The absorption of the same crystal violet solutions were also tested in 1 cm path length standard cuvettes, and these data are plotted in Figure 3.14. By comparing the slope of two calibration curves, it is noticed that there is more than ten times concentration effect of this type of extraction under unit path length.

As previously stated, in the particular detector used, the 75 μm bore capillary has an average effective path length of 37 μm. Thus, the path length ratio between the two cases is 270.3. However, the slope ratio observed is 13.6. If we make the reasonable assumption that the absorptivity of crystal violet is essentially the same in aqueous borate and TBAP containing $CHCl_3$, it is readily apparent that the concentration of the dye in the front interface zone is more than an order of magnitude higher than in the corresponding aqueous solution. In other words, more than an order of magnitude concentration in the organic solvent interface has occurred.

3.3 Experiments with Ion-Pair Extractable Anionic Samples

This section concerns the extraction of anionic species that are not sufficiently hydrophobic to be extracted directly into $CHCl_3$ unless a hydrophobic pairing ion, such as NBu_4^+, is present. It was found that such species shows an altogether different behavior

compared with that of crystal violet. The anionic dye Eosin Y and the anionic metal complex Cobalt-(4-(2-pyridylazo)-resorcinol) (Co-PAR) were studied as typical examples.

3.3.1 Properties of the Extractable Species

3.3.1.1 Eosin Y

The structure of Eosin Y is shown in Figure 3.15. It is usually supplied as the sodium salt and is soluble in water in that form, yielding an orange solution. A solution of Eosin Y is very stable, and can be stored for months. The Eosin Y sample was made in 2 mM borate, pH = 9.2, the maximum absorption wavelength is around 500 nm with $\varepsilon \approx 10^5$. Eosin Y is not significantly dissolved by or directly extracted into $CHCl_3$. However, when TBAP is added to $CHCl_3$, Eosin Y is readily extracted into it, virtually quantitatively. This occurs because the NBu_4^+ cations associate with Eosin Y anions to form ion pairs that are extracted. The extracted Eosin Y in $CHCl_3$ also shows maximum absorption around 500 nm.

3.3.1.2 Cobalt-(4-(2-pyridylazo)-resorcinol)

PAR is the acronym for 4-(2-pyridylazo)-resorcinol. The structure is shown in Figure 3.16. It is a highly sensitive photometric reagent for wide variety of metal ions. It is slightly soluble in water, e.g., 50 mg/l at 10°C. It is more soluble in acidic or alkaline solutions. PAR chelates Co^{2+} ion to form Co-PAR metal chelates. In our experiment, Co-PAR is made in 2 mM $Na_2B_4O_7$, the maximum absorption wavelength is around 510 nm with $\varepsilon \approx 5\times10^4$. The stoichiometry of the Co-PAR complex has not been fully elucidated. The phenolic OH group of the PAR ligand is deprotonated at higher pH to give a chelate with a greater negative charge or a greater ligand to metal ratio.[65] At the same time, the deprotonation of the OH group results in an increase in molar absorptivity

of the chelate, resulting in greater photometric sensitivity. The negatively charged Co-PAR can be extracted into organic solvents as an ion pair with NBu_4^+.

Test tube extraction experiments show there is very little extraction of the Co-PAR complex into $CHCl_3$ in the absence of TBAP. The extractability into $CHCl_3$ does not change upon the addition of $NaClO_4$. This confirms that Co-PAR is an anionic chelate in 2 mM $Na_2B_4O_7$ solution.

3.3.2 Output Characteristics

Figure 3.17 shows the typical output from an extraction experiment with Eosin Y. One trace shows the extraction signal detected at 500 nm; the other shows the "background" signal detected at 620 nm, where there is no significant absorption by Eosin Y. Figure 3.18 shows the net absorption obtained by subtraction of the background signal.

Note that the phase boundary is located at the discontinuity of the curve in Figure 3.18. It is readily noticed that some Eosin Y is extracted and concentrated in the organic zone. The distribution of the dye matches the distribution of crystal violet in the organic segment under the high electric field as described in a previous section. We presume that this is due to the fact that the dye in the organic zone is fully associated with NBu_4^+ and the observed dye distribution reflects the original distribution of the NBu_4^+ cation which results from dissociation and redistribution of TBAP.

However, it is also apparent that the maximum concentration of Eosin Y occurs in the aqueous phase, not at the interface layer or the organic phase. Our current understanding, admittedly incomplete, as to why this occurs, is presented in the next section.

3.3.3 The Behavior of Eosin Y in the Extraction System: Suggested Mechanism

It is relatively straightforward to understand the distribution of Eosin Y in the organic segment. Because of polarization of the organic segment under high electric field, unpaired NBu_4^+ cation concentration decreases exponentially from the front edge of the organic segment. Since the NBu_4^+ ion is directly responsible for the extraction of Eosin Y, the distribution of the latter reflects the initial distribution of the former. This would also suggest that there is less dissociation of the NBu_4^+-$Eosin^-$ ion pair once formed, relative to NBu_4^+-ClO_4^-.

The distribution of Eosin Y in the aqueous phase ahead of the organic segment is related to the leakage of the QAS, specifically NBu_4^+, out of the $CHCl_3$ phase. The aqueous phase Eosin Y concentration exhibits a maximum about 1 cm ahead of the interface. One plausible reason for this behavior is that as NBu_4^+ ions move out of the organic segment on the front of the segment and move towards the cathode, they meet Eosin Y anions moving in the opposite direction. We hypothesize that a sufficiently stable ion pair is formed even in the aqueous phase between these two species such that there is no net electrophoretic movement of the ion-pair. Because the supply of the Eosin anions in the immediate neighborhood of the segment is exhausted, it is reasonable that the maximum ion pair concentration is some distance away from the segment.

One potential way to test this hypothesis is to use different quaternary ammonium bromide or perchlorate salts where the size of the quaternary ammonium group is varied in $CHCl_3$. Experiments were attempted with TPrAB, TBAP, TPAB, THAB and TOAB. Of these, TPrAB does not dissolve in sufficient amount in $CHCl_3$ to make a stable system. The others were dissolved in amounts equimolar to 0.1 g/ml TBAP. As had been mentioned in a previous section (section 3.1.4.2.1), TOAB does not leak significantly from the organic segment, the overall current decreases markedly because much of the voltage

is dissipated across the organic segment. This causes EOF to decrease. The injected organic segment did not pass through the detector in 10 min and the experiment was terminated.

With TBAP (Figure 3.19), the aqueous phase peak occurs 2.96 s (or 0.8 cm) ahead of the front edge of the organic phase. With THAB (Figure 3.20), the aqueous phase peak is less pronounced, as may be expected, since less of the QAS comes out of the segment. It is also apparent that a greater amount of dye is extracted in the organic segment for THAB relative to TBAP. Moreover, the aqueous phase peak for THAB is closer (2.62 s or 0.7 cm) to the interface edge than in the case of TBAP. This is expected as well since the NHx_4^+ cation is less mobile than the NBu_4^+ cation.

The above scenario, however, fails to explain the observed results for the experiment with TPAB (Figure 3.21). The aqueous phase peak is narrow, high relative to TBAP and is further away (4.0 s, 1.1 cm) from the interface than with TBAP.

The dependence of the extraction signals on the concentration of the same QAS was also studied. For TBAP, it was found that there was no significant change of the aqueous phase peak height when different amounts of TBAP was used (see Figure 3.22).

3.3.3.1 "Extraction" Efficiency for Eosin Y

Here as the "extraction signal" we consider the total Eosin Y signal in the neighborhood of the organic segment. This includes both the aqueous phase and the organic phase signals as shown in Figure 3.17. The total mass and the extraction efficiency of analyte is computed in the same fashion as that for crystal violet (equations 3.8-3.9, section 3.2.3.3).

For the data Figure 3.18, in which the Eosin Y concentration solution is 1 ppm, 605 pg Eosin Y was computed to be present in the peak zone. In a second experiment when 3 ppm Eosin Y was used, the extraction zone was computed to contain 1.80 ng, almost

exactly three times the first result. Relative to the total amount of Eosin Y present in the capillary ahead of the organic segment, 37.4% is present in the peak zone.

3.3.3.2 The Unique Necessity of Electric Field for the Extraction

Once the capillary is filled with the Eosin Y containing sample, and the QAS containing organic segment is injected by electroosmosis, if the organic segment is made to elute through the detector by gravity, rather than by applying electric field, it was remarkable that there was no positive aqueous phase signal. The organic segment also showed no evidence of Eosin Y accumulation at the front edge.

In summary, the aqueous phase concentration and front edge accumulation in the organic phase are observed only when aqueous Eosin Y samples are extracted under high electric field. Obviously all aspects of the output signal are dependent on the presence of the electric field.

Can Eosin Y leak out of the organic segment? A sample of Eosin Y was first extracted into $CHCl_3$ containing QAS. This colored segment was injected and eluted out under high electric field, using the same aqueous electrolyte of 2 mM $Na_2B_4O_7$. No signal due to Eosin Y in the aqueous phase was observed suggesting no leakage occurs from the segment. If the Eosin Y loading in the organic phase was too high (this also means that the perchlorate was largely replaced), an open circuit resulted quickly after injection. This suggests that the NBu_4^+-$Eosin^-$ ion-pair is not nearly as easily dissociated as NBu_4^+-ClO_4^- and formation of an aqueous interface film may thus be hindered.

3.3.3.3 Adsorption Experiments with Eosin Y

Physical adsorption is a universal phenomenon in surface chemistry. For crystal violet (section 3.2.3.2), we have argued that it is indeed adsorption that leads to the signal.

this should be different for Eosin Y which is negatively charged and should not adsorb markedly on silica at alkaline pH.

A capillary was first washed with 2 mM $Na_2B_4O_7$, dried with compressed air, than filled with 2 mM $Na_2B_4O_7$. One end of the capillary was then lifted to a certain height and the capillary was rinsed with 1.6 ppm Eosin Y solution (made in 2 mM $Na_2B_4O_7$) by gravity. After measuring the flow rate under such conditions, it was possible to calculate the total volume of the Eosin Y solution passed through the capillary by recording the rinse time. Finally TBAP-loaded $CHCl_3$ was injected and eluted out by applying high voltage.

Figure 3.23 shows the dependence of the positive absorbance signal in the aqueous phase upon the rinse volume. A plateau signal is reached after rinsing the capillary with 1-2 µl Eosin Y solution, no further increase occurs with a greater rinse volume. The total volume of the capillary from the anode to the detector, as the segment is first introduced, is 1.8 µl. These results suggest that adsorption is not involved, the maximum signal is reached by the time the whole capillary is filled with the Eosin Y solution, and does not increase thereafter.

To see if a greater signal can be obtained by promoting surface adsorption, we deliberately created an uncharged hydrophobic surface by reacting the interior of a small length of capillary (~ 5 cm) with octadecyltrichlorosilane. This was then connected to the standard capillaries. Stable and reproducible output signals unfortunately could not be attained, primarily because of frequent occurrences of an open circuit. When the organic segment passed through the hydrophobic capillary: (much like the interposition of a PVC tube mentioned in section 3.1.4.1), the aqueous film surrounding the segment could not be maintained. The resistance of the segment is dramatically increased wherein heat production results in bubbles and an open circuit.

3.3.4 Calibration Results for Anionic Analytes Extractable as Ion-Pairs

3.3.4.1 Eosin Y

Parts per billion level Eosin Y solutions were made in 2 mM $Na_2B_4O_7$ to construct a calibration plot. Figure 3.24 shows the signals resulting from different concentrations of Eosin Y. Figure 3.25 shows the calibration plot. Note, that the ordinate plotted is the peak height of the positive aqueous phase signal. The absorbance of the same Eosin Y test solutions were also measured in a standard 1 cm path length cell. By comparing the slope of the two calibration plots as in the case of crystal violet, it was found that at the peak, the aqueous phase concentration is a factor of 14 times greater than that in the original solution.

3.3.4.2 Cobalt-(4-(2-pyridylazo)-resorcinol)

Calibration data for the Co^{2+} ion as the Co-PAR anionic complex was also obtained. These results show facile determination of ppb levels of metal ions, not easily attainable in capillary systems with typical commercial detectors due to the limited radial path length.

The Co^{2+} standard solutions were made in 2 mM $Na_2B_4O_7$ containing 10 ppm PAR. Figure 3.26 shows the signals obtained from filling the capillary with different concentrations of Co-PAR solutions. Figure 3.27 shows the calibration plot. As before, the aqueous phase positive peak heights are plotted as the ordinate. The reproducibility of the signals are good for capillary scale experiments (mean RSD is 1.75%). The linearity of response is also good, with a linear r^2 value of 0.99901 . The absorbance of the same Co solutions were also measured in 1 cm standard cell (see Figure 3.28). It is thus possible to conclude from the slopes in Figure 3.27 and 3.28 that at the aqueous phase peak in the capillary, the Co-PAR concentration is 6.3 times higher.

3.4 Experiments With Ion-Pair Extractable Cation

Cationic ion-pair extractable species were also used to study the pattern of aqueous phase concentration and extraction in a capillary under high electric field. The metal chelate $Fe(\varrho\text{-Phen})_3^{2+}$ was studied as a typical example of this category.

3.4.1 Properties of $Fe(\varrho\text{-Phen})_3^{2+}$

1,10-Phenanthroline, also called ϱ-Phenanthroline or 4,5-Phenanthroline (see Figure 3.29), is usually obtained as the monohydrate, a white crystalline powder. It is reasonably soluble in water (~3.3 g/l at room temperature), and much more soluble in alcohol, acetone and dilute acid. Aqueous ϱ-Phen solutions are colorless and do not absorb in the visible region.

ϱ-Phen usually behaves as an uncharged ligand, and forms cationic metal chelates which retain the positive charge of central metal ions. Ferrous ions complex with ϱ-Phen forming the tris-(ϱ-Phenanthroline) complex ($Fe(\varrho\text{-Phen})_3^{2+}$). It is an orange-red chelate, with a stability constant log β_3 of 10.03 (20 °C, I = 0.1), a λ_{max} of 510 nm, and an $\varepsilon_{max} \approx 10^4$.

Metal-(ϱ-Phen) cationic chelates tend to form ion-pairs with mono- or divalent bulky anions, e.g., ClO_4^-, that are insoluble in water. $Fe(\varrho\text{-Phen})_3^{2+}(ClO_4^-)_2$, can be extracted into polar organic solvents of high dielectric constant. $Fe(\varrho\text{-Phen})_3^{2+}$ is not significantly extracted to $CHCl_3$ if only hard anions. e.g., Cl^-, is present.

3.4.2 Output Characteristics

Figure 3.30 shows a typical output from an extraction experiment with $Fe(\varrho\text{-Phen})_3^{2+}(ClO_4^-)_2$. The solid line is the extraction signal detected at 510 nm; the dashed line is the "background" signal detected at 620 nm, at which there is no significant

absorption by $Fe(\varrho\text{-Phen})_3^{2+}$. Figure 3.31 shows the net absorption due to $Fe(\varrho\text{-Phen})_3^{2+}$ by subtracting the background signal from the first.

Note that as mentioned in section 3.2.2, the detector used is not a dual wavelength detector and the "signal" and the "background" data comes from two separate runs. The shoulder in the descending part of the net peak or the negative glitch at ~165 s seen in Figure 3.31 is likely an artifact of the subtraction process.

It is clearly seen from Figure 3.30 that the $Fe(\varrho\text{-Phen})_3^{2+}$ chelate is extracted and concentrated in the rear part of organic zone. This is exactly opposite of the behavior displayed by crystal violet, a hydrophobic dye that is extracted without the necessity of ion-pairing with perchlorate. The distribution of the extracted $Fe(\varrho\text{-Phen})_3^{2+}$ matches the envisioned distribution of the unpaired perchlorate group in the organic segment under high electric field, the mirror image of the case for the extraction of Eosin Y (see section 3.3.2).

3.4.3 Mechanism of Extraction and Concentration

The mechanism of extraction of $Fe(\varrho\text{-Phen})_3^{2+}$ is conceptually similar to that of crystal violet, in that it is most likely extracted via wall adsorption and then through the aqueous film surrounding the segment. As in the case of crystal violet, the net absorption signal due to extracted $Fe(\varrho\text{-Phen})_3^{2+}$ shows no significant dependence on whether or not $Fe(\varrho\text{-Phen})_3^{2+}$ is present in the aqueous electrolyte trailing the organic segment.

The marked difference between crystal violet and $Fe(\varrho\text{-Phen})_3^{2+}$ is in the manner in which these species are distributed in the extracted zone (compare Figure 3.8 vs. 3.30). While crystal violet behaves in the same manner we envision NBu_4^+ to be distributed in the polarized segment, $Fe(\varrho\text{-Phen})_3^{2+}$ is distributed in the organic segment in the same manner we envision ClO_4^- to be distributed in the organic segment. We believe that this

difference is because of the fact $Fe(o\text{-Phen})_3^{2+}$ can be extracted into the organic segment only as an ion-pair with the hydrophobic perchlorate. It therefore enters the segment through the film into the rear edge of the segment where polarization results in a higher concentration of perchlorate. Once in the segment, the ion associate has no net charge and can diffuse into the rest of the segment. Nevertheless, an exponentially charging concentration profile with the maximum concentration being in the rear edge is expected and this is observed. Crystal violet is a member of the cationic triphenylmethane dye class where it can exist in tautomeric equilibrium. For the chloride form for example, the two forms can be the salt like form ($Ph_3C^+Cl^-$) and the nonionic form ($Ph_3C\text{-}Cl$).[68] It may be extracted in the cationic form. The electron deficiency represented by the cation may be sufficiently delocalized due to the extensive conjugation and be mitigated by the presence of the three electron donating amino groups to permit it to exist as the cation even in the organic solvent and therefore be distributed as a positive ion in a polarized segment.

Note that the distribution of $Fe(o\text{-Phen})_3^{2+}$ (or Eosin Y) in the organic segment occupies a larger portion of the segment than does crystal violet. This supports the contention that in the case of these extracted ion pairs, once formed, the charge-neutral ion pairs diffusively migrate into the rest of the segment.

3.4.3.1 Role of Perchlorate in the Extraction of $Fe(o\text{-Phen})_3^{2+}$

If NBu_4^+ and ClO_4^- are present without polarization in the organic segment (as would be the case in the absence of an electric field) there will be no local excesses of either ion, and $Fe(o\text{-Phen})_3^{2+}$ will have to compete with NBu_4^+ to be extracted. If the metal chelate must be associated with ClO_4^- to be extracted, clearly an unpolarized segment would not promote extraction. This is indeed observed. If after filling the capillary with $Fe(o\text{-Phen})_3^{2+}$ and introducing the organic segment by electroosmosis, the voltage is turned off and the segment carried to the detector by gravity, no significant

extraction peak (at least a situation where Fe(o-Phen)$_3^{2+}$ is inhomogeneously distributed in the organic segment) can be observed.

3.4.3.2 Dependence of Distribution of Fe(o-Phen)$_3^{2+}$ upon the Direction of Polarization of the Segment

If we were to reverse the polarity of the power supply, the direction of polarization of the organic segment will be reversed. However, electroosmotic flow will also be reversed and it would not be possible to carry the segment to the detector by electroosmotic flow. This was circumvented in the following manner. After the capillary was filled with analyte solution and the organic segment introduced by electroosmosis in the usual manner using positive high voltage, the polarity of the power supply was reversed and a positive pneumatic pressure was simultaneously applied at the high voltage end of the capillary to drive the segment to the detector against electroosmotic flow. (Applying pneumatic pressure to induce flow unfortunately results in frequent air bubbles. Glitches in the signal output due to these were removed by software.)

Figure 3.32 shows the detector output at 510 nm; while Figure 3.33 shows the detector output at 620 nm. In comparing Figure 3.32 and Figure 3.33, it can be noted that Fe(o-Phen)$_3^{2+}$ is concentrated in this case in the front part of the organic segment. Reversing the polarization of the segment indeed reversed the distribution the Fe(o-Phen)$_3^{2+}$ in the organic segment.

A careful examination of Figures 3.32 and 3.33 shows, however, that the extraction peak is significantly smaller in this case. This may be due to pneumatic pumping, that results in a parabolic flow profile. The shape of the organic segment is accordingly distorted, with the aqueous film surrounding the front part of organic segment becoming thicker (Figure 3.34). The intensity of polarization thus becomes smaller and less extraction occurs.

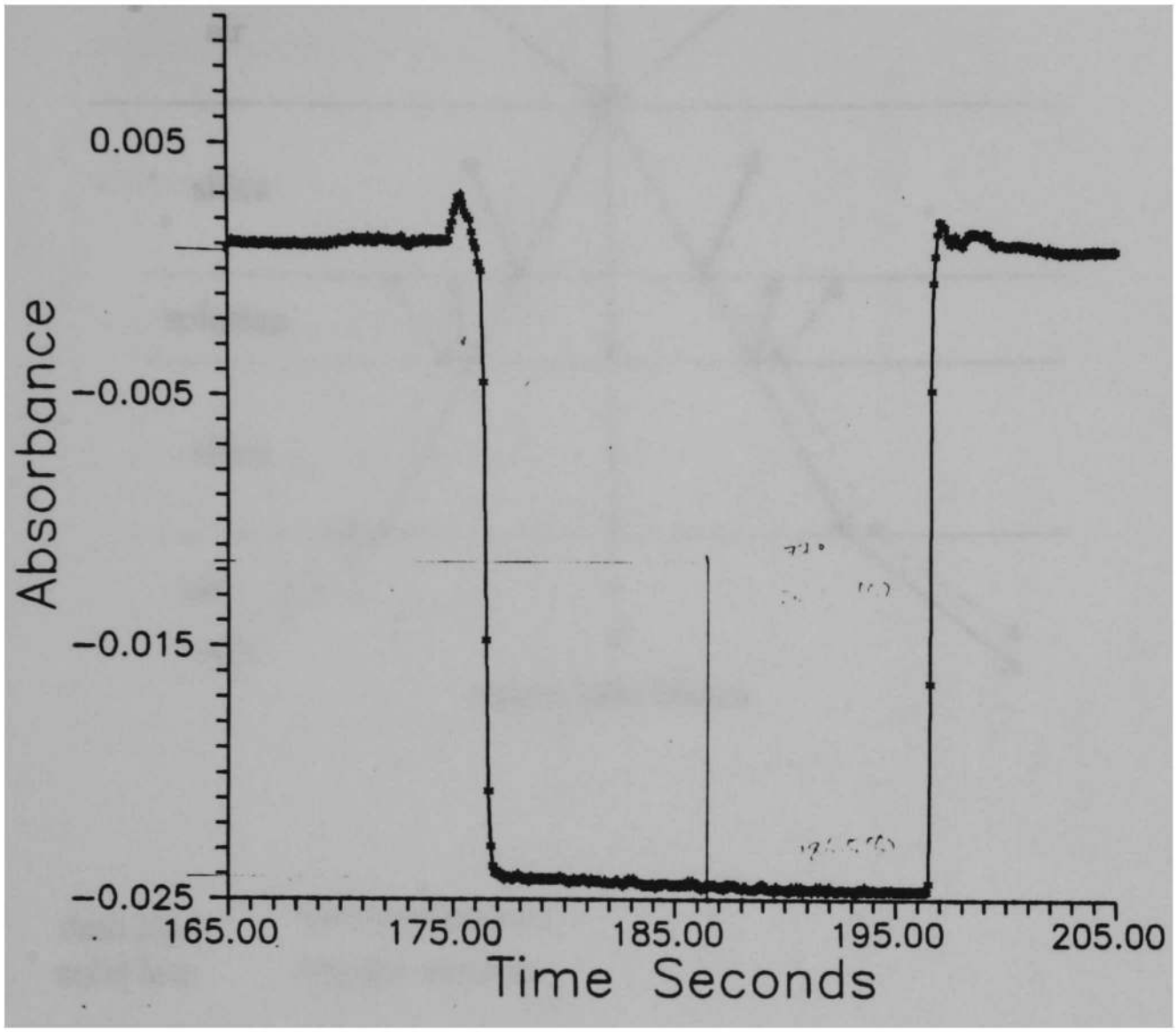

Experimental Conditions

high voltage	15 kV across 50 cm 75 μm ID/350 μm OD capillary
organic phase	0.1 g/ml TBAP in $CHCl_3$
aqueous phase	2 mM $Na_2B_4O_7$
detection wavelength	600 nm
injection time	20 seconds

Figure 3.1 Output from a Blank Sample Injection.

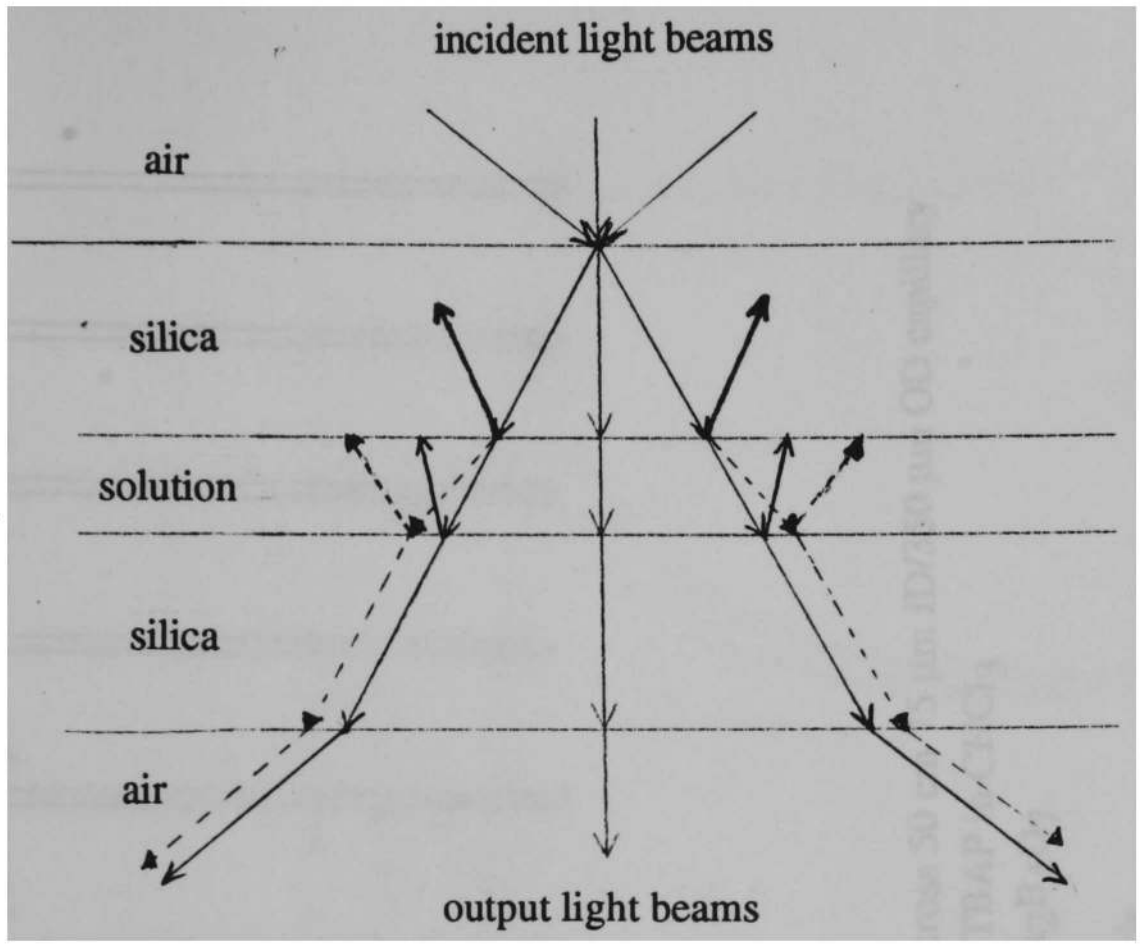

dash line	aqueous medium
solid line	organic medium

Figure 3.2 Ray Tracing Diagram.

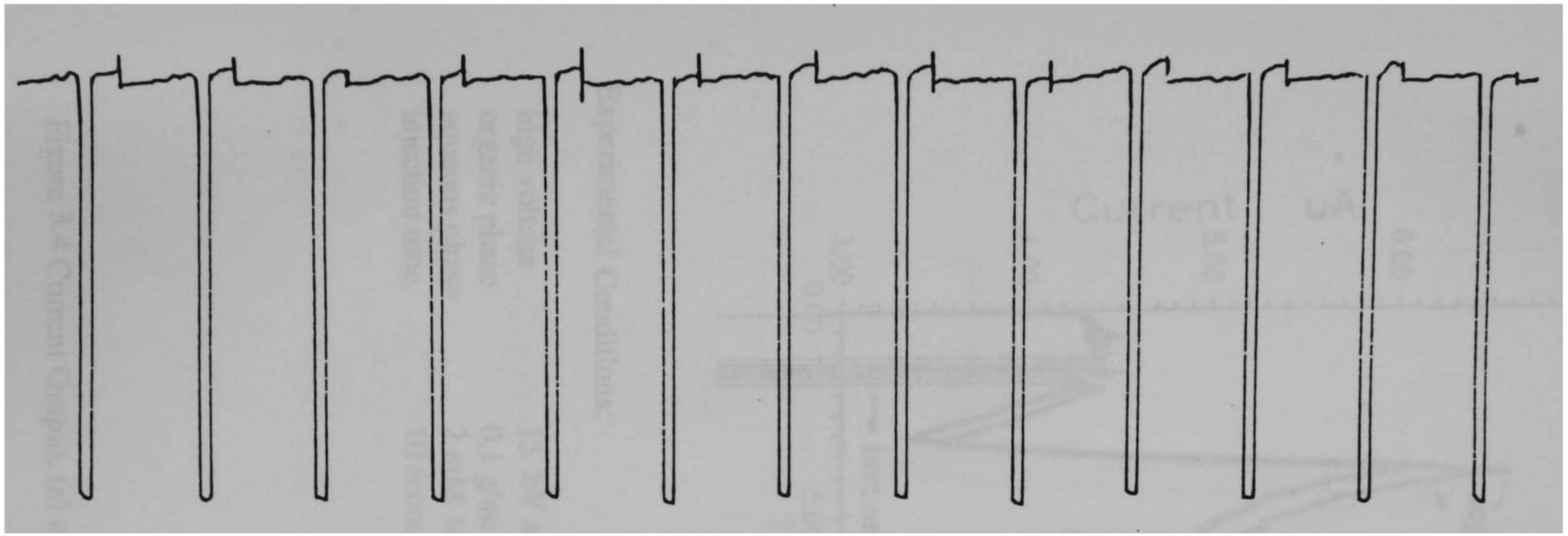

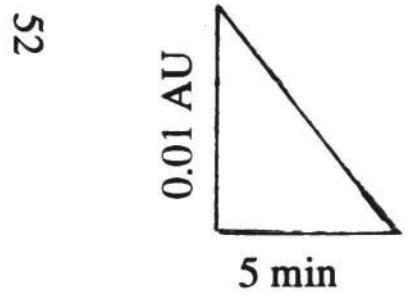

Experimental Conditions

high voltage	15 kV across 50 cm 75 μm ID/350 μm OD capillary
organic phase	0.1 g/ml TBAP in $CHCl_3$
aqueous phase	2 mM $Na_2B_4O_7$
detection wavelength	600 nm
injection time	20 seconds

Figure 3.3 Output of Repeated Injections from QAS Containing Chloroform Segments.

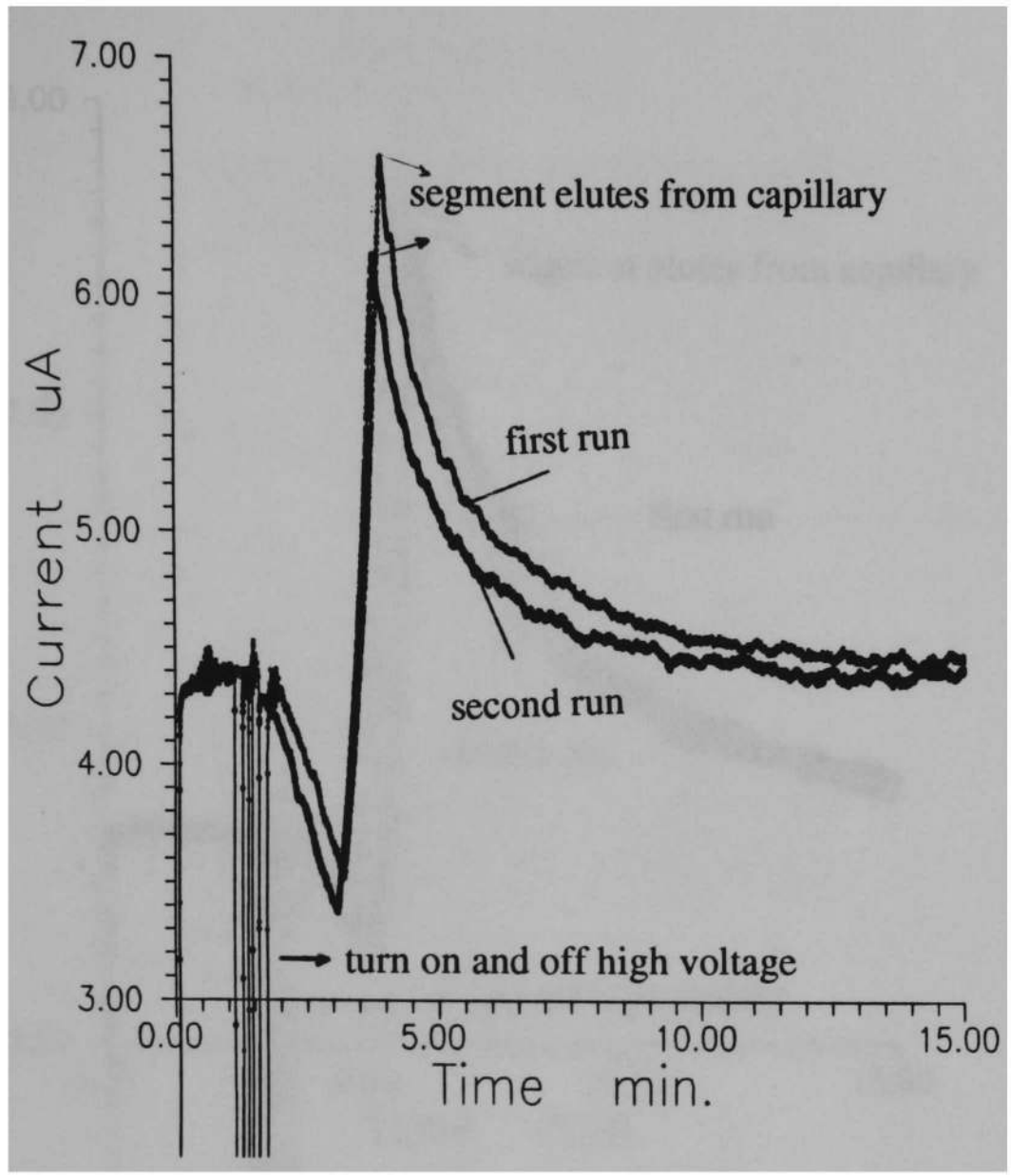

Experimental Conditions:

high voltage	15 kV across 50 cm 75 μm ID/350 μm OD capillary
organic phase	0.1 g/ml TBAP in $CHCl_3$
aqueous phase	2 mM $Na_2B_4O_7$
injection time	10 seconds

Figure 3.4 Current Output. (a) organic phase: 0.1 g/ml TBAP in $CHCl_3$.

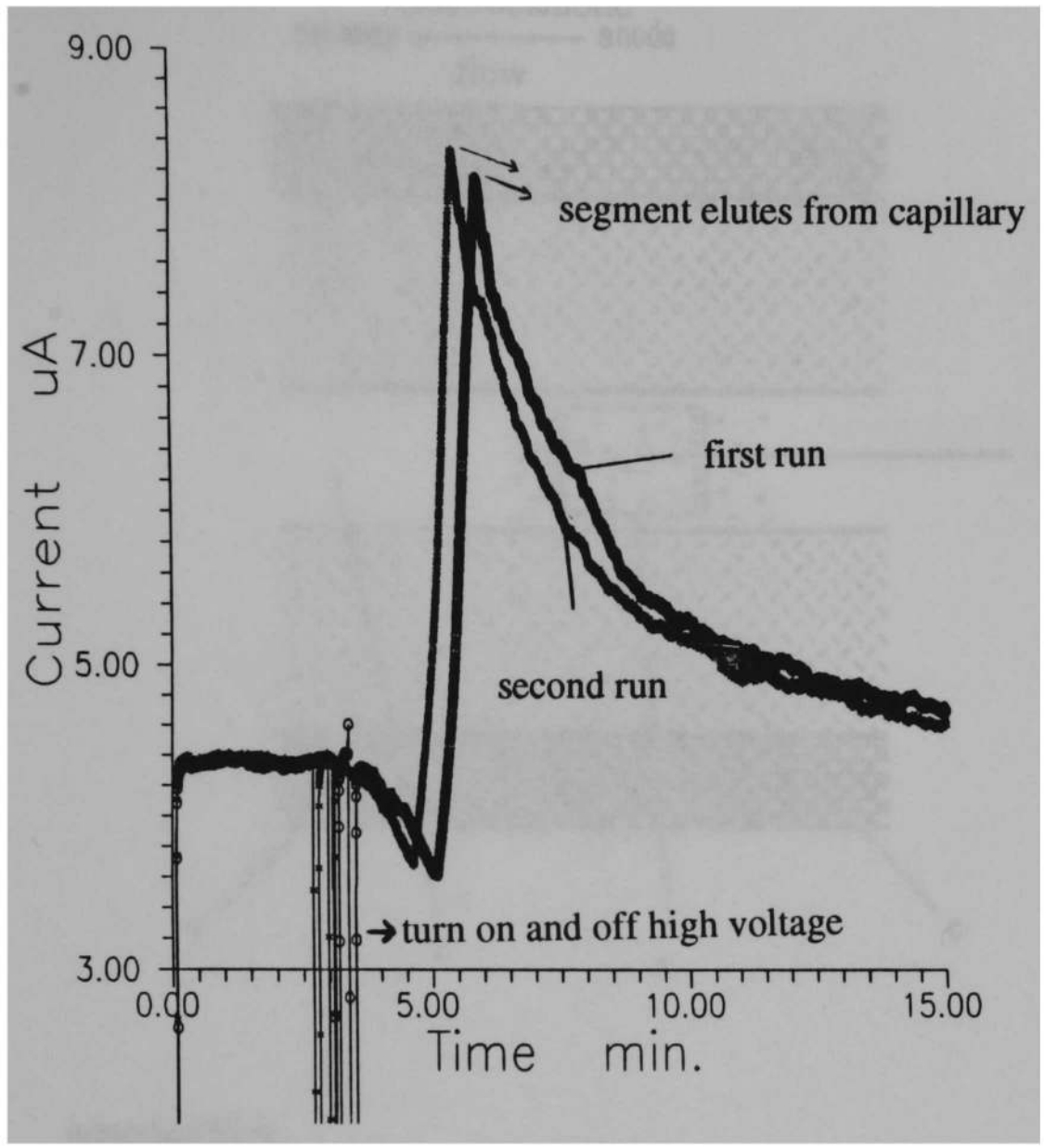

Experimental Conditions

high voltage	15 kV across 50 cm 75 μm ID/350 μm OD capillary
organic phase	0.2 g/ml TBAP in $CHCl_3$
aqueous phase	2 mM $Na_2B_4O_7$
injection time	10 seconds

Figure 3.5 Current Output. (b) organic phase: 0.2 g/ml TBAP in $CHCl_3$.

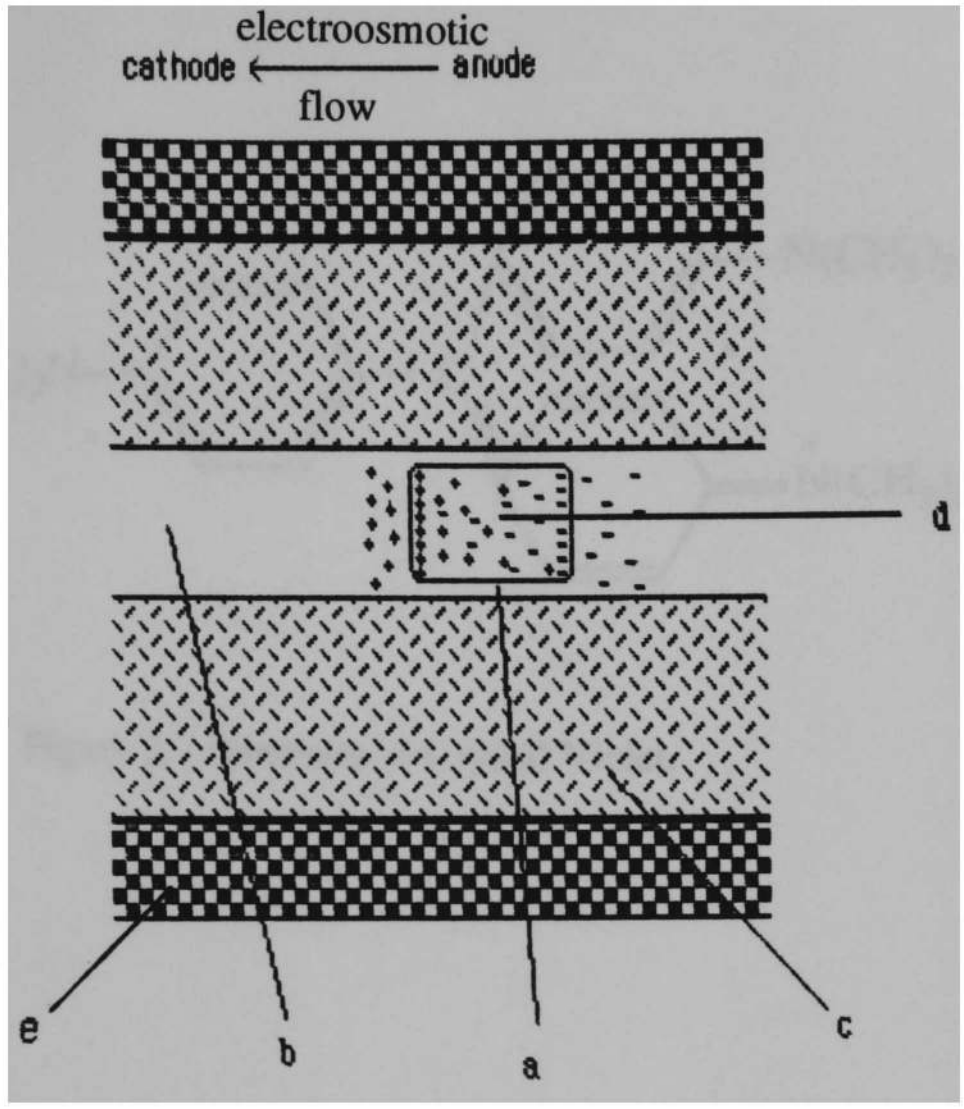

a aqueous film
b bulk electrolytes, 2 mM sodium borate
c 75 μm ID/350 μm OD capillary
d organic segment
e polyimide coating

\+ quaternary ammonium cation or net positive charge in organic segment
\- pairing anion or net negative charge in organic segment

Figure 3.6 Polarization of Organic Segment under High Electric field .

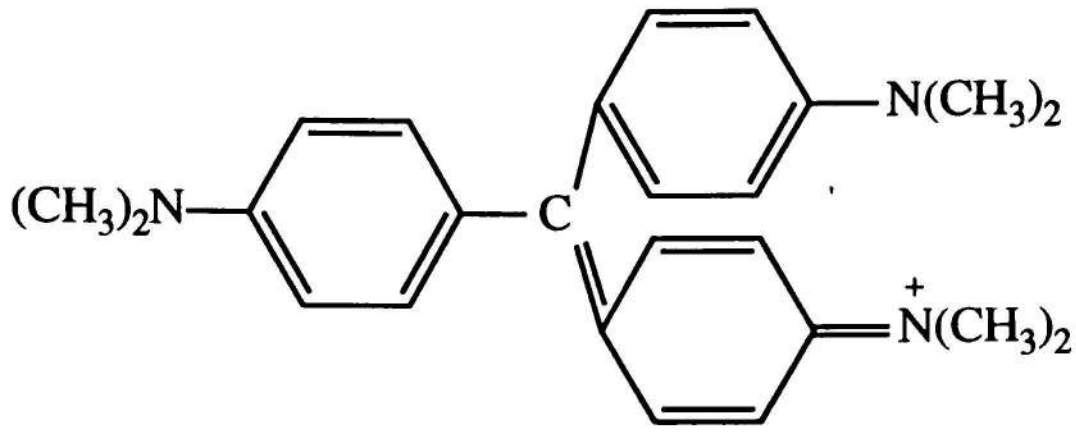

Figure 3.7 Structure of Crystal Violet.

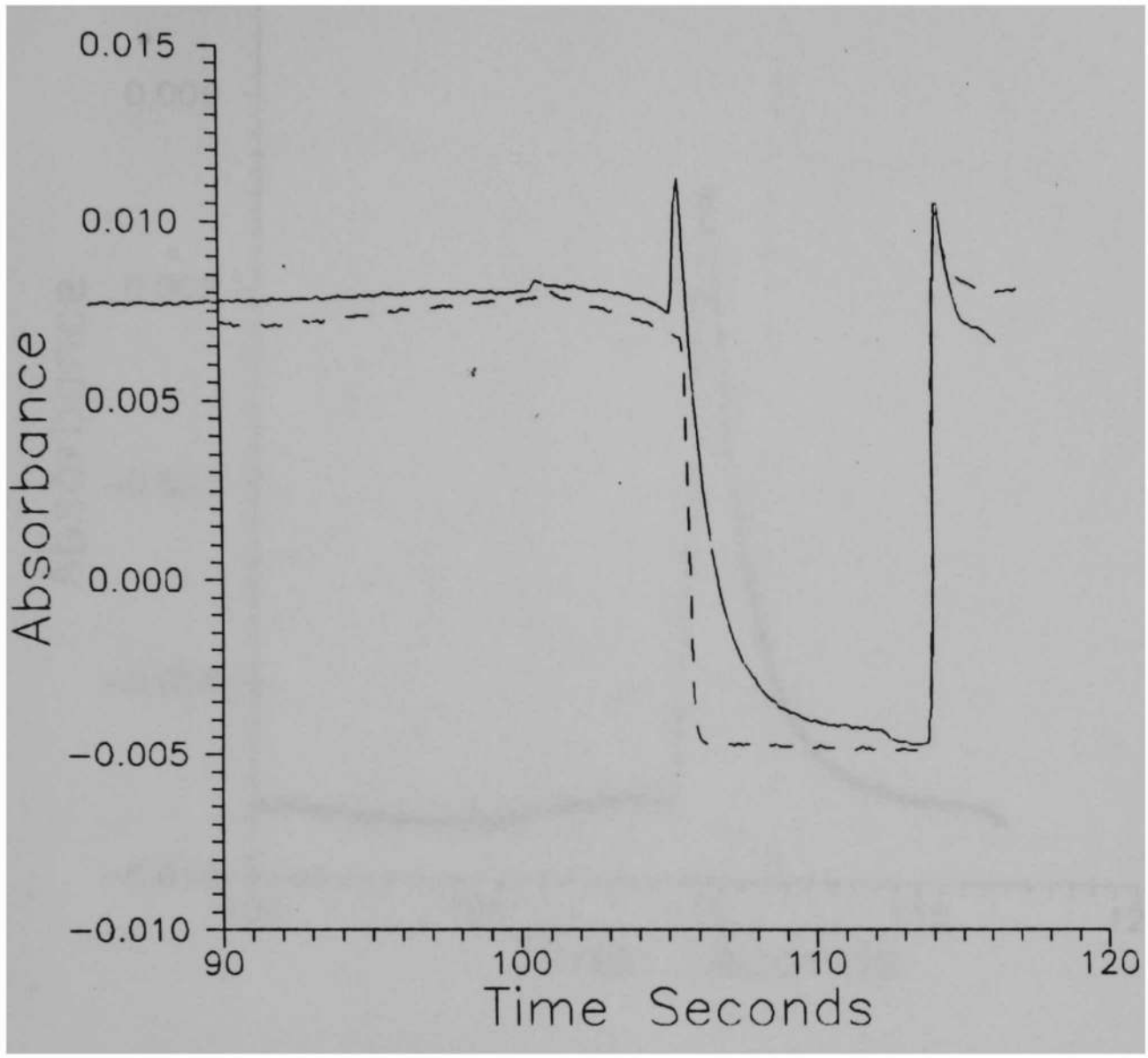

Experimental Conditions:

high voltage	15 kV across 50 cm 75 μm ID/350 μm OD capillary
organic phase	0.1 g/ml TBAP in $CHCl_3$
aqueous phase	0.23 ppm crystal violet in 2 mM $Na_2B_4O_7$
detection wavelength	600 nm/720 nm
injection time	10 seconds
solid line	$\lambda = 600$ nm
dash line	$\lambda = 720$ nm

Figure 3.8 Crystal Violet Output.
(a) organic phase: 0.1 g/ml TBAP in $CHCl_3$.

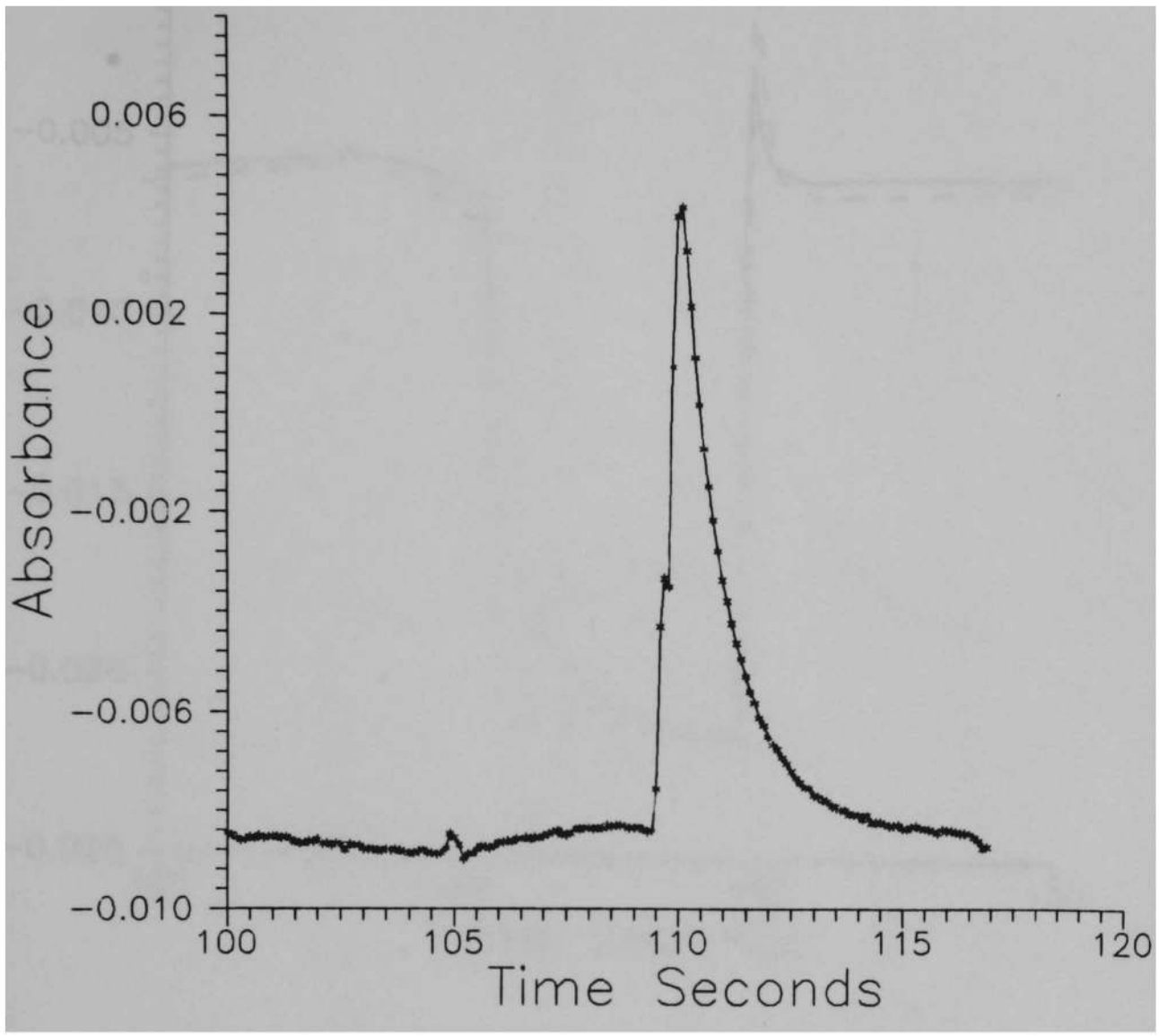

Experimental Conditions

high voltage	15 kV across 50 cm 75 μm ID/350 μm OD capillary
organic phase	0.1 g/ml TBAP in $CHCl_3$
aqueous phase	0.23 ppm crystal violet in 2 mM $Na_2B_4O_7$
detection wavelength	600 nm/720 nm
injection time	10 seconds

Figure 3.9 Net Crystal Violet Extraction Signal.
(a) organic phase: 0.1 g/ml TBAP in $CHCl_3$.

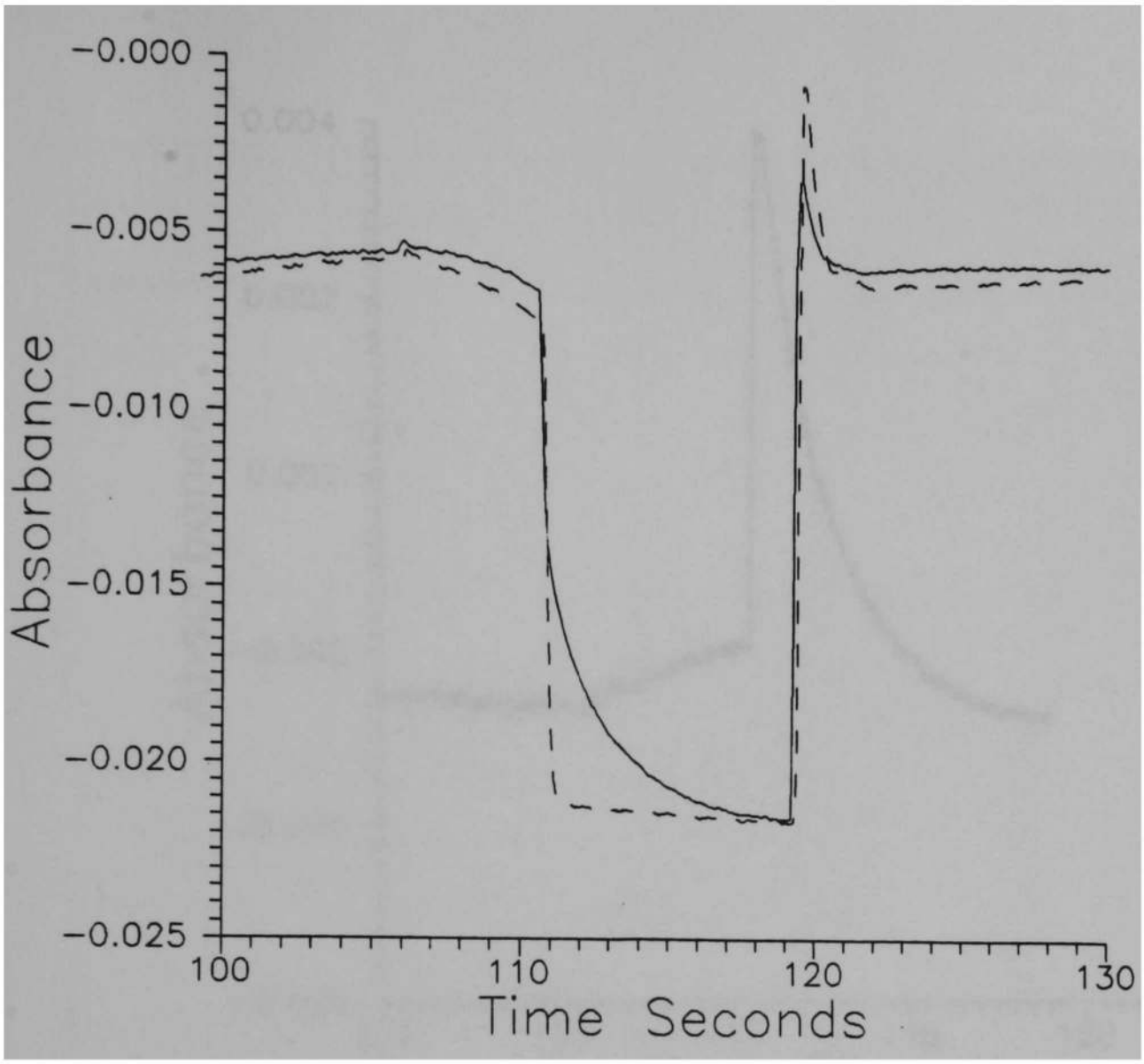

Experimental Conditions

high voltage	15 kV across 50 cm 75 μm ID/350 μm OD capillary
organic phase	0.2 g/ml TBAP in $CHCl_3$
aqueous phase	0.23 ppm crystal violet in 2 mM $Na_2B_4O_7$.
detection wavelength	600 nm/720 nm
injection time	10 seconds
solid line	λ = 600 nm
dash line	λ = 720 nm

Figure 3.10 Crystal Violet Output.
(b) organic phase: 0.2 g/ml TBAP in $CHCl_3$.

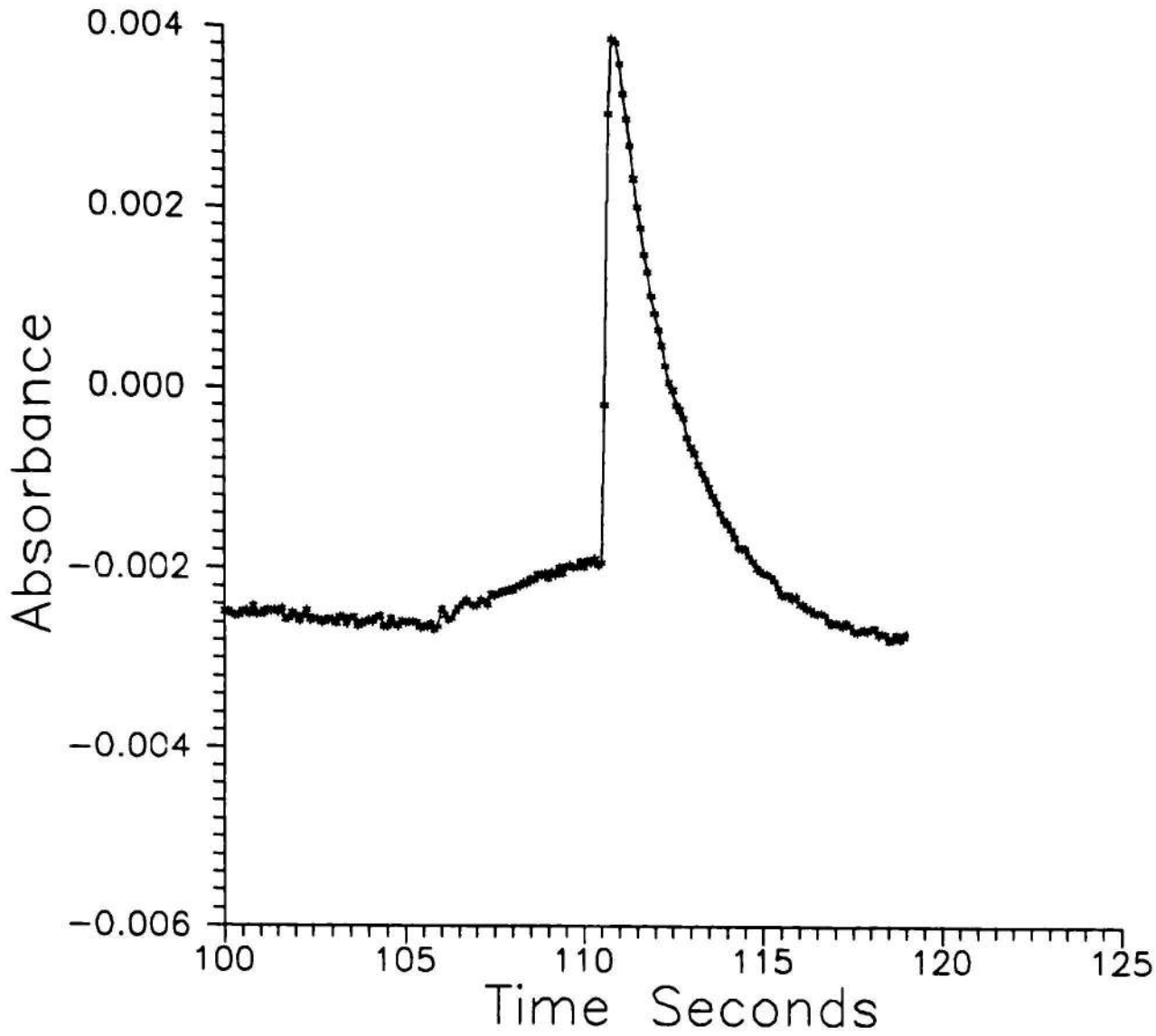

Experimental Conditions

high voltage	15 kV across 50 cm 75 μm ID/350 μm OD capillary
organic phase	0.2 g/ml TBAP in $CHCl_3$
aqueous phase	0.23 ppm crystal violet in 2 mM $Na_2B_4O_7$
detection wavelength	600 nm/720 nm
injection time	10 seconds

Figure 3.11 Net Crystal Violet Extraction Signal.
(b) organic phase: 0.2 g/ml TBAP in $CHCl_3$.

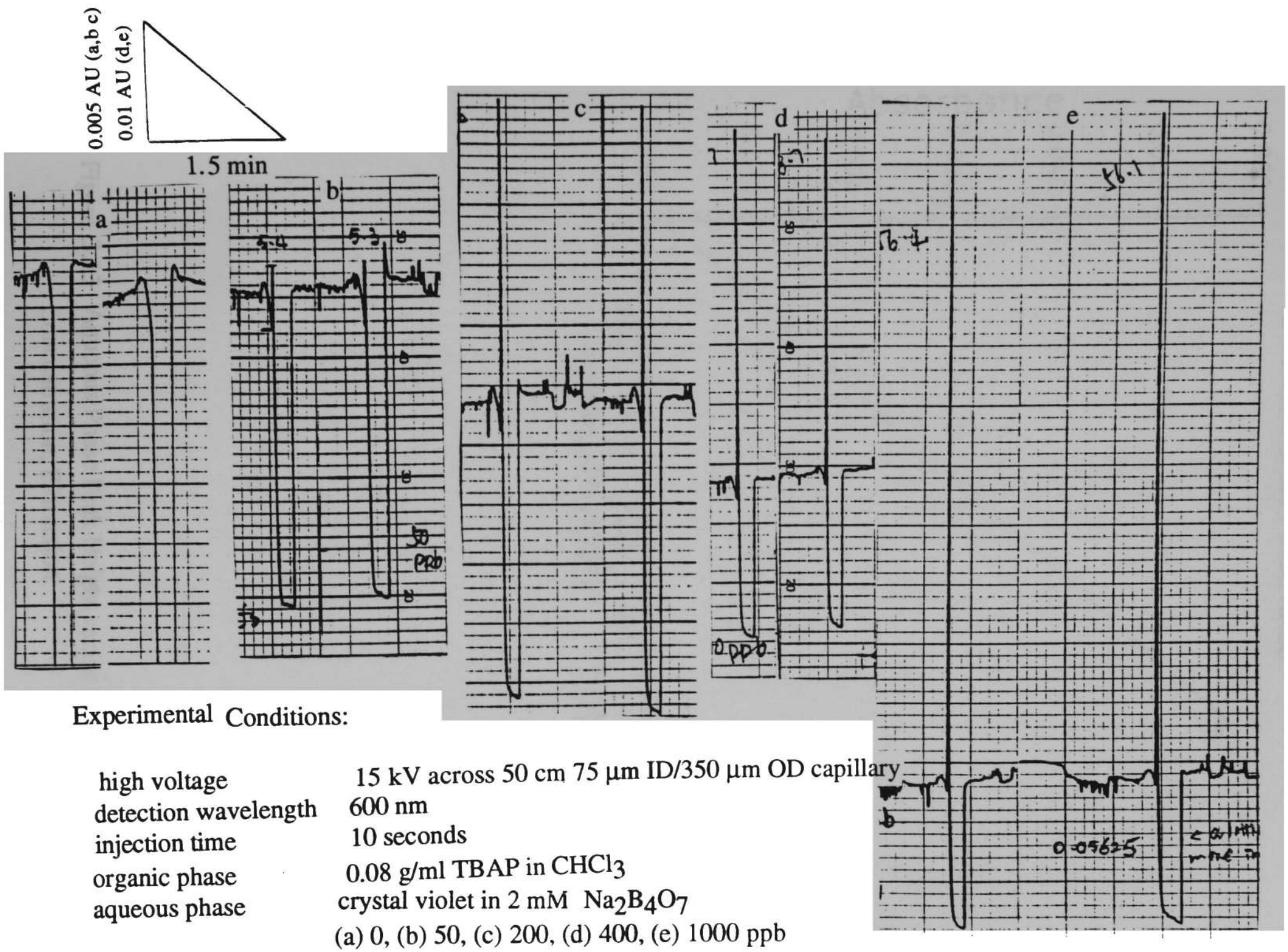

Experimental Conditions:

high voltage	15 kV across 50 cm 75 µm ID/350 µm OD capillary
detection wavelength	600 nm
injection time	10 seconds
organic phase	0.08 g/ml TBAP in $CHCl_3$
aqueous phase	crystal violet in 2 mM $Na_2B_4O_7$
	(a) 0, (b) 50, (c) 200, (d) 400, (e) 1000 ppb

Figure 3.12 Recorder Output, Extraction of Crystal Violet at Different Concentrations.

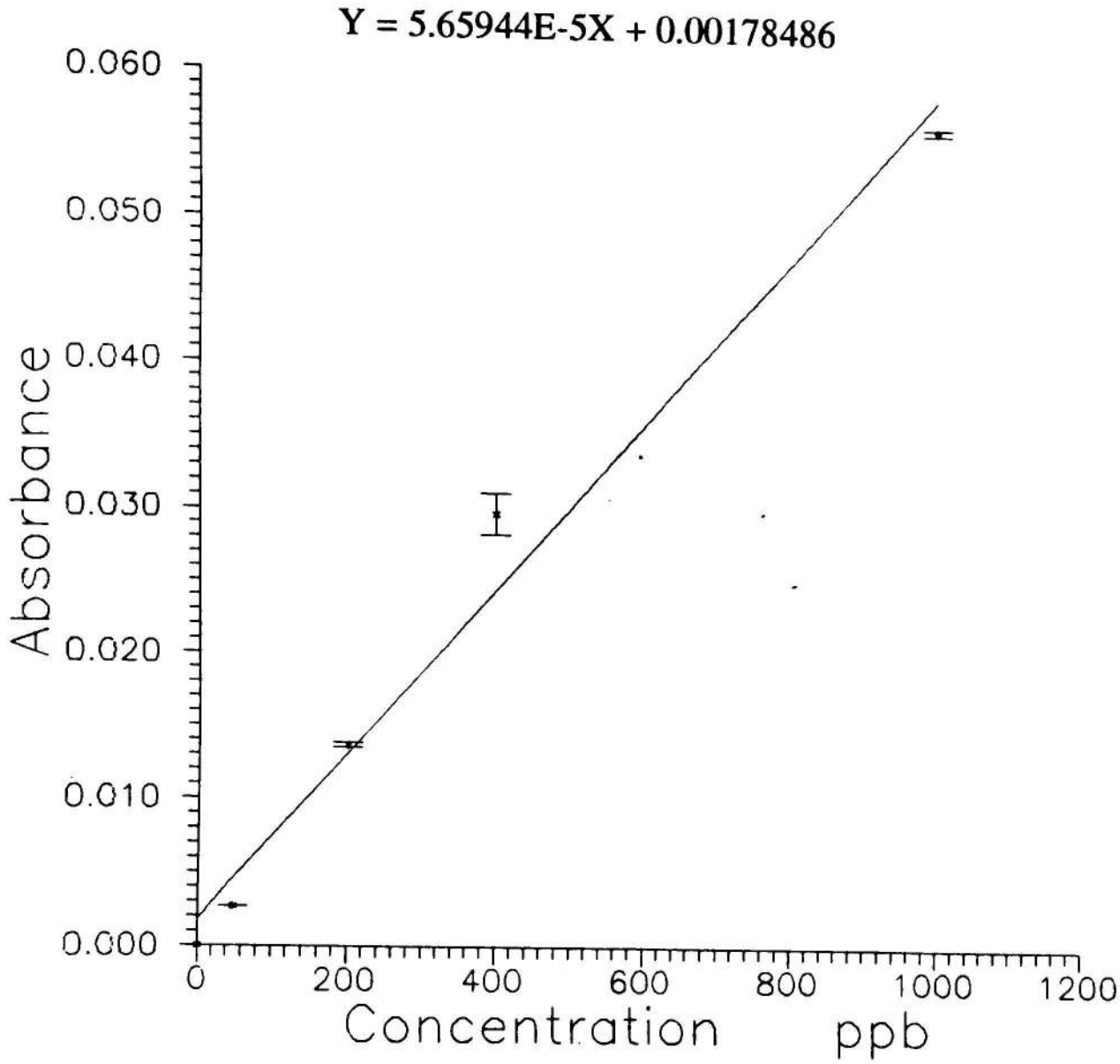

Figure 3.13 Aqueous Phase Peak Height versus Crystal Violet Concentration, Extraction.

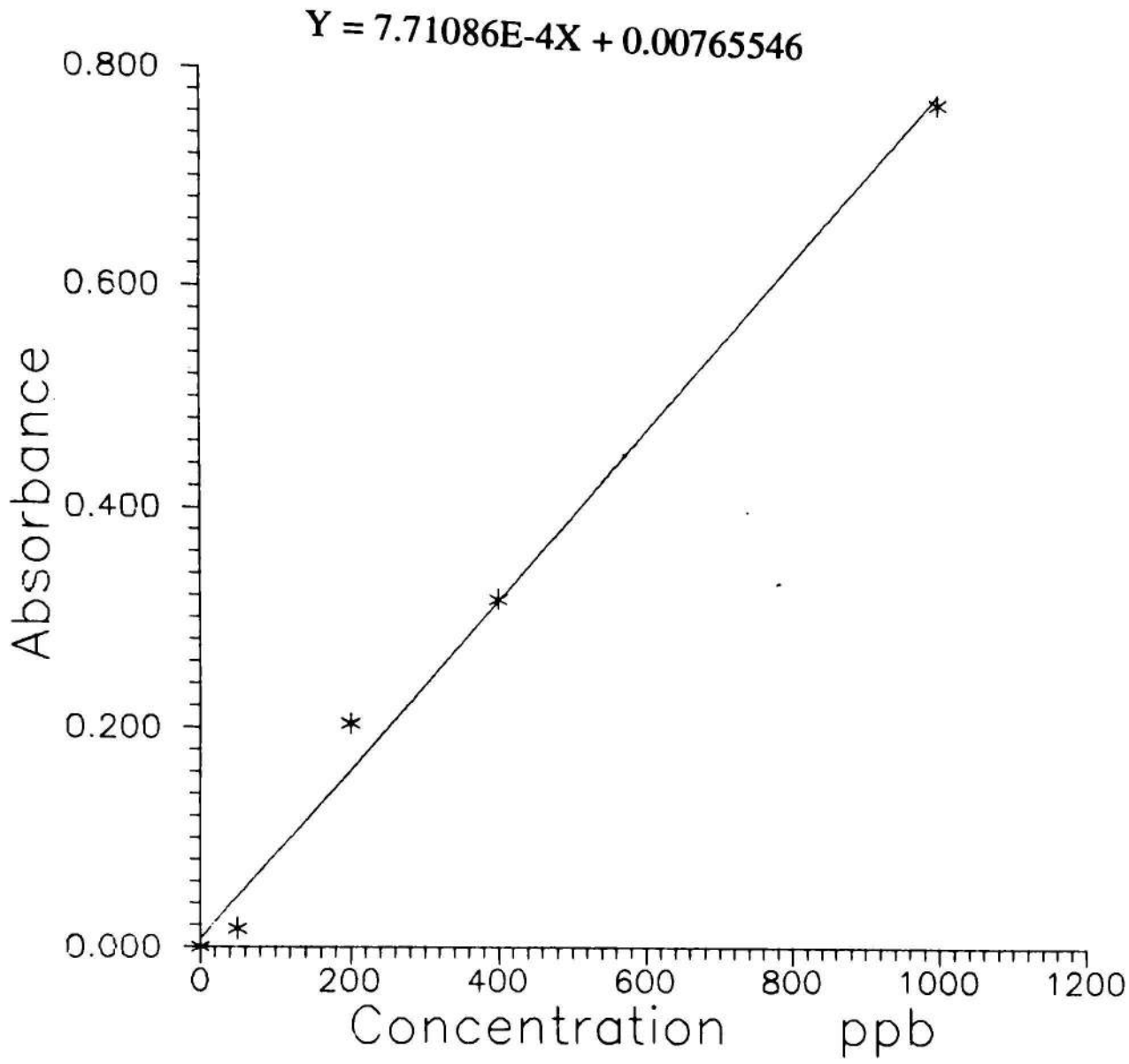

Figure 3.14 Calibration of Crystal Violet in 1 cm Cell.

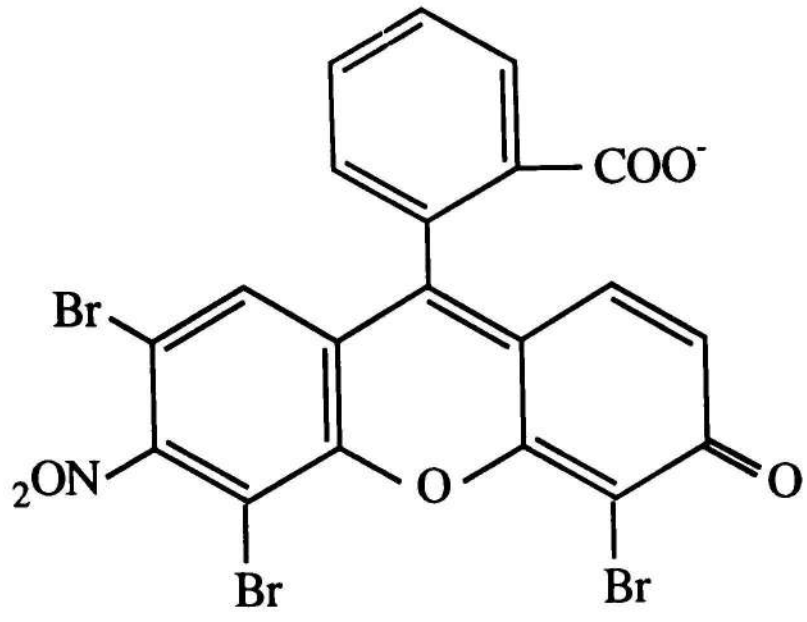

Figure 3.15 Structure of Eosin Y.

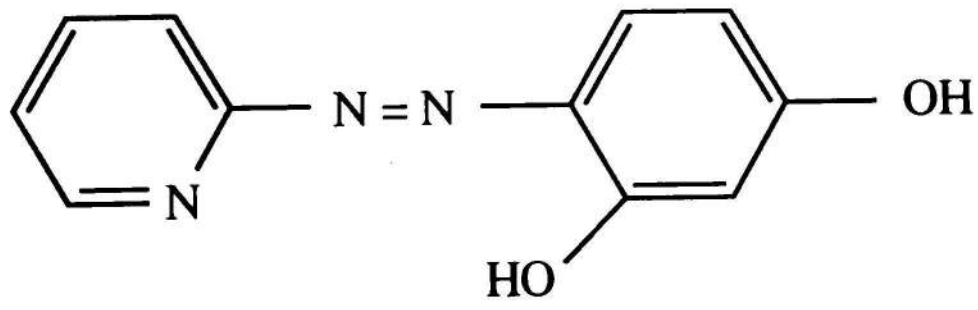

Figure 3.16 Structure of 4-(2-pyridylazo)-resorcinol (PAR).

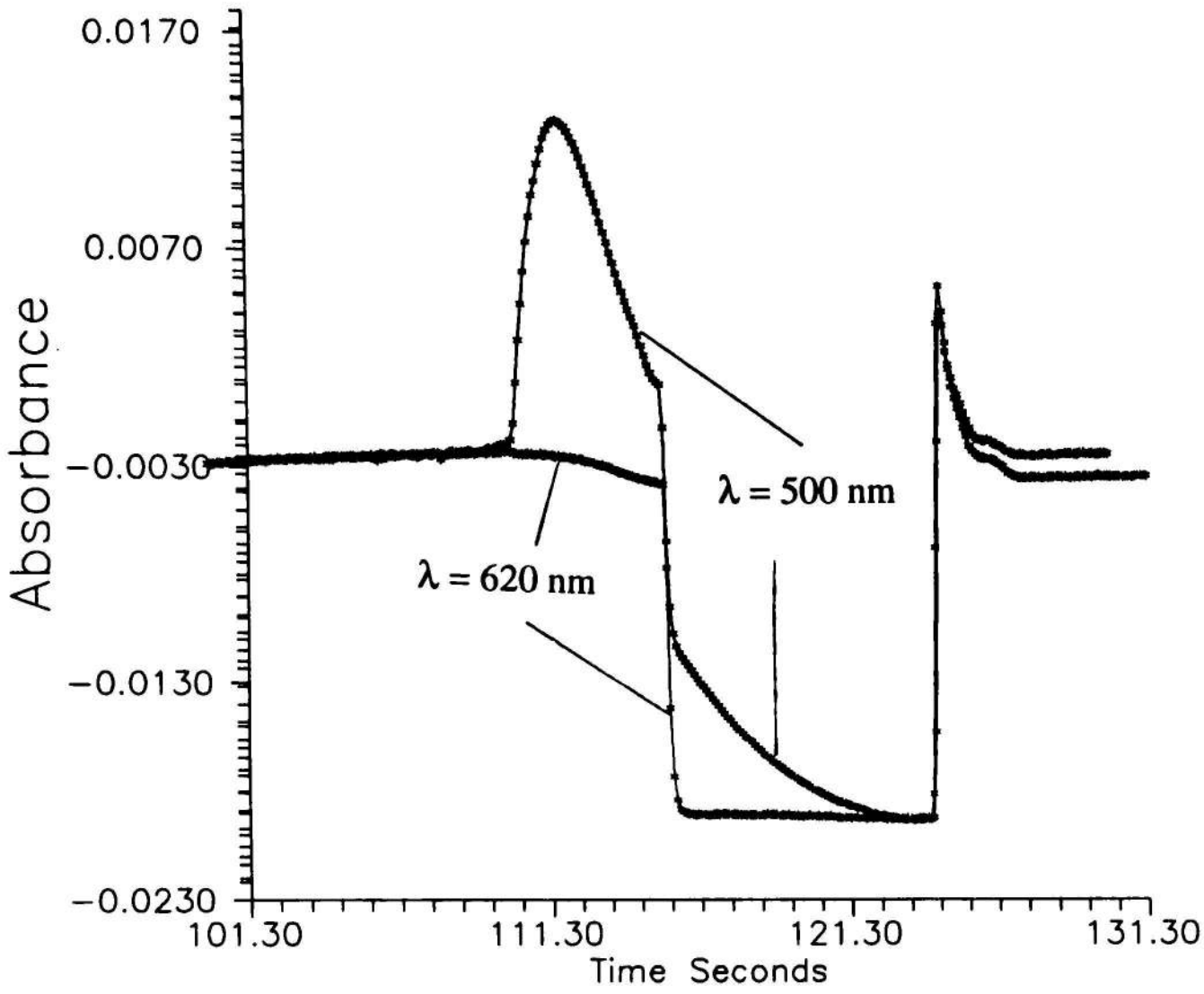

Experimental Conditions

high voltage	15 kV across 50 cm 75 μm ID/350 μm OD capillary
organic phase	0.2 g/ml TBAP in $CHCl_3$
aqueous phase	1 ppm Eosin Y in 2 mM $Na_2B_4O_7$
detection wavelength	500 nm/620 nm
injection time	10 seconds

Figure 3.17 Signal Output from Eosin Y Extraction.

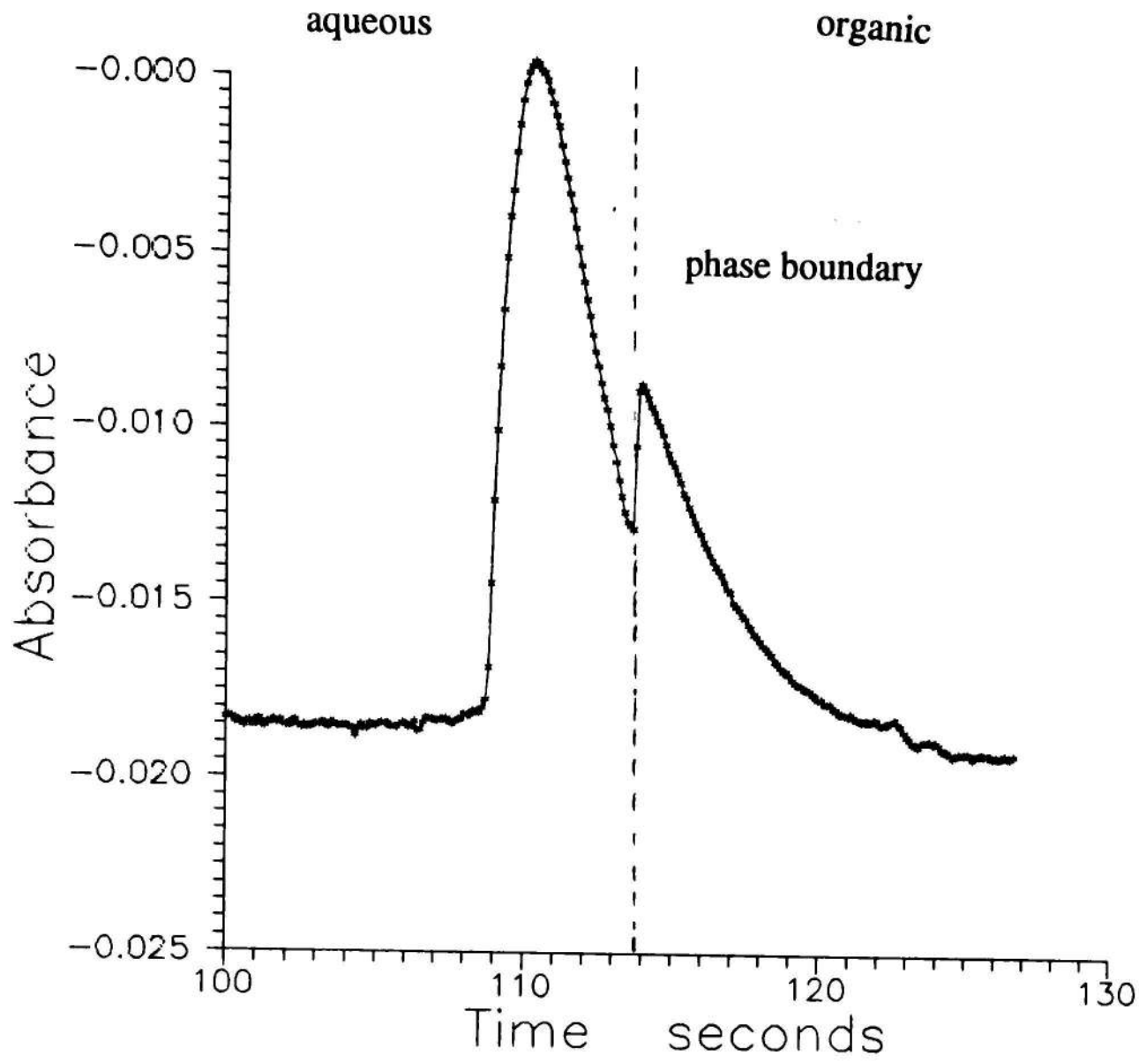

Experiment Conditions:

high voltage	15 kV across 50 cm 75 µm ID/350 µm OD capillary
organic phase	0.2 g/ml TBAP in $CHCl_3$
aqueous phase	1 ppm Eosin Y in 2 mM $Na_2B_4O_7$
detection wavelength	500 nm/620 nm
injection time	10 seconds

Figure 3.18 Net Signal from Eosin Y Extraction.

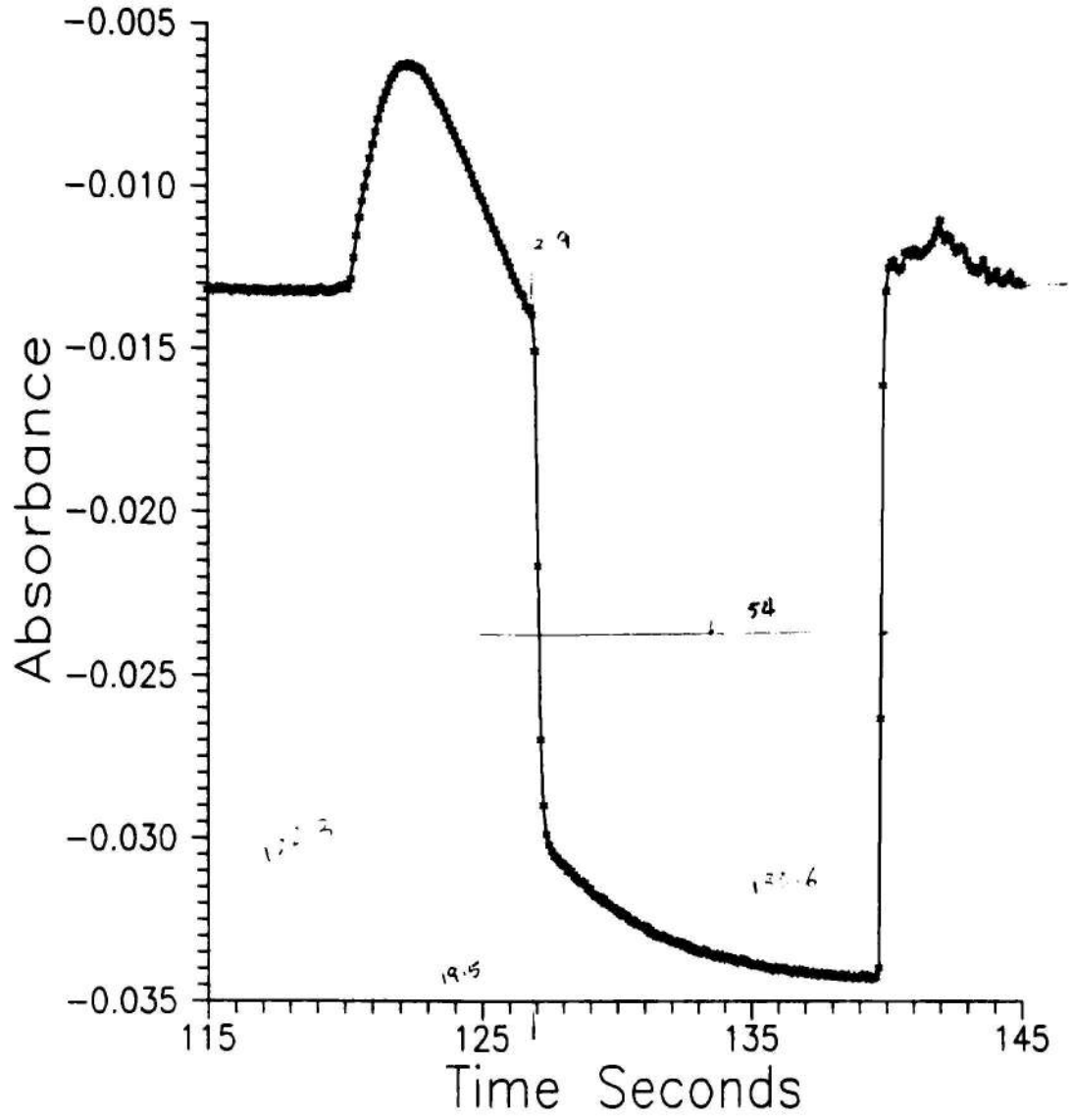

Experimental Conditions

high voltage	15 kV across 50 cm 75 μm ID/350 μm OD capillary
organic phase	0.1 g/ml TBAP in $CHCl_3$
aqueous phase	0.5 ppm Eosin Y in 2 mM $Na_2B_4O_7$
detection wavelength	500 nm
injection time	10 seconds

Figure 3.19 Eosin Y Extraction Experiment Using TBAP in $CHCl_3$.

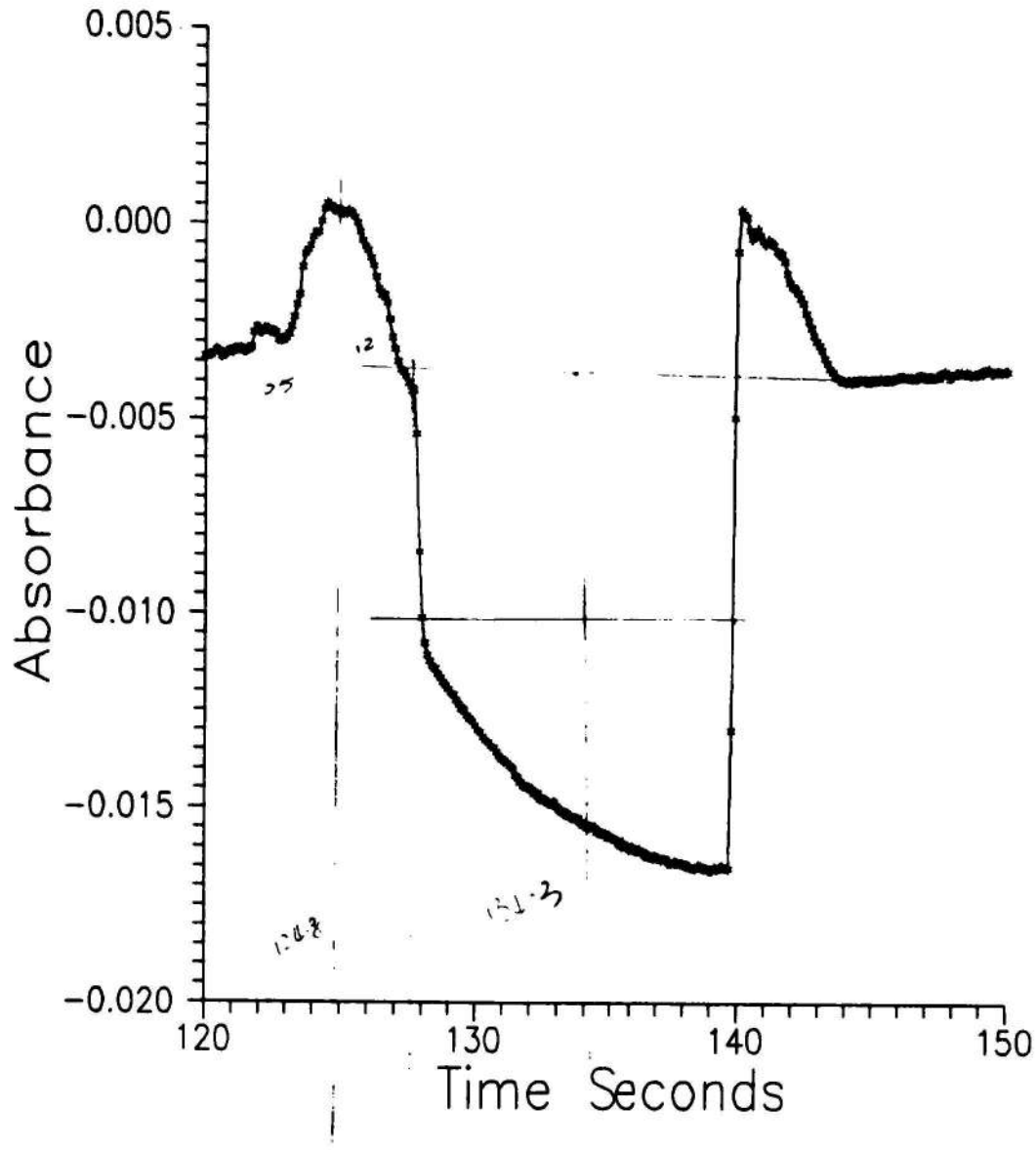

Experimental Conditions

high voltage	15 kV across 50 cm 75 μm ID/350 μm OD capillary
organic phase	0.1271 g/ml THAB in $CHCl_3$
aqueous phase	0.5 ppm Eosin Y in 2 mM $Na_2B_4O_7$
detection wavelength	500 nm
injection time	10 seconds

Figure 3.20 Eosin Y Extraction Experiment Using THAB in $CHCl_3$.

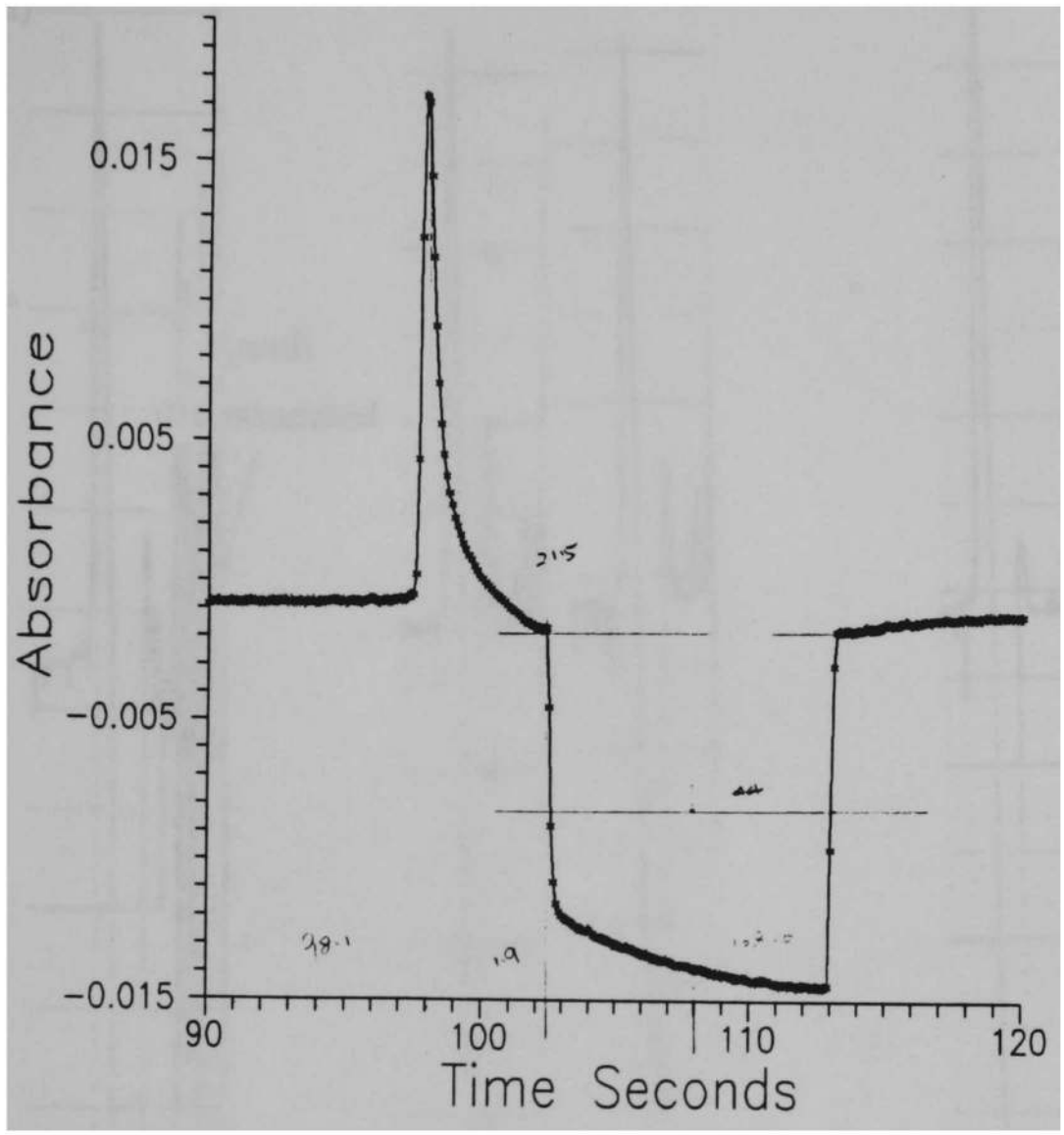

Experimental Conditions

high voltage	15 kV across 50 cm 75 μm ID/350 μm OD capillary
organic phase	0.1107 g/ml TPAB in $CHCl_3$
aqueous phase	0.5 ppm Eosin Y in 2 mM $Na_2B_4O_7$
detection wavelength	500 nm
injection time	10 seconds

Figure 3.21 Eosin Y Extraction Experiment Using TPAB in $CHCl_3$.

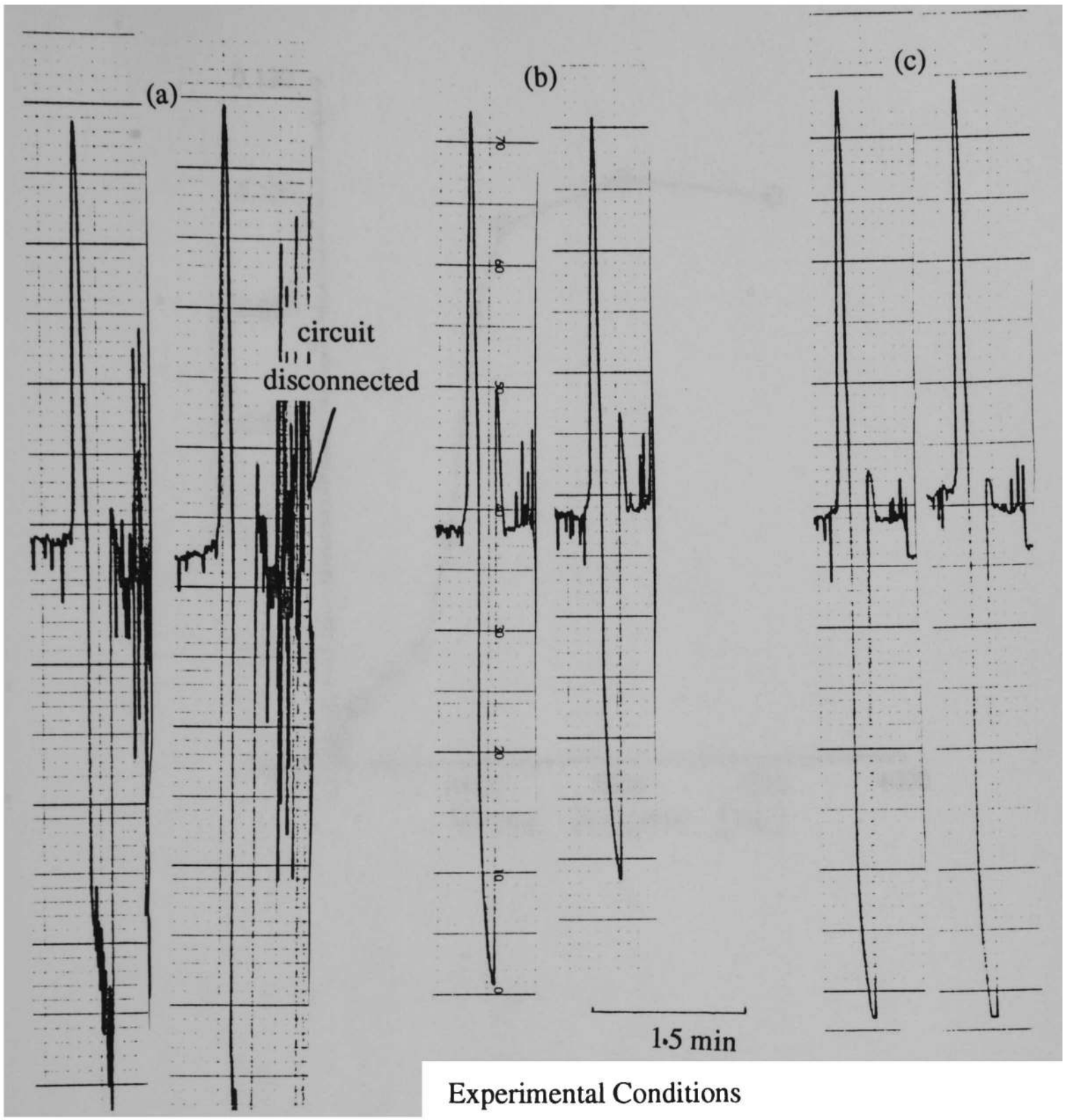

Experimental Conditions

high voltage	15 kV across 50 cm 75 μm ID/350 μm OD capillary
organic phase	different amount of TBAP in $CHCl_3$
	(a) 0.05 g/ml, (b) 0.1 g/ml, (c) 0.18 g/ml.
aqueous phase	1.6 ppm Eosin Y in 2 mM $Na_2B_4O_7$
detection wavelength	500 nm
injection time	10 seconds
full scale	0.05 AU

Figure 3.22 Independence of Aqueous Phase Peak Height on the Amount of TBAP for the Extraction of Eosin Y.

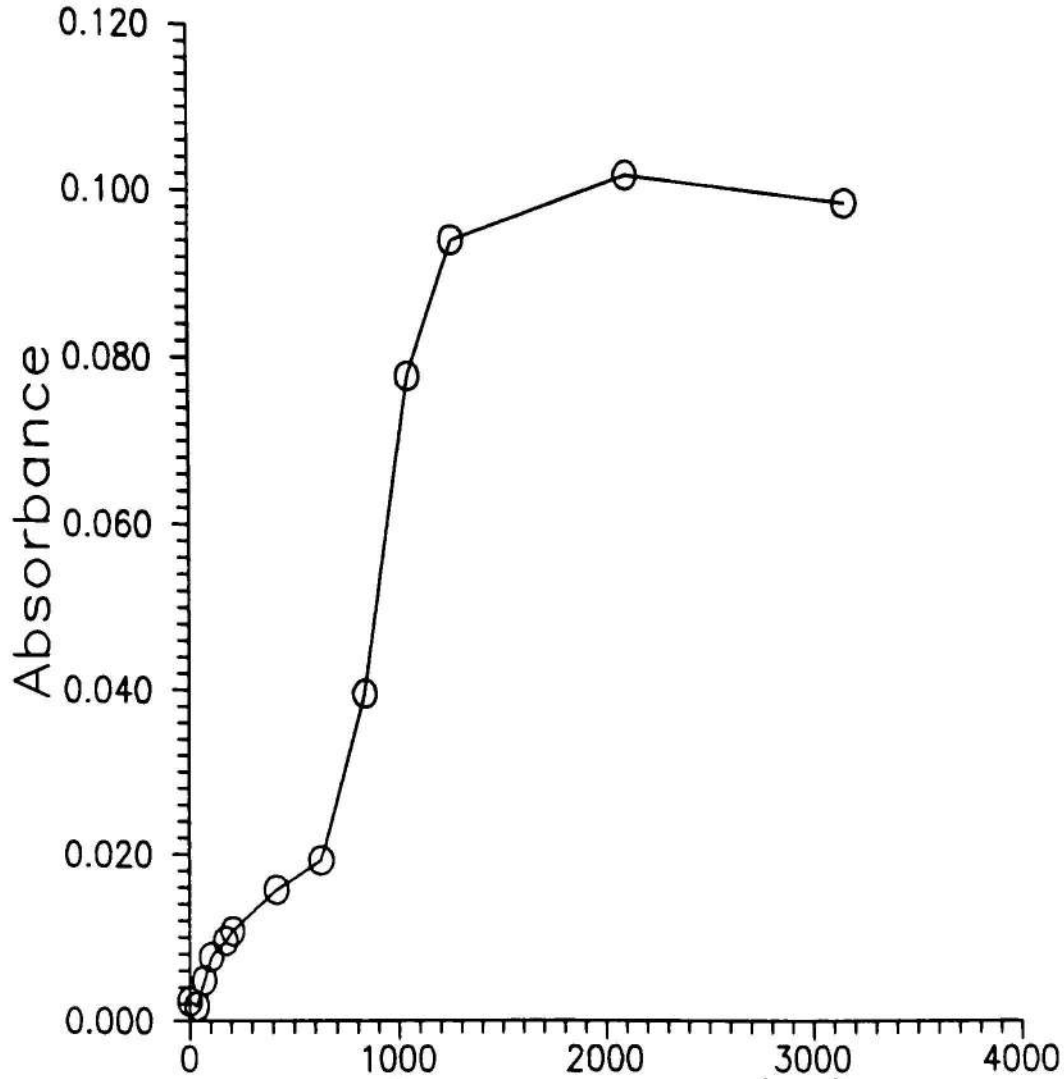

Figure 3.23 Effect of the Eosin Y Solution Rinse Volume on the Positive Aqueous Phase signal.

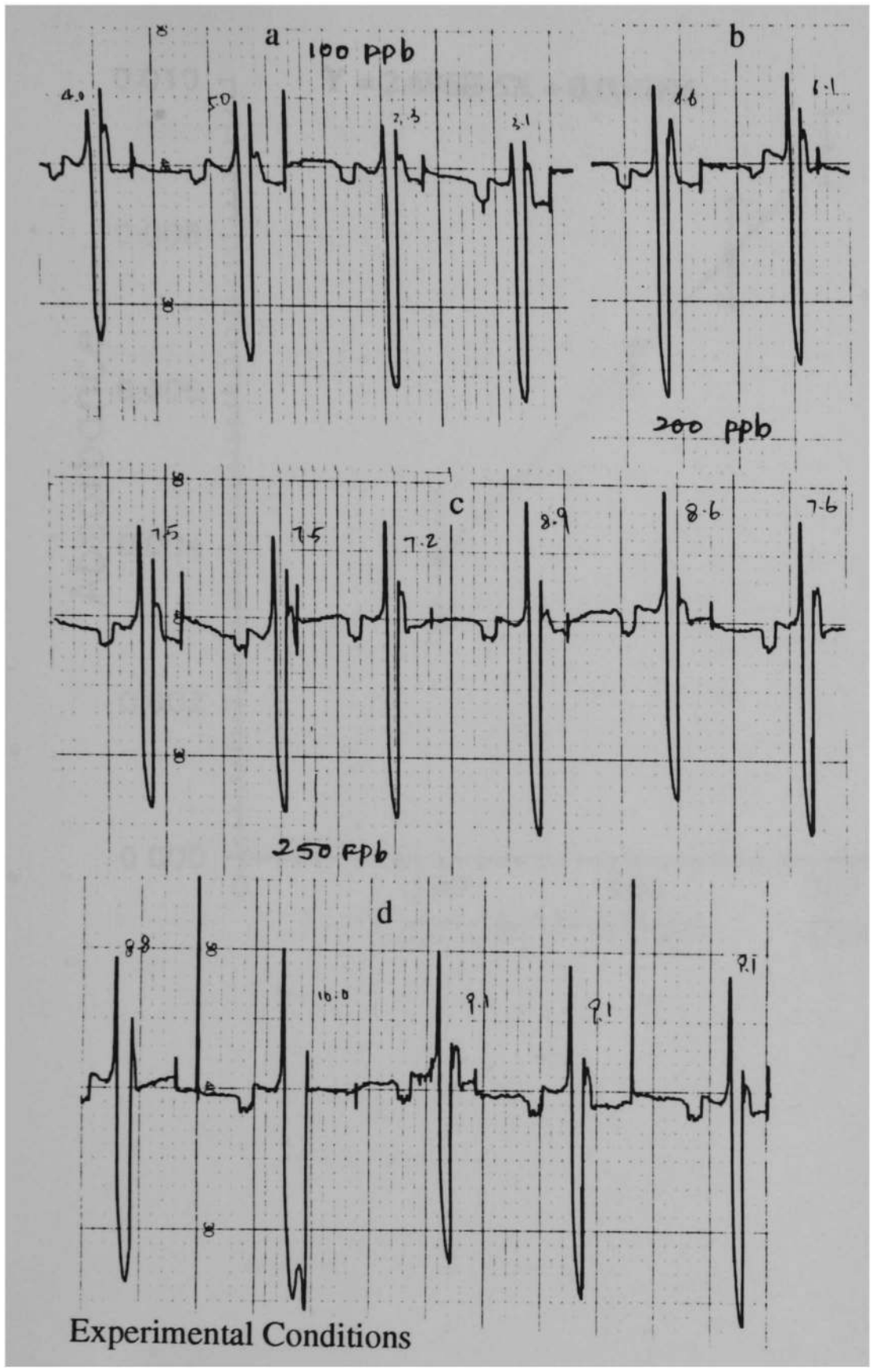

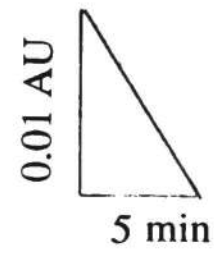

high voltage	15 kV across 50 cm 75 µm ID/350 µm OD capillary
organic phase	0.4 g/ml TBAP in $CHCl_3$
aqueous phase	Eosin Y in 2 mM $Na_2B_4O_7$ (a) 100, (b) 200, (c) 250, (d) 300 ppb
detection wavelength	500 nm
injection time	30 seconds

Figure 3.24 Recorder Output, Extraction of Eosin Y at Different Concentrations.

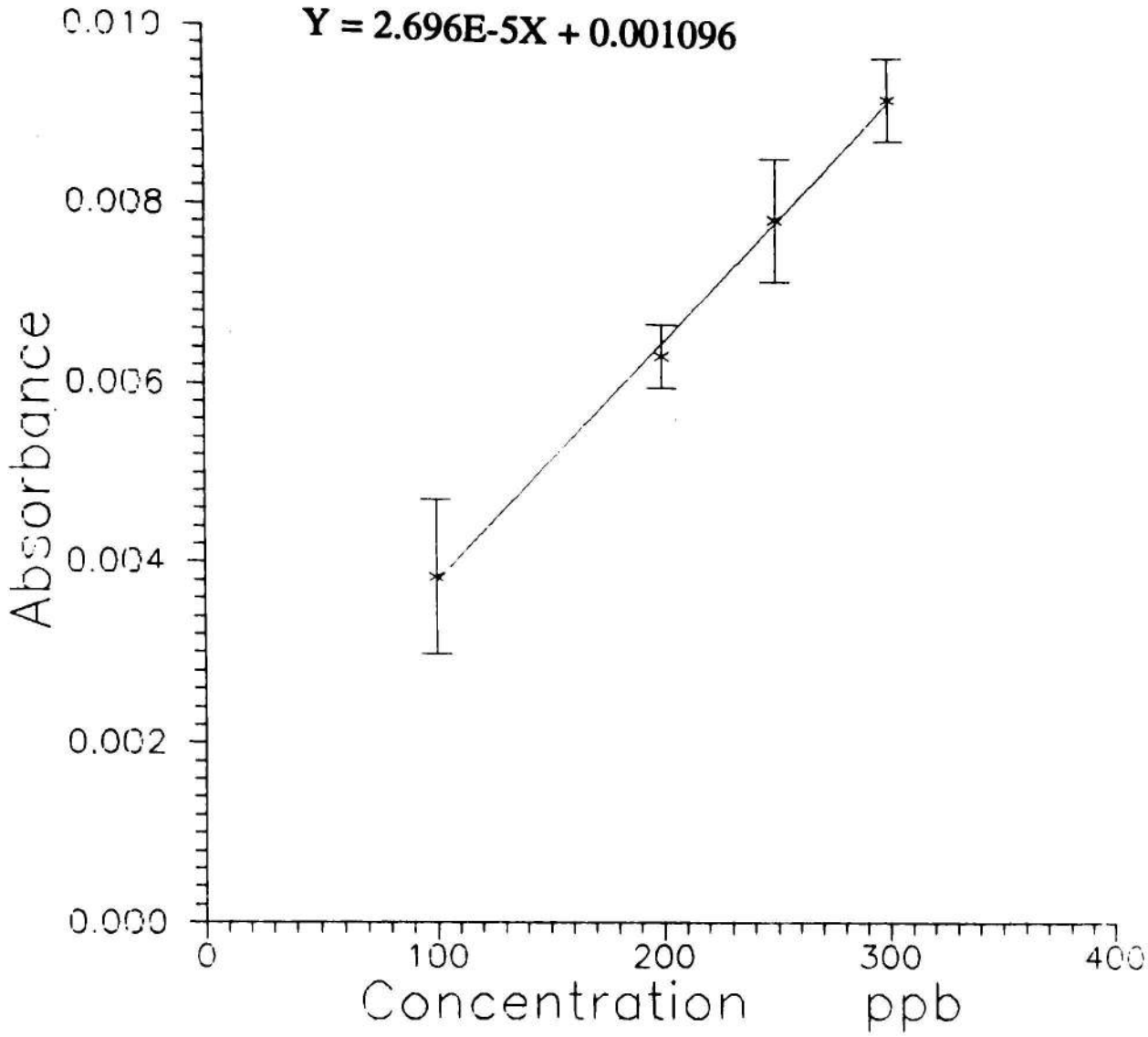

Figure 3.25 Aqueous Phase Peak Height versus Eosin Y Concentration, Extraction.

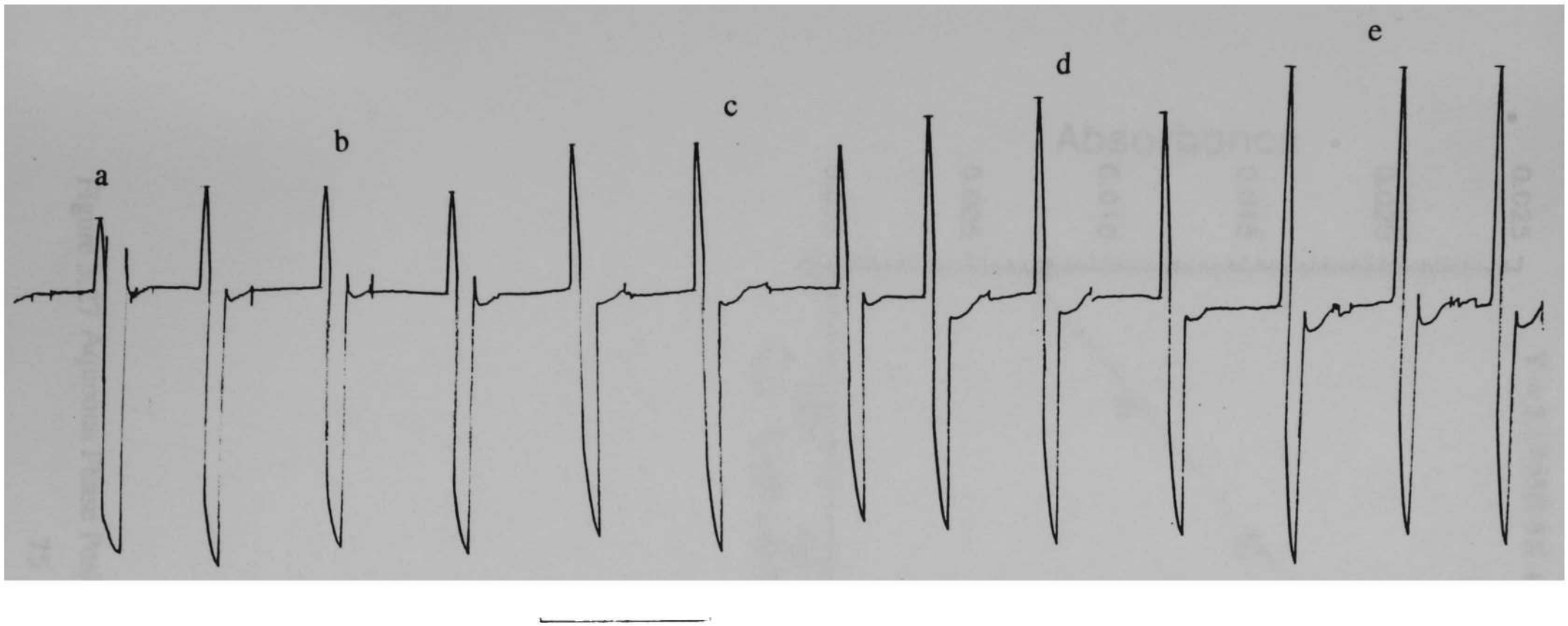

Experimental Conditions

high voltage	15 kV across 50 cm 75 µm ID/350 µm OD capillary
organic phase	0.2 g/ml TBAP in $CHCl_3$
aqueous phase	Co-PAR in 2 mM $Na_2B_4O_7$ (a) 0, (b) 200, (c) 400, (d) 600, (e) 800 ppb
detection wavelength	510 nm
injection time	10 seconds
full scale	0.1 AU

Figure 3.26 Recorder Output, Extraction of Co-PAR at Different Concentrations.

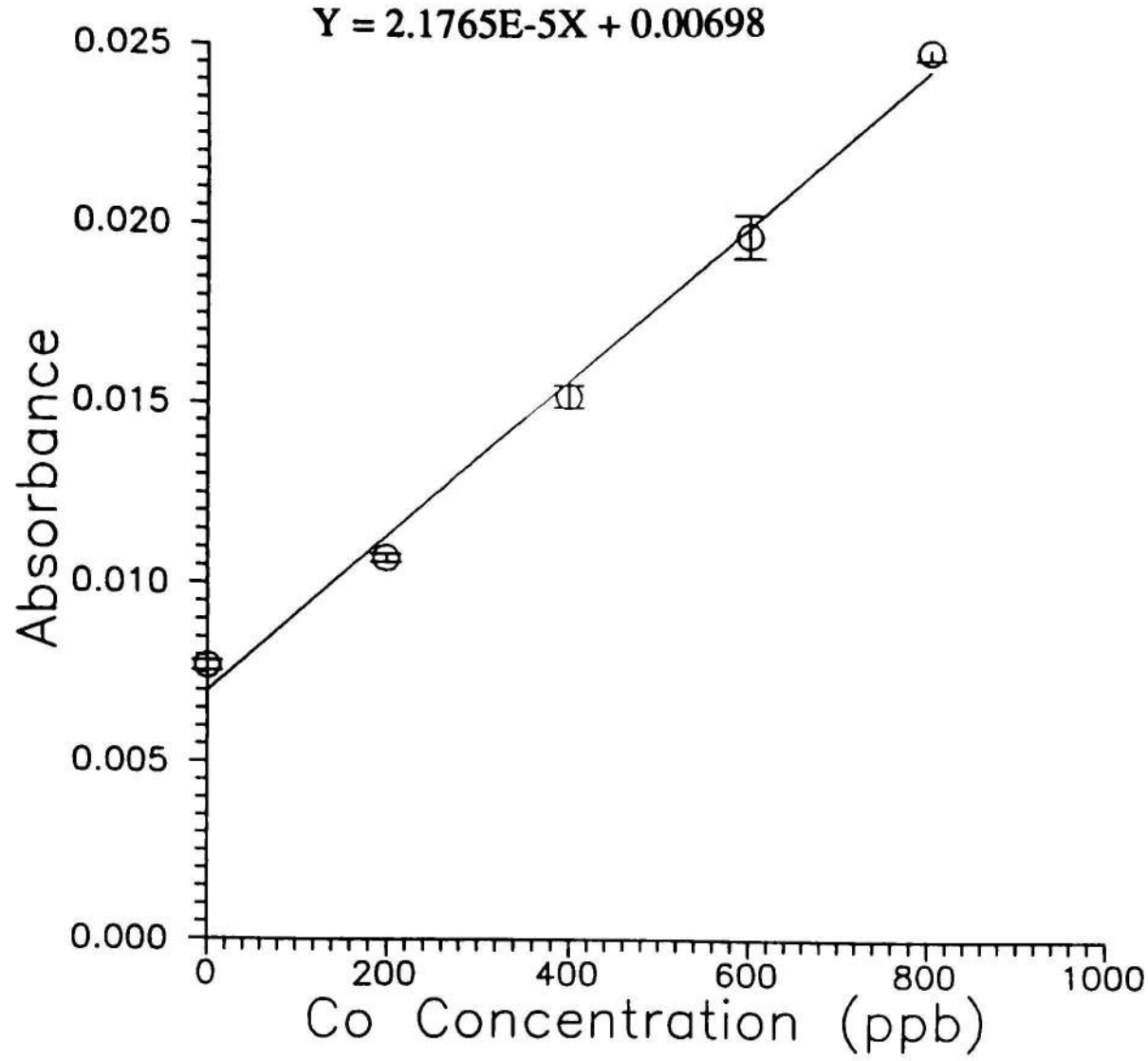

Figure 3.27 Aqueous Phase Peak Height versus Co^{2+} Concentration, Extraction.

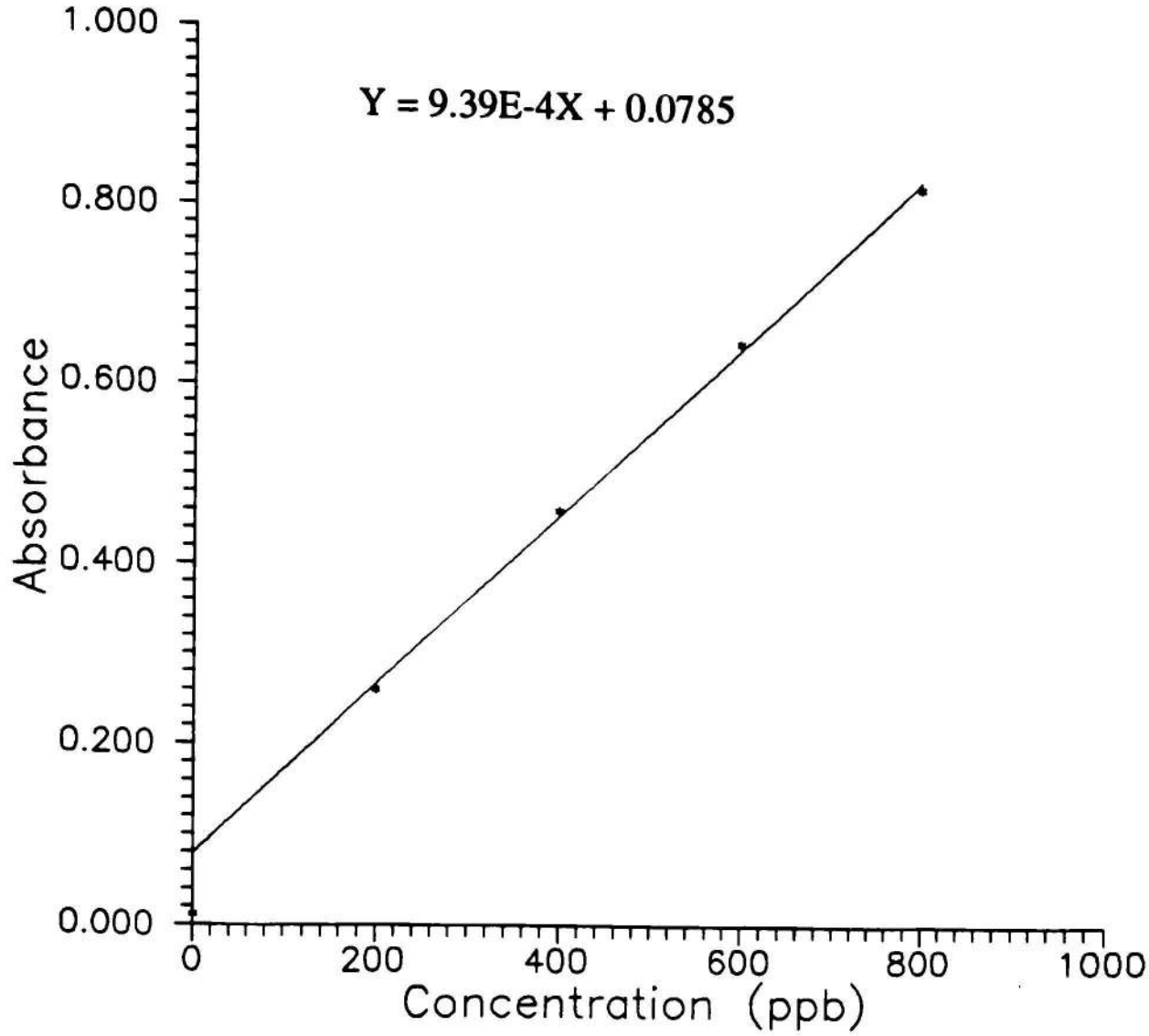

Figure 3.28 Calibration of Co-PAR in 1 cm Cell.

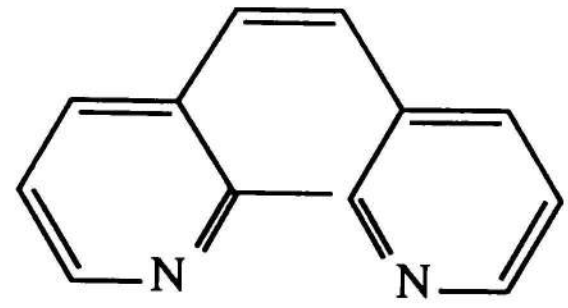

Figure 3.29 Structure of ϱ-Phenanthroline.

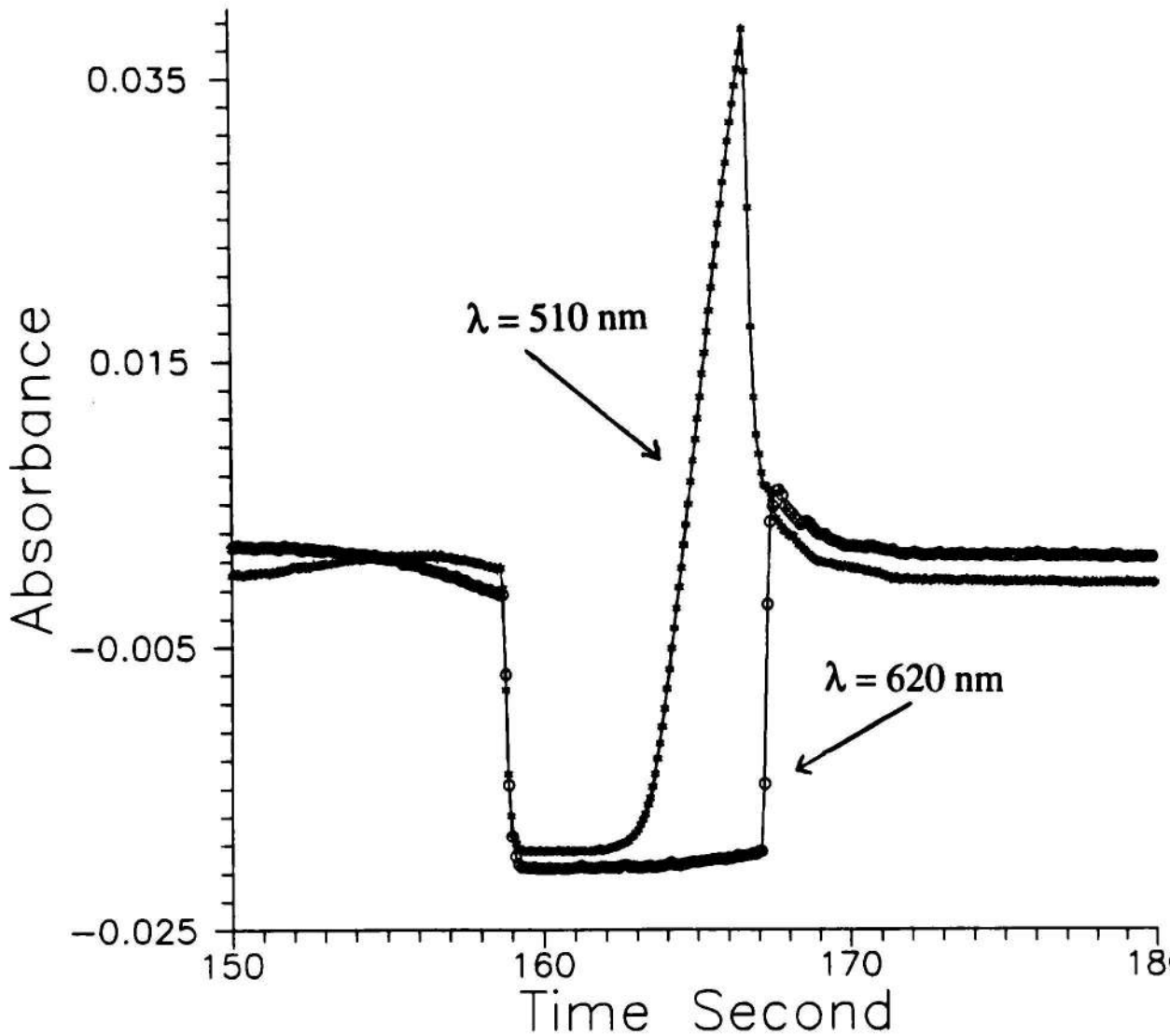

Experimental Conditions

high voltage	15 kV across 50 cm 75 µm ID/350 µm OD capillary
organic phase	0.1 g/ml TBAP in $CHCl_3$
aqueous phase	700 ppb Fe-(ϱ-Phen)$_3^{2+}$ in 2 mM $Na_2B_4O_7$ + 1 mM ϱ-Phen
detection wavelength	510 nm/620 nm
injection time	10 seconds

Figure 3. 30 Fe-(ϱ-Phen)$_3^{2+}$ Output.

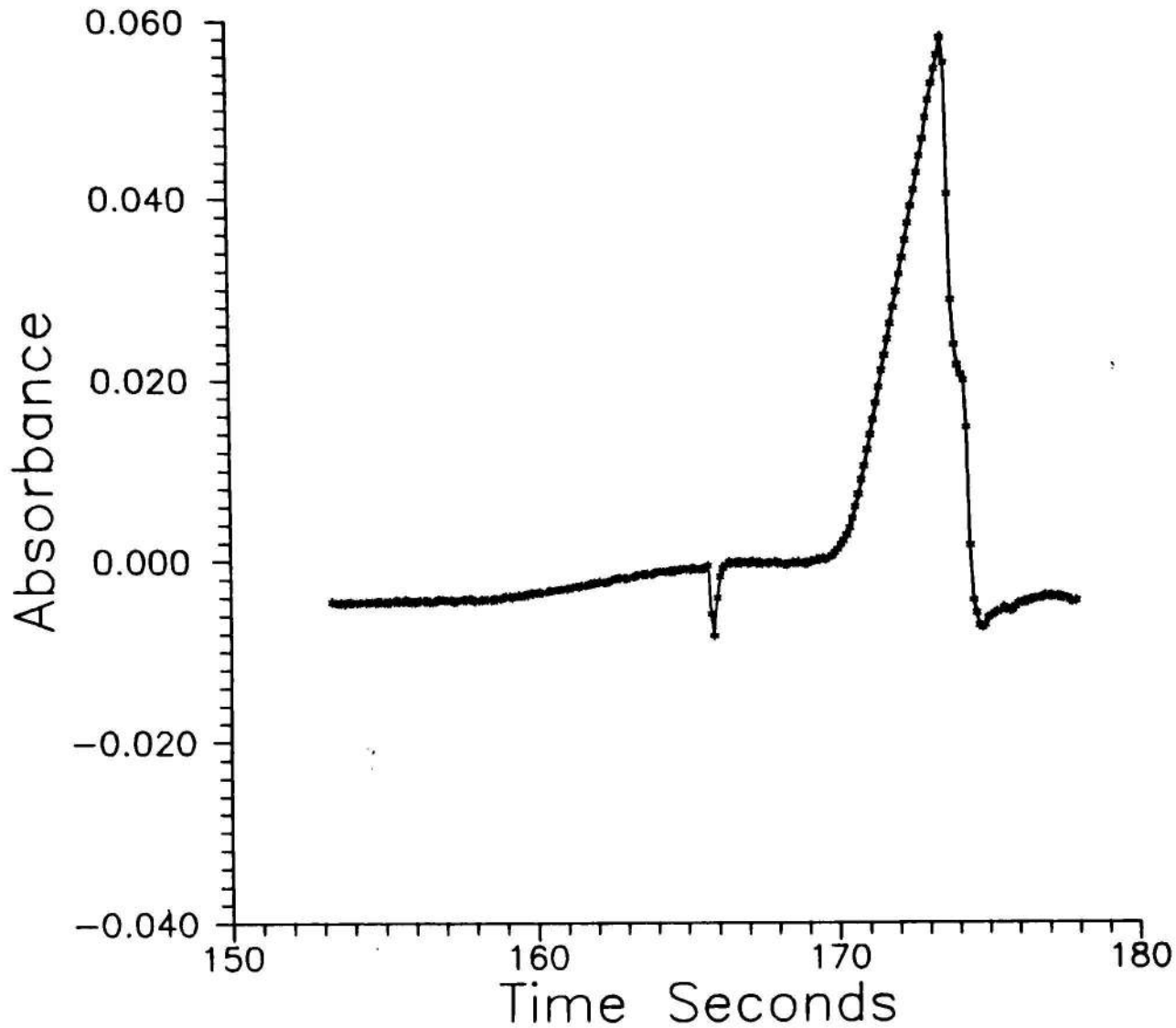

Experimental Conditions

high voltage	15 kV across 50 cm 75 µm ID/350 µm OD capillary
organic phase	0.1 g/ml TBAP in $CHCl_3$
aqueous phase	700 ppb Fe-(ϱ-Phen)$_3^{2+}$ in 2 mM $Na_2B_4O_7$ + 1 mM ϱ-Phen
detection wavelength	510 nm/620 nm
injection time	10 seconds

Figure 3.31 Net Fe-(ϱ-Phen)$_3^{2+}$ Extraction Signal.

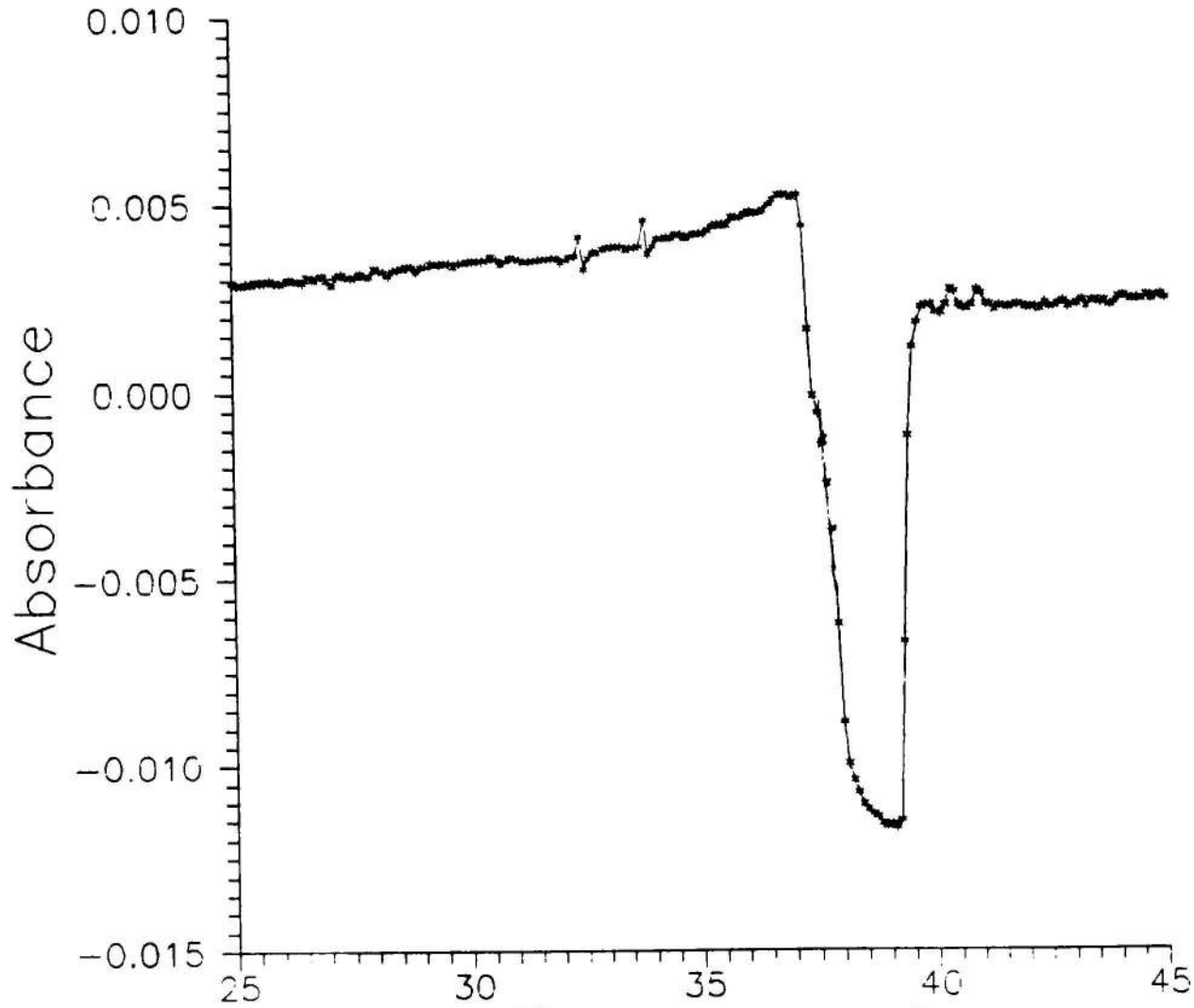

Experimental Conditions

organic phase	0.1 g/ml TBAP in $CHCl_3$
aqueous phase	700 ppb Fe-(ϱ-Phen)$_3^{2+}$ in 2 mM $Na_2B_4O_7$ + 1 mM ϱ-Phen
detection wavelength	510 nm
injection time	10 seconds
high voltage	-15 kV across 50 cm 75 µm ID/350 µm OD capillary & compressed air pumping

Figure 3.32 Fe-(ϱ-Phen)$_3^{2+}$ Output with Reverse Polarized High Voltage & Compressed Air Pumping (a).

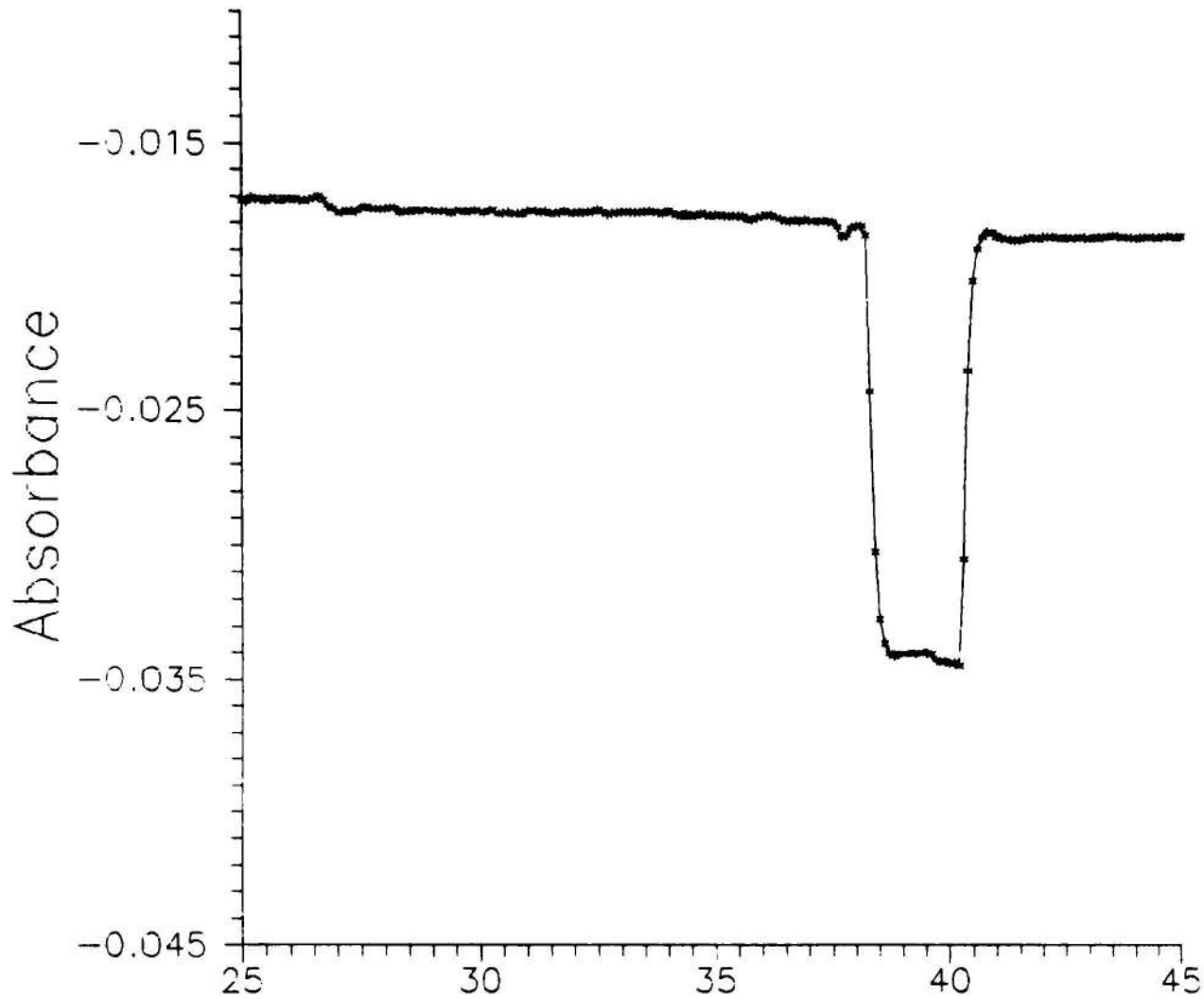

Experimental Conditions

organic phase	0.1 g/ml TBAP in $CHCl_3$
aqueous phase	700 ppb Fe-(ϱ-Phen)$_3^{2+}$ in 2 mM $Na_2B_4O_7$ + 1 mM ϱ-Phen
detection wavelength	620 nm
injection time	10 seconds
high voltage	-15 kV across 50 cm 75 µm ID/350 µm OD capillary & compressed air pumping

Figure 3.33 Fe-(ϱ-Phen)$_3^{2+}$ Output with Reverse Polarized High Voltage & Compressed Air Pumping (b).

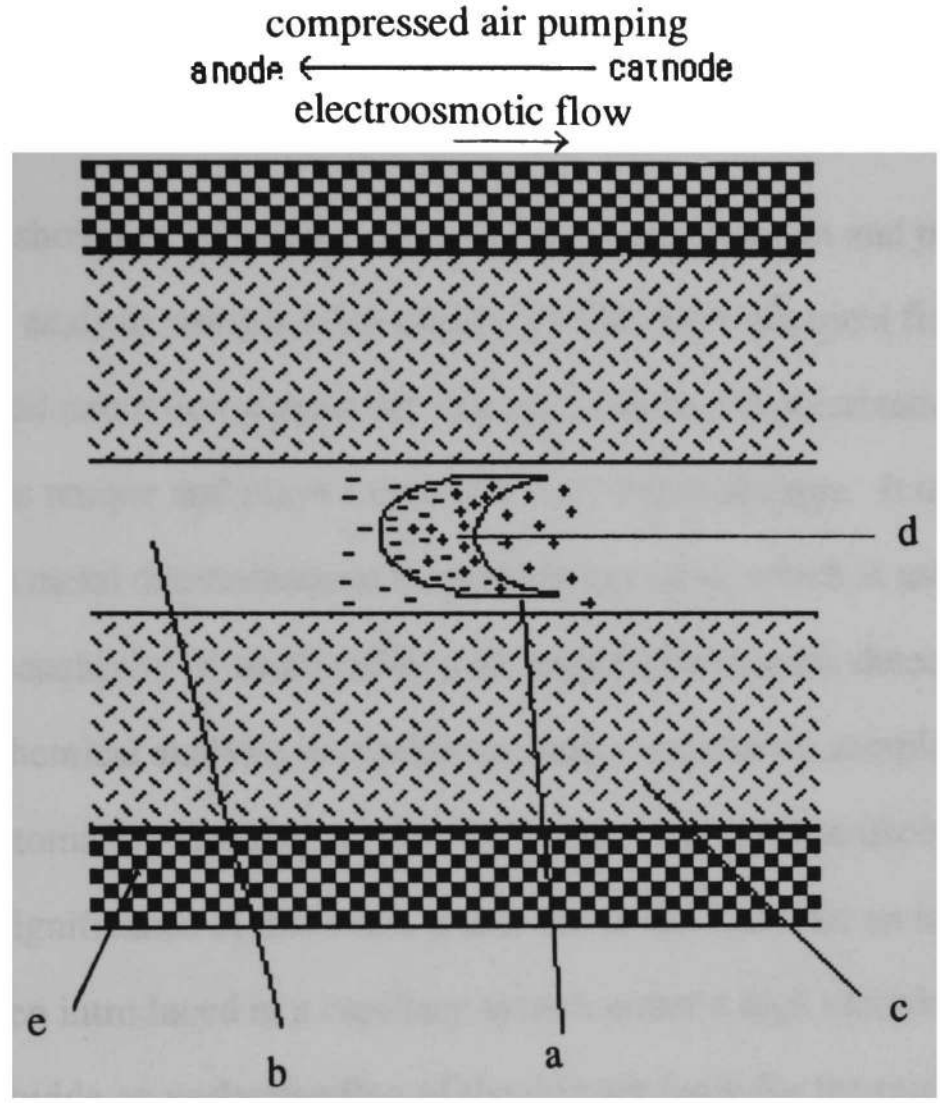

a aqueous film
b bulk electrolytes
c 75 μm ID/350 μm OD capillary
d organic segment
e polyimide coating

\+ quaternary ammonium cation or net positive charge in organic segment
\- pairing anion or net negative charge in organic segment

Figure 3. 34 Polarization of Organic Segment under Reverse Polarized High Voltage & Compressed Air Pumping.

CHAPTER IV

CONCLUSION

The work shown in this thesis presents a new phenomenon and potentially a new tool in chemical analysis using a silica capillary under high electrical field. The unusual concentration and extraction signals are dependent upon the polarization of the organic segment. This is unique and plays a crucial role in this technique. It offers opportunities to perform trace metal determinations in capillary systems, which is usually not possible due to the low sensitivity of small radial path length photometric detectors. Other inherent advantages of chemical analysis in capillary systems, e.g., small sample consumption, feasibility of automation and high sample throughput, are not sacrificed.

Another significance of this work is that this is the first time an immiscible organic segment has been introduced in a capillary system under a high electric field. I have attempted to provide an understanding of the driving force for the migration of an organic segment in such a system. In addition, this provides a novel avenue of quantitatively delivering nanoliter quantity of organic solvents with excellent reproducibility.

REFERENCES

1 Kertes, A. S. and Marcus, Y., ed., *Solvent Extraction Research*, Wiley & Sons, Inc.: New York, 1969.

2 Morrison, G. H. and Freiser, H., *Solvent Extraction in Analytical Chemistry*, John Wiley & Sons, Inc.: New York, 1957, p4.

3 Dyrssen, D.; Liljenzin, J.-O. and Rydberg, J., ed., *Solvent Extraction Chemistry*, Wiley & Sons, Inc.: New York, 1967.

4 IUPAC, *Spectrophotometric Data for Colorimetric Analysis*, Butterworths: London, 1963.

5 Sandell, E. B.and Onishi, H., *Photometric Determination of Traces of Metals. General Aspects*, Wiley & Sons, Inc.: New York, 1978.

6 Onishi, H., *Photometric Determination of Traces of Metals. Individual Metals, Aluminum to Lithium,* Wiley & Sons, Inc.: New York, 1986.

7 Ruzicka, J. and Hansen, E. H., *Flow Injection Analysis*, John Wiley & Sons, Inc.: New York, 1981, p76.

8 Karlberg, B. and Thelander, S., *Anal. Chim. Acta*, 98, 1978, p1.

9 Bergamin-Filho, H.; Medeiros, J. X.; Reis, B. F. and Zagatto, E. A. G., *Anal. Chim. Acta*, 101, 1978, p9.

10 Kuban, V., *Critical Reviews in Analytical Chemistry*, 22(6), 1991, p477.

11 Thommen, C.; Fromageat, A.; Ubergfel, P. and Widmer, H. M., *Anal. Chim. Acta*, 234, 1990, p141.

12 Liu, H. and Dasgupta, P. K., "Flow-Injection Extraction without Phase Separation Based on Dual-Wavelength Spectrophotometry," *Anal. Chim. Acta*, to be published.

13 Kuban, V. and Ingman, F., *Anal. Chim. Acta*, 245, 1991, p251.

14 Snyder, L. R. and Adler, H. J., *Anal. Chem.*, 48, 1976a, p1017.

15 Snyder, L. R. and Adler, H. J., *Anal. Chem.*, 48, 1976b, p1022.

16 Nord, L. and Karlberg, B., *Anal. Chim. Acta*, 164, 1984, p233.

17 Ruzicka, J. and Hansen, E. H., *Flow Injection Analysis*, John Wiley & Sons, Inc.: New York, 1981, p109.

18 Olesik, S. V.; French, S. B. and Novotny, M., *Anal. Chem.*, 58, 1986, p2256.

19 Tissjen, R., *Anal. Chim. Acta*, 114, 1980, p71.

20 van der Linden, W. E., *Anal. Chim. Acta*, 180, 1986, p20.

21 Jorgenson, J. W. and Lukacs, K. D., *Anal. Chem.*, 53, 1981, p1298.

22 Grossman, P. D. and Colburn, J. C., *Capillary Electrophoresis. Theory and Practice,* Academic Press, Inc.: New York, 1992.

23 Jandik, P. and Bonn, G., *Capillary Electrophoresis of Small Molecules and Ions*, VCH: New York, 1993.

24 Harmon, B. J.; Patterson, D. H. and Regnier, F. E., *Anal. Chem.*, 65, 1993, p2655.

25 Bao, J. and Regnier, F. E., *J. Chromatogr.*, 608, 1992, p217.

26 Liu, S. and Dasgupta, P. K., *Anal. Chim. Acta*, 268, 1992, p1.

27 Liu, S. and Dasgupta, P. K., *Anal. Chim. Acta*, 283, 1993, p739.

28 Rose, D. J. and Jorgenson, J. W., *Anal. Chem.*, 60, 1988, p624.

29 Huang, X., Gordon, M. J. and Zare, R. N., *Anal. Chem.*, 60, 1988, p377.

30 Tsuda, T. and Zare, R. N., *J. Chromatogr.*, 264, 1983, p385.

31 Deml, M.; Foret, F. and Bocek, P., *J. Chromatogr.*, 320, 1985, p159.

32 Tehrani, J.; Macomber, R. and Day, L., *High Resolut. Chromatogr.*, 14, 1991, p10.

33 Tsuda, T.; Mizuno, T. and Akiyama, *J., Anal. Chem.*, 59, 1987, p799.

34 Dordon, G. B., *United States Patent*, 5061361, Oct. 15, 1991.

35 Grant, I. H. and Steuer, J., *Microcolumn Sep.*, 2, 1990, p14.

36 Chervet, J. P.; Vrsem, M.; Salzmann, J. P. and Vannoort, R. W., *J. High Resolut. Chromatogr.*, 12, 1989, p278.

37 Chervet, J. P., *United States Patent*, 5057216, Oct. 15, 1991.

38 Liu, S. and Dasgupta, P. K., *Anal. Chim. Acta*, 283, 1993, p747.

39 Liu, H.; Dasgupta, P. K. and Zheng, H., *Talanta*, 40(9), 1993, p1331.

40 Wang, T.; Aiken, J. H.; Huie, C. W. and Hartwick, R. A., *Anal. Chem.*, 63, 1991, p1372.

41 Dasgupta, P. K. and Rhee, J.-S., *Anal. Chem.*, 59, 1987, p783.

42 Jandik, P. and Bonn, G., *Capillary Electrophoresis of Small Molecules and Ions*, VCH: New York, 1993, p21.

43 Hammann, C. H. and Vielstich, W., *Electrochemie I, 2nd ed.*, VCH: Weinheim, Germany, 1985.

44 Smoluchowski, M. V., *Physik. Z.*, 6, 1905, p530.

45 Unger, K. K.; *Porous Silica, J. Chromatogr. Library, Vol. 16*, Elsevier Co.: Amsterdam, 1979.

46 Stevens, T. S. and Cortes, H. J., *Anal. Chem.* 55, 1983, p1365.

47 Davies, J. T. and Rideal, E. K., *Interfacial Phenomena*, Academic Press: New York, 1963.

48 Altria, K. D. and Simpson, C. F., *Chromatographia*, 24, 1987, p527.

49 Whitehead, R. and Rice, C. C., *J. Phys. Chem.* 69, 1965, p233.

50 Ghowsi, K. and Gale, R. J., *J. Chromatogr.*,559, 1991, p95.

51 Hayes, M. A. and Ewing, A.G., *Anal. Chem.*, 64, 1992, p512.

52 Kazarinov, V. E., ed., *The Interface Structure and Electrochemical Processes at the Boundary between Two Immiscible Liquids*, Springer-Verlag: New York, 1987, p4.

53 Ward, W.J., *AIChE J.*, 16, 1970, p808.

54 Koryta, J., *Electrochim. Acta*, 24, 1979, p293.

55 Samec, Z.; Marecek, V.; Koryta, J. and Khalil, W., *ibid.*, 83, 1977, p83.

56 Samec, Z.; Marecek, V.; Weber, J., *J. Electroanal. Chem.*, 100, 1979, p841.

57 Gavach, C. and Henry, F., *J. Electroanal. Chem.*, 54, 1974, p361.

58 Koryta, J.; Vanysek, P. and Brezina, M., *ibid.*, 75, 1977, p211.

59 Osakai, T.; Kakutani, T. and Senda, M., *Rev. Polarogr.*, Kyoto, 27, 1981, p51.

60 Kihara, S.; Yoshida, Z. and Fujinaga, T., *Bunseki*, Kagaku, 31, 1982, pE297.

61 Koryta, J., *Electrochim. Acta*, 24 1979, p293.

62 Du, G.; Koryta, J.; Ruth, W. and Vanysek, P., J. *Electroanal. Chem.*, 159, 1983, p413.

63 Kar, S.; Dasgupta, P. K.; Liu, H. and Hwang, H., submitted.

64 Bishop, E., ed., *Indicators*, Pergamon Press: New York, 1972, p185.

65 Cheng, K. L.; Ueno, K. and Imamura, T., *Handbook of Organic Analytical Reagents*, CRC Press: Boca Raton, Florida, 1982, p195.

66 Zheng, H., *Research Report*, Nov. 1993.

67 Zheng, H., *Research Report*, May 1992.

68 Dasgupta, P. K.; Decesare, K. B. and Ullreu, J. C., *Anal. Chem.*, 52, 1980, p1912.

69 Tsuda, T.; Sweedler, J. V. and Zare, R. N., *Anal. Chem.*, 62, 1990, p2149.

70 Dolnic, V.; Cobb, K. A. and Novotyn, M., *J. Microcol. Sep.*, 2, 1990, p299.

APPENDIX A

OTHER VERSION OF VALVE INJECTOR

The second version of the valve injector is shown in Figure A.1. A polyetheretherketone (PEEK) tubing was used for sample stream instead of capillaries. Two small holes (~350 μm) were drilled on the PEEK tubing and aligned with C_1 and C_2 so that C_1 and C_2 would meet inside the PEEK tubing. The original thought behind this design was to improve the sealing of the injection area and to avoid using capillaries as sample lines since they are fragile. Unfortunately, due to the mechining difficulty (PEEK is extremely hard), it did not reach our original expectation. The sealing was worse than the first version, and because the two small holes on the PEEK tubing were not polished, it created more resistance for the movemnet of C_2 in the injection area and resulted in tiny bubbles. The RSD for repeated injections was 3.7% ($n \geq 6$, see Figure A.3).

The third version of valve injector is shown in Figure A.2. The sample stream was in the hole drilled in the Plexiglas block, no extra tubing was used. The hole for holding C_1 and C_2 was drilled larger so that two Teflon capillaries (~380 μm I.D.) were used as sleeves of C_1 and C_2. The purpose of this design was to decrease the resistance for the movemnet of C_2 so that it would prevent bubbles production during the injection process. However the Teflon sleeve was too large for C_2 (~350 μm O.D.) in this case, it resulted in severe leakage. The RSD for repeated injection was 7.6% ($n \geq 10$, see Figure A.4).

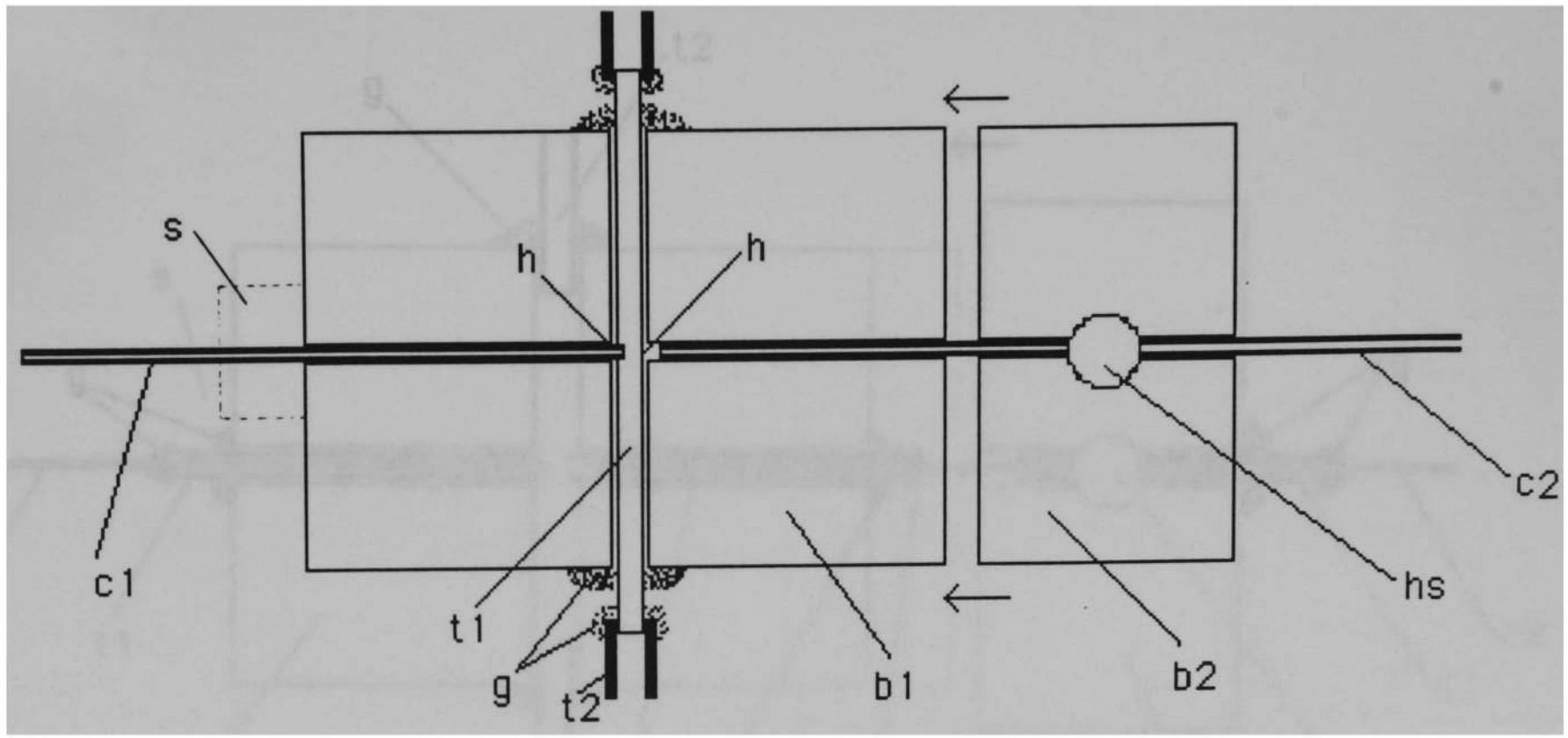

b1, b2	Plexiglas blocks	t2	Teflon tubing
c1, c2	75 µm ID / 350 µm OD capillaries	g	glue
hs	hole for screw to fix c2	s	screw for adjusting capillary displacement
t1	Polyetheretherketone (PEEK) tubing constituting sample line	h	350 µm holes drilled on t1

Figure A.1 Second Version of the Valve Injector.

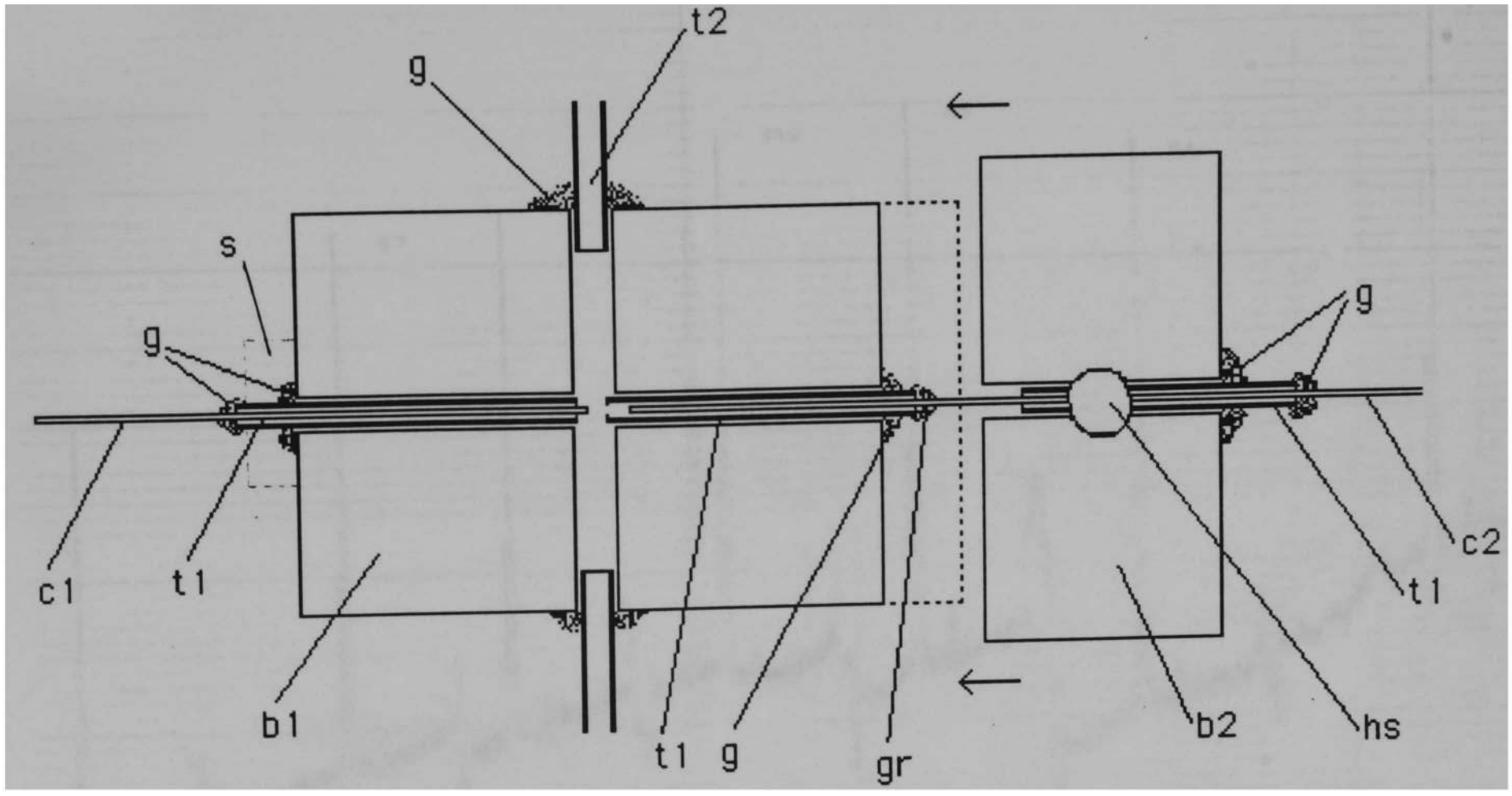

b1, b2	Plexiglas blocks	t2	Teflon tubing constituting sample line
c1, c2	75 µm ID / 350 µm OD capillaries	g	glue
hs	hole for screw to fix c2	gr	viscous high vacuum fluorocarbon grease
t1	380 µm ID sleeve Teflon tubing	s	screw for adjusting capillary displacement

Figure A.2 Third Version of the Valve Injector.

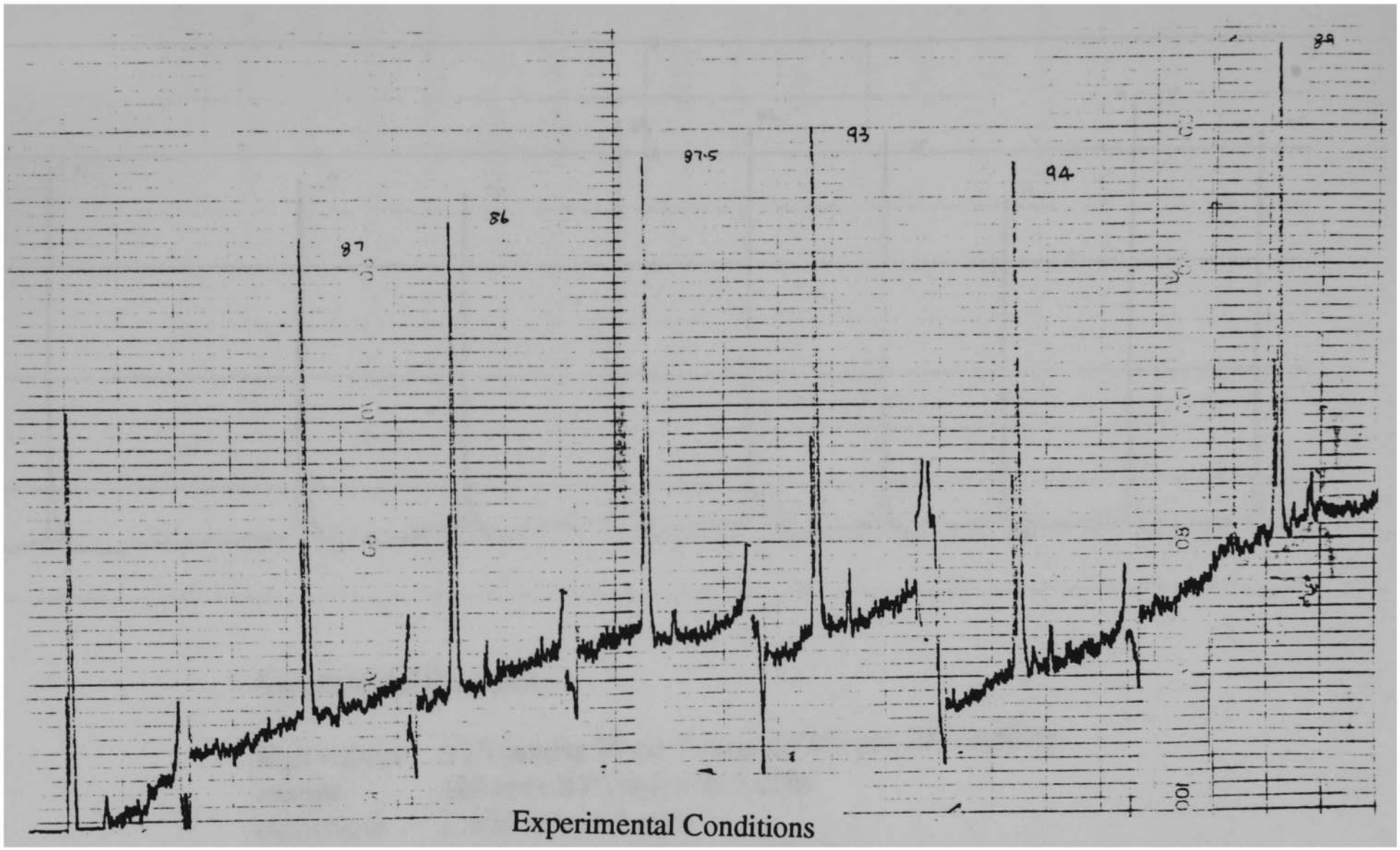

high voltage	9 kV across 50 cm 75 µm ID/350 µm OD capillary	detector	LINEAR UVIS 200 λ = 618 nm
sample	100 ppm BTB in 0.01N NaOH	full scale	0.1 AU
electrolyte	2 mM sodium borate	paper speed	60 mm / hr.

Figure A.3 Results from the Second Version of the Valve Injector .

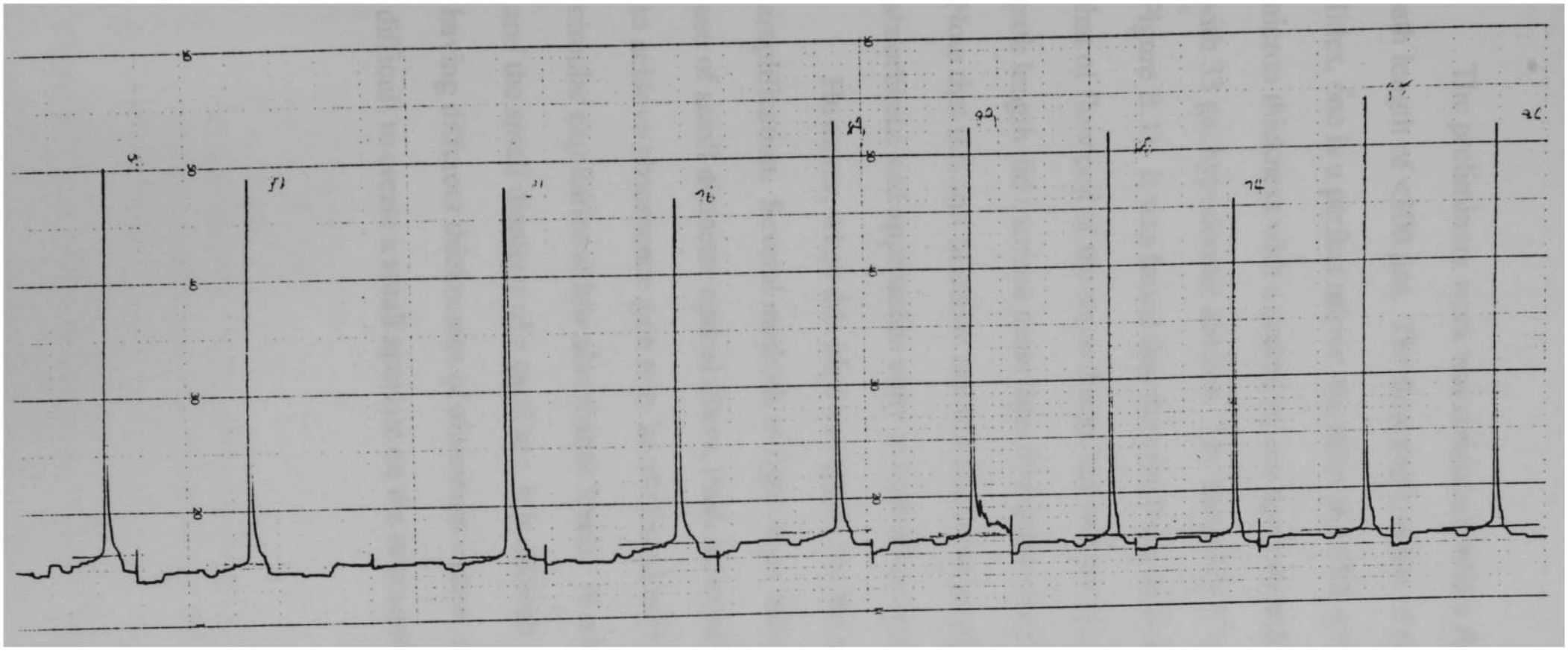

Experimental Conditions

high voltage	9 kV across 50 cm 75 µm ID/350 µm OD capillary
sample	100 ppm BTB in 0.01N NaOH
electrolyte	2 mM sodium borate
detector	LINEAR UVIS 200 $\lambda = 618$ nm
full scale	0.1 AU
paper speed	60 mm / hr.

Figure A.4 Results from the Third Version of the Valve Injector .

APPENDIX B

MULTIREFLECTION DETECTION CELL

The preliminary work was conducted with a flat flow cell with a geometrical light path length of <300 μm. The flow cell consists of two aluminum coated thin microscope slides, one is a perfect mirror, the other is a 95% reflective partial mirror; a thin film of 75 micron thickness with a central square aperture and liquid inlet and outlet apertures made with 33 ga. hypodermic needles. The assembly is held together by epoxy adhesive (see Figure B.1). It was found that the sensitivity increased more than five times relative to that of flow cell of the same design but without mirrors. This implies that the effective path length did increase more than five times when incident light beams are multireflected. Note that this sort of etalon cell is a nonlinear amplifier and the gain is high only at low absorbance and approaches unity at high absorbance.

However, when this idea was applied to the capillary system, there was no obvious amplification. Several methods of light beam introduction were investigated, including the use of small diameter optical fibers, flush mounted light emitting diodes, etc. The failure to achieve absorbance gain may be attributed to the severe stray light effect with the circular capillaries at low absorbance levels. In addition, because of the physical geometry and the small diameter of a capillary, it is difficult to exactly meet the requirements of having different thicknesses of aluminum coated on each half of the capillary. It was also difficult to create a small aperture on the deposited aluminum.

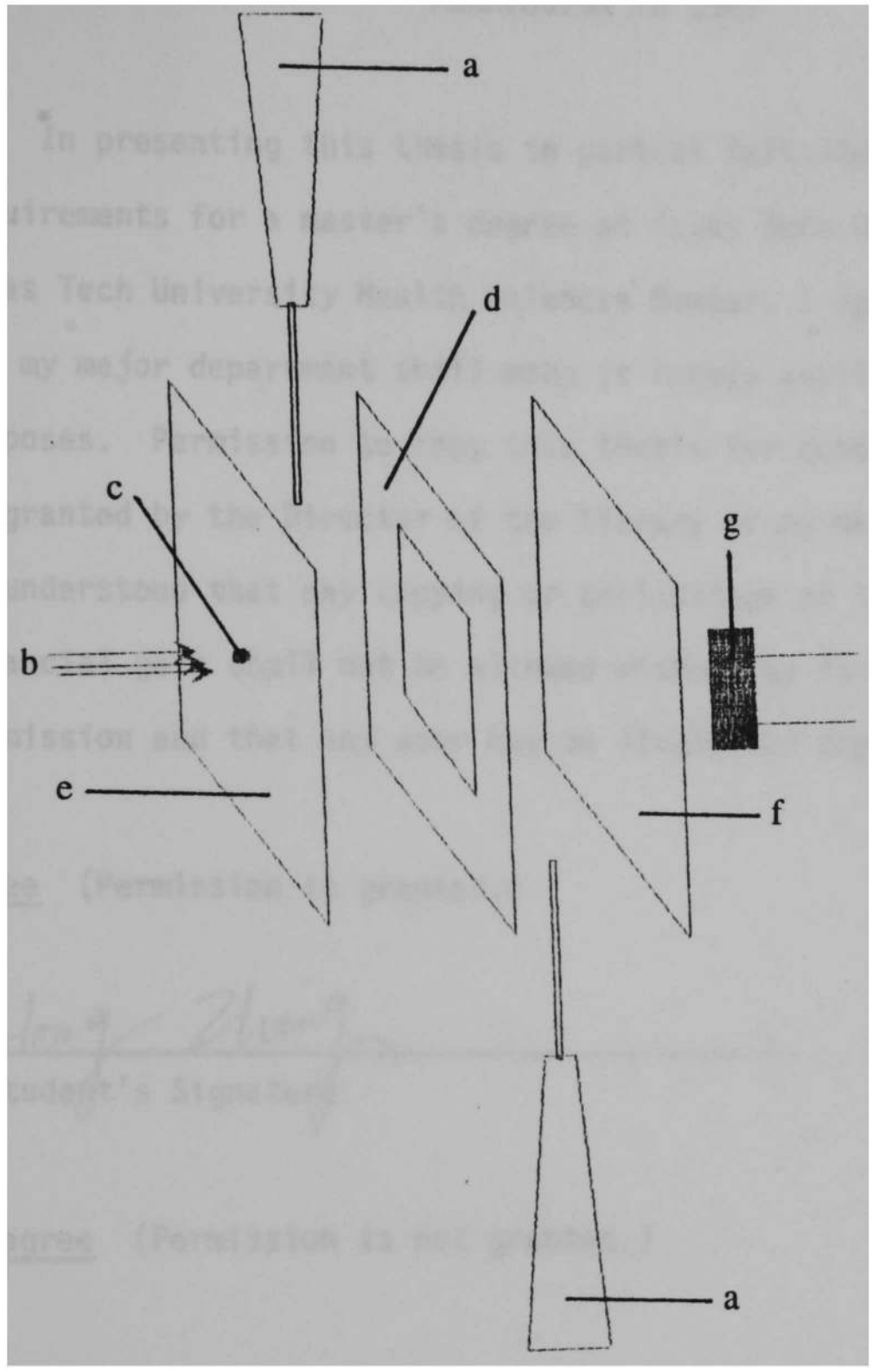

a needle 30G1/2
b incident light beams
c hole <150 μm
d film 75 μm
e microscope slide coated with aluminum 100% reflectivity
f microscope slide coated with aluminum 95% reflectivity 5% transmissibility
g photodiode

Figure B.1 Mutireflection Detection in Small Flow Cell Using Conventional Light Beams.